Delft University of Technology

Integrated Electrical Steady-State Power Flow Simulations on Transmission and Distribution Networks

Kootte, M.E.

Important note
To cite this publication, please use the final published version (if applicable).
Please check the document version above.

Integrated Electrical Steady-State Power Flow

Simulations on Transmission and Distribution Networks

Integrated Electrical Steady-State Power Flow
Simulations on Transmission and Distribution Networks

Proefschrift

ter verkrijging van de graad van doctor

aan de Technische Universiteit Delft,

op gezag van de Rector Magnificus Prof. dr. ir. T.H.J.J. van der Hagen

voorzitter van het College voor Promoties,

in het openbaar te verdedigen op

donderdag 25 april om 10:00 uur

door

Maria Eliza KOOTTE

Wiskundig Ingenieur, Technische Universiteit Delft, Nederland

geboren te Rotterdam, Nederland.

Dit proefschrift is goedgekeurd door de promotoren.

Samenstelling promotiecommissie:

Rector Magnificus	voorzitter
Prof.dr.ir. C. Vuik	Technische Universiteit Delft, promotor
Prof.dr.ir. M.B. van Gijzen	Technische Universiteit Delft, promotor

Onafhankelijke leden:

Prof.dr. M. Vlasiou	Universiteit Twente
Dr. S. Grundel	Max Planck Institute Magdeburg, Duitsland
Dr. S.H. Tindemans	Technische Universiteit Delft
Prof.dr.ir. Z. Lukszo	Technische Universiteit Delft
Prof.dr.ir. H.X. Lin	Technische Universiteit Delft

De auteur wil graag J.E. Romate bedanken voor zijn bijdragen aan dit proefschrift.

An electronic version of this dissertation is available at
http://repository.tudelft.nl/.

"Laat het maar moeilijk zijn."

— Nasrdin Dchar, Familiekroniek

Contents

Summary

Integrated electrical power flow simulations are concerned with solving the steady-state load flow problem on integrated transmission and distribution electricity networks. We have developed a framework to run these simulations efficiently, whilst keeping in mind the differences between these network types and accommodating the practical considerations of system operators. We need such a framework to analyse the interaction that these systems might have as a result of the energy transition.

The steady-state load flow (or power flow) problem is the problem of computing voltages in an electricity network given the admittance on branches and power consumption and generation at the buses in a network. This is done by solving the power flow equation: A nonlinear equation that relates the voltage, power, and admittance in a network. Transmission and distribution networks differ in topology and characteristics such that these networks are modelled and solved in different manners. The most important difference is that the transmission network is balanced and we therefore only have to regard a single phase in power flow computations whilst distribution networks are not balanced and require three-phase simulations.

To develop a framework to run integrated power flow simulations, we have worked in two stages. Firstly, we have studied how we can model an integrated network. We have found two ways of modelling an integrated network: using a homogeneous configuration in which both networks are modelled using three phases and using a hybrid network configuration in which both networks keep their original configuration but in which the coupling substation takes care of the phase dimension mismatch between the two sides. Next to that, we have found two ways of solving an integrated system: either by coupling them into one system and solving that as a whole (we call this the unified approach) or by keeping two separate systems and iterating between these networks (we call this the Manager-Fellow Splitting (MFS) method).

In total, we obtained four methods that were subject to our numerical assessment study: the unified method applied to hybrid networks (the interconnected method) or to homogeneous networks (the full three-phase method) and the MFS method applied to hybrid (MFS-hybrid) or homogeneous (MFS-homo) networks.

We have performed simulations in Matpower on a small scale to compare the performance of these four methods which gave us an idea of their performances in larger and more realistic settings. We have concluded that the unified methods are generally faster than MFS methods and that a hybrid network configuration leads to faster results, making the interconnected method the most efficient.

As the increasing rise of photo-voltaic penetration at the distribution level might lead to an additional imbalance in transmission networks, we have investigated whether this imbalance is indeed induced. We have seen that even with high PV penetration levels, the effects on the transmission grid are negligible. Therefore we have con-

cluded that hybrid network configurations are also sufficient to analyse integrated power flow simulations.

In the second stage, we have focused on the efficiency of these simulations. During every Newton-Raphson iteration in power flow simulations, a linear system is solved. We have therefore studied several Krylov subspace and preconditioning techniques that can solve this linear system efficiently. As it is difficult to judge upfront which techniques work best to solve power flow problems, we have first applied them to separate network problems to get insight into their performance. Afterwards, we applied the best-performing Krylov and preconditioning combinations to integrated network simulations. During this stage, we applied them to networks up to a size of 800,000 buses as we were interested in efficient scaling of the methods that were originally the object of study. As hybrid network configurations were sufficient to analyse interaction on integrated systems and performed better than homogeneous configurations, we only considered the hybrid unified and hybrid MFS methods.

The results were somewhat different than our initial assessment study as the MFS methods were performing better (in terms of CPU time) than unified methods. Furthermore, preconditioned Krylov subspace methods had a similar performance to direct methods. It is difficult to judge why this happened. The reason for the first observation could be that the library in which we performed these simulations, PETSc, is optimised for parallel computations in which multiple smaller blocks are solved at the same time whilst we were doing only sequential computations. The unified methods have to solve a larger block than the MFS methods. An explanation for the second observation could be the way that the large test cases are built which is by connecting multiple of the same test cases to each other with only one branch connecting them.

During the development of this integration framework, we have striven to incorporate operational convenience for Transmission and Distribution System Operators (TSOs and DSOs). To get an idea of their concerns and considerations, we have consulted several reports written by the European Union that reflect on TSO and DSO interaction. In this way, we got an insight into the opportunities for increased TSO-DSO cooperation but also into the challenges that arise. Besides financial and regulatory challenges, we saw that SOs can be somewhat reluctant to increase cooperation because of the expected computational burden and data privacy concerns. SOs often lack awareness of the latest advances in scientific computing that decrease computational burden and handle privacy issues. The way this framework is built can take away a part of their concerns.

The focus of this framework was mainly on creating a numerical basis to run integrated power flow simulations. Therefore, during our analysis, we made simplifications in the design of the test cases that were input to our assessment and in the studies we performed (electrical elements, topology, and steady-state operation respectively). We would therefore recommend continuing the assessment study on more realistic test cases and under different conditions such as dynamic analysis, contingency analysis or optimal flow computations.

Lastly, we think that these simulations could benefit from High-Performance Computing techniques to make them even more efficient. It should be relatively easy to implement this in PETSc.

Samenvatting

Geïntegreerde elektrische load-flow simulaties worden uitgevoerd om het stationaire load-flow probleem op geïntegreerde transmissie en distributie netwerken op te lossen. Wij hebben een raamwerk ontwikkeld dat deze simulaties op een efficiënte manier uitvoert, rekening houdend met de eisen en praktische bezwaren van transmissie en distributie netbeheerders (TNBs en DNBs). Een dergelijk raamwerk is nodig om de mogelijke interactie tussen deze twee netwerken —die door de energie transitie wordt veroorzaakt— te simuleren.

Het stationaire load-flow probleem koppelt de spanning in een netwerk aan de admittantie (een officiële benaming van de weerstand) van de netwerkkabels en het vermogen dat in een elektriciteitsnetwerk geconsumeerd en geproduceerd wordt. Het is een niet-lineair probleem, bestaande uit complexe eenheden dat wordt opgelost met een iteratieve methode. Omdat transmissie en distributie netwerken een verschillende topologie en karakter hebben, verschilt het per netwerk hoe het load-flow probleem wordt gemodelleerd en opgelost. Het belangrijkste verschil is dat het transmissie netwerk gebalanceerd is waardoor driefasig vermogen als eenfasig gemodelleerd kan worden. Distributie netwerken zijn niet gebalanceerd, waardoor driefasige simulaties nodig zijn bij de analyse van distributie netwerken.

We hebben de ontwikkeling van het raamwerk in twee stappen aangepakt. Als eerste hebben we gekeken hoe een geïntegreerd transmissie en distributie systeem gemodelleerd moet worden, rekening houdend met het verschil in fasen tussen de netwerken. De eerste methode is om het transmissie netwerk ook driefasig te modelleren, zodat de twee netwerken gemakkelijk gekoppeld kunnen worden. Dit noemen we een homogene netwerk configuratie. De tweede manier is om het transmissie netwerk eenfasig te houden en bij de koppeling rekening te houden met het faseverschil. Dit noemen we een hybride netwerk configuratie. Daarnaast hebben we ook twee manieren om het geïntegreerde systeem op te lossen. De eerste manier is om het gekoppelde systeem als geheel in een keer op te lossen: de geünificeerde methode. De tweede manier is om te itereren tussen de twee aparte methoden. Dit noemen we de Manager-Fellow Splitsing (MFS) methode.

We hebben hierdoor in totaal vier methoden die we onderwerpen aan een numerieke assessment studie: de geünificeerde methode toegepast op hybride netwerken (Geïnterconnecteerde methode) of op homogene netwerken (de volledige driefasige (V3F) methode) en de MFS methode toegepast op elk van die twee, wat leidt tot de MFS-hybride en MFS-homo methode.

We hebben simulaties op kleine test netwerken uitgevoerd in het softwareprogramma Matpower om de numerieke prestatie van deze vier methodes te onderzoeken zodat we een idee krijgen van het gedrag van deze methoden in een grote en meer realistische test omgeving. We hebben geconcludeerd dat geünificeerde methoden over het algemeen leiden tot snellere simulaties dan MFS methoden. Hetzelfde geldt voor

hybride netwerk configuraties ten opzichte van homogene configuraties. Dit maakt de geïnterconnecteerde methode het meest efficiënt.

Naast efficiëntie hebben we rekening gehouden met toename van zonne-energie op distributie netwerken door de energie transitie dat gevolgen kan hebben op transmissie netwerken: Deze kunnen ongebalanceerd worden. Hybride netwerk configuraties kunnen dit effect niet simuleren. We hebben daarom een studie uitgevoerd waarin we de penetratie van zonne-energie op het distributienet in verschillende fases laten toenemen en de resultaten van hybride en homogene netwerken vergelijken. Hieruit bleek dat de toename van zonne-energie op dit moment niet leidt tot extra onbalans op transmissie netwerken. Hybride netwerken zijn dus niet alleen efficiënter maar ook voldoende om de interactie tussen de twee netwerken vast te leggen.

In de tweede stap in de ontwikkeling van het raamwerk, hebben we gefocust op de efficiëntie van deze simulaties. In load-flow simulaties wordt er in elke Newton-Raphson iteratie een lineair systeem opgelost. Dit systeem kan efficiënter worden opgelost als verschillende Krylov subspace methoden in combinatie met preconditioners worden toegepast. Omdat het moeilijk is om op voorhand te beslissen welke combinaties goed resultaat leveren, hebben we ze eerst getest op aparte transmissie en distributie netwerken. Vervolgens hebben we de best presterende methoden toegepast op geïntegreerde netwerken met een grootte tot 800,000 knooppunten, omdat we geïnteresseerd zijn in de efficiëntie van de methoden. Vanwege de efficiëntie en bruikbaarheid van hybride netwerk configuraties, hebben we deze grote simulaties alleen op deze configuratie toegepast.

De resultaten van de simulaties waren anders dan die van de numerieke assessment uitgevoerd in Matpower. De MFS methoden waren namelijk sneller dan de geünificeerde methoden. Daarnaast zagen we ook dat directe methoden net zo snel waren als gepreconditioneerde Krylov subspace methoden. Het is moeilijk om te zeggen wat tot deze verschillende resultaten heeft geleid. Het eerste zou verklaard kunnen worden in de manier waarop het programma PETSc, waarin we de grote simulaties hebben uitgevoerd, is opgebouwd. Het zou kunnen dat het geoptimaliseerd is voor het oplossen van meerdere kleine blokken. Het tweede kan eventueel verklaard worden door hoe de test netwerken zijn gecreëerd. Het grote netwerk is namelijk handmatig ontwikkeld door verschillende kleine netwerken met één kabel aan elkaar te koppelen.

Tijdens de ontwikkeling van het raamwerk hebben we altijd de toepasbaarheid voor netbeheerders in ons achterhoofd gehouden. Om goed op de hoogte te zijn van de behoeftes en eisen van netbeheerders, hebben we een studie gedaan naar de ontwikkeling omtrent TNB-DNB samenwerking in de Europese Unie. Hier zagen we dat deze samenwerking leidt tot kansen om spanningen op het net te verminderen, maar dat het ook leidt tot uitdagingen. Deze uitdagingen zijn zowel financieel, operationeel als procedureel van aard. Ook zijn netbeheerders vaak terughoudend vanwege computationele bezwaren en omdat het uitwisselen van gegevens tussen netbeheerders vanwege privacy redenen niet zomaar is toegestaan. Netbeheerders zijn vaak niet op de hoogte van de ontwikkelingen in de numerieke analyse die de computationele last kan verlichten. De manier waarop dit raamwerk is ontwikkeld, kan een deel van die uitdagingen wegnemen.

De focus gedurende dit proefschrift lag voornamelijk op het creëren van een nume-rieke basis om geïntegreerde load-flow simulaties uit te voeren. Daarom hebben we tijdens de ontwikkeling van het raamwerk een aantal keuzes gemaakt om een en ander te versimpelen. Bijvoorbeeld in het ontwerp van de test netwerken en bij het onderwerpen aan bepaalde studies. Zo hebben we alleen stationaire analyse gedaan. Eén van de aanbevelingen is om in het vervolg onderzoek de methodes te testen op meer realistische netwerken en ook te onderzoeken hoe ze presteren bij dynamische analyse, contingentie analyse of optimale load-flow studies.

Tot slot denken we dat deze simulaties nog efficiënter kunnen als technieken uit de High-Performance Computing worden toegepast. Het zou relatief makkelijk moeten zijn om dit te implementeren in PETSc.

1

Introduction

Electrical power systems provide us with a supply of electrical energy. The commodity of supply for us consumers conceals the complexity behind these systems but the millions of buses that are part of an electricity network are continuously assessed by system operators (SOs). Power flow simulations are the backbone of safe operations of the electrical power grid. These simulations are based on power (or load) flow equations: Equations that relate the generation and consumption of electrical power in electricity networks by assessing the voltage, power, and admittance at the buses in these networks. Numerical Analysis (NA) is at the heart of these simulations: NA makes sure that simulations can run efficiently despite the size of electrical grids and the complexity of the power flow equation.

In this study, we distinguish between two types of electrical grids: High-Voltage Transmission grids and Medium/ Low-Voltage Distribution grids. Currently, they are analysed separately. However, the energy transition requires that these networks be analysed as integrated systems such that the influences that the networks have on each other can be monitored. The integration of these two systems comes with challenges that are related to the different designs of the two separate systems and the distinct ways that these systems are solved. Furthermore, a challenge arises as the size of the system increases when these two systems are integrated into one. In this thesis, we derive a framework to model and solve transmission and distribution systems as an integrated system and use numerical analysis techniques to solve the integrated system efficiently.

The Dutch power system

The electrical power system provides the generation, transmission and distribution of electrical energy. The Dutch power system consists of one transmission network, operated by the Transmission System Operator (TSO), and several distribution networks, operated by Distribution System Operators (DSOs). TenneT is the Dutch TSO. Stedin, Liander, Enexis, Westland Infra, and RENDO are the Dutch DSOs. The transmission network supplies the generation and transport of high-voltage power ($150 - 380$ kV in the Netherlands) over large distances on overhead cables to substations or directly
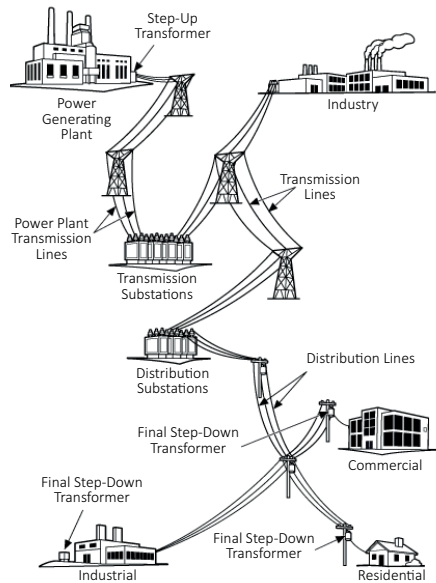
Figure 1.1: A schematic electrical power grid [1] including the transmission and distribution grid. Power is generated at bulk power plants and transported over transmission lines directly to industry and substations. At these substations, power is transported further over distribution lines to residential and commercial consumers. Note that in the Netherlands, the distribution network primarily comprises underground infrastructure.

to large-scale consumers. At the substations, power is transformed to lower voltage levels, from which it is further transported on distribution networks. These networks are responsible for the supply of electrical power to end consumers. It operates on medium voltage levels (around $10 - 66$ kV) and low voltage levels (below 1 kV). Figure 1.1 represents an electrical power system.

The design of the electrical power system is efficient and safe: The supply of power on high-voltage Alternating Current (AC) using three phases reduces voltage drops and power losses, and minimises the use of conductors (the material that allows the flow of charge in an electricity network). The use of gradually varying voltage levels, makes the distribution of power to end consumers efficient. The use of underground distribution cables provides natural isolation and a risk-averse environment. The European system operates on a frequency of 50 Hz [2], meaning the number of oscillations per second of AC.
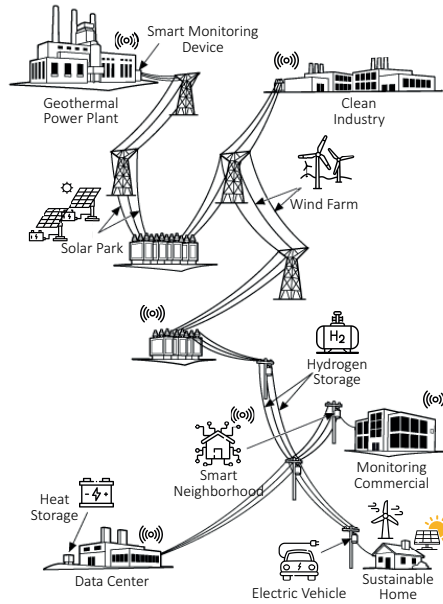
Figure 1.2: Sustainable Electricity grid of the future (Adapted from [1]) in which electric appliances can constantly be monitored. Loads and generators are replaced with their renewable and sustainable counterparts. New electric loads, such as data centres and electric vehicles have arisen. Battery and hydrogen storage are part of the new grid.

The energy transition

Traditionally, the electrical system is a centralised, passive top-down network where electricity is generated in large power plants at the transmission level and further transported to lower-level customers. Currently, the electrical power system is changing to a decentralised, active bottom-up network. This has different immediate causes, amongst which are the development of Renewable Energy Sources (RES) and the electrification of different sectors [3]. Renewable resources, such as solar panels and wind turbines, are often connected to the electrical power system at the distribution level; either as large-scale utility Photo-Voltaic (PV) power plants or as rooftop solar panels at the household level. Electrification is induced by the transport sector (electric vehicles), heat suppliers (Combined Heat and Power plants, electric central heating), and the energy absorption of data centres. Figure 1.2 represents an energy-transitioned grid.

The changing environment requires a more detailed analysis of the electricity network and the interaction between transmission and distribution networks. Integrated transmission-distribution network models can be used to study this interaction [4].

Load flow studies

System operators perform load flow studies to analyse their power systems. Steady-state load flow — or power flow — analysis gives insight into the state of the system. It is used to monitor voltages and power in the network and forms a basis for daily operation or (long-term) planning of electrical power systems. For operation purposes,

load flow studies are performed to evaluate the power systems' performances when conditions are suddenly changing, such as in the event of power outages or blackouts. In planning, load flow studies form the basis for the evaluation of expansion plans.

Numerical Analysis

The size and complexity of electrical power computations — non-linear equations in which millions of nodes need to be assessed — require numerical methods to provide quick results to these analyses. Well-known numerical methods such as the Newton-Raphson method are one of the most common ways to solve transmission and distribution systems. Additionally, several other NA techniques such as Krylov subspace methods, line search techniques, and reordering methods are frequently encountered to gain additional speed-up of load flow computations. Furthermore, load flow equations often form the basis for time-consuming procedures such as optimal power flow — in which the optimal allocation of generators is assessed — or contingency analysis, in which the power system is assessed whether it is still stable when one (N-1 contingency) or multiple outages are happening. It is therefore important to evaluate the numerical performance of electrical power systems and to solve load flow equations efficiently and robustly.

Integrated network analysis

Integrated transmission-distribution network models are employed to study the interaction between transmission and distribution networks. The study of integrated network models is an emerging field [5]. A literature review shows that multiple approaches exist that can roughly be categorised into 1) co-simulation frameworks that can study multiple domains with their own suitable solver and 2) stand-alone analysis frameworks that study integrated network models in one software program [6]. The focus of this work is on stand-alone frameworks. Although co-simulation frameworks are beneficial for simultaneous analysis of large — millions of buses — transmission and distribution networks due to their modular nature and suitability for HPC architectures [3], we expect a competitive advantage for stand-alone models soon: Co-simulation methods — which are the antitheses of stand-alone methods — are valuable and practical for system operators, but can never live up to the numerical performances of stand-alone methods: Efficiently integrated stand-alone models require significantly less communication and should therefore be competitive to co-simulation techniques.

It is not straightforward to integrate separate electricity networks. The networks have different characteristics which has resulted in different network models that cannot be easily integrated. The most important difference is that the transmission network is balanced: Power is generated in three phases but the voltage and current of other phases have the same magnitude and an equal phase shift amongst them. Therefore, only one phase of the transmission network is modelled and computed, from which the other two phases are deducted. We call this a single-phase model. The distribution network is in general not balanced, due to the unequal mutual coupling between phases on the lines and unbalanced loads installed along the distribution feeder, and thus modelled using all three phases [7], hence the need for a three-phase model. Furthermore, the distinct characteristics have led to the development of different algorithms to solve the transmission or distribution power flow problem [8].

Practical considerations

Besides the technical complexity of electricity network models, we have the issue of confidentiality that makes SOs less inclined to cooperate and do integrated system analyses. SOs are not willing — due to financial or operational reasons — or not allowed to share network information with other system operators. One can reason that the ongoing energy transition and electrification are going to push the limits of conventional models until they do not suffice anymore. Probably, legislation and current behaviour will then follow the necessary change towards the use of integrated network models. Furthermore, technical advances in distributed computing allow system operators to share data and to do integrated analysis without full data sharing between entities [9]. In this work, we address the different needs of the system operators and the possibility of doing a fully integrated network analysis under legal and practical considerations.

Focus

We will develop a framework to run efficient stand-alone power flow computations on integrated transmission-distribution systems. Thus far, several integration techniques have been developed and tested on small-size transmission and distribution networks to test the feasibility of the methods [10] [11]. In this work, we compare the performance of these existing stand-alone methods on convergence rate and CPU time and their ability to be efficiently scaled to large-size networks by applying them on several transmission-distribution networks. Next, we pay attention to NA techniques, such as Krylov subspace methods, preconditioners, and reordering techniques to efficiently solve the stand-alone methods. We focus on Newton-Krylov solvers as they are robust and have chosen their potential for transmission systems [12]. Special attention is paid to the needs and concerns of transmission and distribution system operators, and specific conditions and design of physical electricity networks to make this framework practical and functional.

Outline

This thesis consists of four parts. Part I focuses on the description of electricity network models and solution methods of separate transmission and distribution systems. Part II is concerned with the analysis of integrated power systems. Part III focuses on iterative computing methods and preconditioning techniques to solve large power systems, while part IV relates the functionality of the developed framework to the developments in TSO-DSO cooperation in Europe.

Integrated Power Systems

Part I Electricity Networks	Part II Integrated Systems	Part III Large Systems	Part IV Looking Ahead
• Power System Analysis • Transmission and Distribution Analysis • Nonlinear Power Flow Solvers	• Integrated Network Analysis • Numerical Results • The Influence of Additional PV Generation	• Linear System Solvers • Numerical Results of Large Power Systems	• Policy Notes on TSO-DSO Interaction in Europe • Conclusion • Discussion
Background	Proof of Concept	Efficient Scaling	Discussion

Figure 1.3: Overview of this Thesis including Parts and Chapters.

Figure 1.3 gives an overview of the four parts and their chapters. Chapter 2 describes the basics of electrical circuit theory and fundamental laws to analyse steady-state power flow systems. Chapter 3 describes the distinct components of transmission and distribution systems and the elements encountered in electricity networks. Chapter 4 pays attention to existing non-linear methods to solve separate transmission and distribution systems. Chapter 5 gives an overview of the possible options to model and solve integrated systems. Chapter 6 gives the results of power flow computations on small integrated systems while Chapter 7 gives the results when these integrated systems are applied to different levels of Photo-Voltaic penetration at the distribution level. In general, Part II is concerned with the proof of concept of integration methods and applicability to the physical conditions of power systems.

The size of integrated systems can become very large, therefore — in Part III of this thesis — we pay attention to the possibilities of iterative methods combined with Newton-Raphson solvers and the possibility to precondition these methods. Chapter 8 gives a literature overview of iterative and preconditioning methods and the results of applying these techniques to separate transmission and distribution networks. Chapter 9 contains the results of the application of these methods to large integrated systems. The last part contains two chapters: Chapter 10 sheds light on the developments in Europe around TSO-DSO cooperation. Chapter 11 contains the conclusion, discussion, and future outlook.

I

Electricity Network Models

2

Power System Analysis

2.1. Introduction

We analyse electrical power systems by creating a mathematical model of the system of interest and the elements it consists of. We use electrical circuit theory to describe the behaviour of these elements. An electrical circuit is the assemblage of devices that connect an electrical power source to a load. An electrical power system can be seen as a connection of multiple electrical circuits. The parameters that form the basis to describe an electrical circuit, are: voltage, current, power, and admittance.

We are interested in performing efficient load flow studies on electrical power systems. A load flow study gives insight into the state of the network which is input for planning and operation purposes of system operators. Load flow studies are performed independent of time and dimension. Temporal disturbances in electrical power grids, called transients, happen within microseconds and then settle to an equilibrium. Therefore, we can assume a steady-state operation in our analyses and use a time-independent approach where we assume the frequency to be constant. Dynamical analyses do study the effect of transients, but that is outside the topic of this thesis.

To perform a load flow study, we need to create a network model that assembles the elements and parameters. In this chapter, we describe how to perform a load flow study on general electrical power systems. It contains a description of the following:

1. The essential parameters and electrical laws that are valid in power systems

2. The concept of an electrical network model

3. The assemblage of elements into the power flow equation that gives insight into the state of the network

4. The derivation of steady-state per-unit phasor representation of the parameters (independent of time, dimensionless) that are input to the power flow equation.

2.2. Power system parameters

2.2.1. Voltage and Current

Power systems connect one or multiple sources to one or multiple loads. The source in a power system causes current to flow and produce an electric voltage in the circuit. In Alternating Current (AC) systems, the waveforms of voltage and current can be assumed to be a sinusoidal function, described by:

$$v(t) = V_{max} \cos(\omega t - \delta_V) \quad \text{and} \quad i(t) = I_{max} \cos(\omega t - \delta_I)$$

V_{max} the amplitude of the voltage

ω the angular frequency in [rad/s]

δ_V the phase angle of the voltage

δ_I the phase angle of the current

Phasor representation

In steady-state analysis, we use the effective phasor notation [12] in the computations. A phasor is a complex number representing a sinusoidal function whose amplitude, angular frequency, and initial phase (φ) are time-invariant. We can derive the phasor of the voltage using the Euler identity, which is the following:

$$e^{\iota\varphi} = \cos(\varphi) + \iota\sin(\varphi),$$

such that we can express $v(t)$ as:

$$
\begin{aligned}
v(t) &= V_{max} \cos(\omega t - \delta_V) \\
&= \text{Re}\{V_{max} e^{\iota\omega t} e^{-\iota\delta_V}\}
\end{aligned}
\tag{2.1}
$$

In complex arithmetic, phasors again produce phasors. Therefore, we can omit the term $e^{\iota\omega t}$ in equation 2.1 and in the rest of the calculations. This simplifies mathematics. We can insert the omitted term before evaluating the final result. The phasor representations of voltage $\mathcal{V}$ and current $\mathcal{I}$ are:

$$\mathcal{V} = V_{max} e^{\iota\delta_V} \quad \text{and} \quad \mathcal{I} = I_{max} e^{\iota\delta_I}$$

In circuit theory, it is common practice to use effective phasor notations, described by the effective value (or Root Mean Square (RMS) value) of the voltage and current. The RMS of the voltage ($|V|$) is found by taking the square root of the mean of $v^2(t)$:

$$\sqrt{\frac{1}{T} \int_0^T v^2 dt} = V_{max} \sqrt{\frac{1}{T} \int_0^T \cos^2(\omega t) dt} = V_{max} \sqrt{\frac{1}{2}} = |V|$$

T the period of the sine wave in $[s]$

The effective value $|V|$ and the peak value of the voltage V_{max} differ by a factor $\sqrt{2}$. The same holds for the current. It is common practice to use the label V for the effective phasor notation. We get the following expressions for the effective Voltage and Current phasors:

$$V = |V| e^{\iota\delta_V} \quad \text{and} \quad I = |I| e^{\iota\delta_I} \tag{2.2}$$

2.2.2. Reactive, Active and Complex Power

Instantaneous power is the time-varying component of power. It is expressed using a relation between the sinusoidal voltage and resistance R, or between the sinusoidal current and resistance:

$$p(t) = \frac{v^2(t)}{R} = i^2(t)R$$

R   the resistance

In steady-state computations, the instantaneous power is not used. Instead, we use the average power, obtained by taking its integral:

$$P = \frac{1}{T} \int_0^T p(t)dt$$

Next to the average component of power, we also have an oscillating component, as a result of the sinusoidal function. The average and oscillating components are derived simultaneously when rewriting the instantaneous power. To achieve this, we first need to express the sinusoidal voltage and current using a reference frame that is in phase with the voltage phase angle. Using the phase shift (ϕ) between voltage and current phase angles:

$$\phi = \delta_V - \delta_I,$$

we can express voltage and current using the following functions:

$$v(t) = V_{max} \cos(\omega t) \quad \text{and} \quad i(t) = I_{max} \cos(\omega t - \phi) \tag{2.3}$$

Using equation 2.3, we can rewrite the instantaneous power in the following way, from which we derive P and Q:

$$\begin{aligned}
p(t) &= v(t)i(t) \\
&= 2|V||I| \cos(\omega t) \cos(\omega t - \phi) \\
&= |V||I| \cos(\phi)[1 + \cos(2\omega t)] + |V||I| \sin(\phi) \sin(2\omega t) \\
&= P[1 + \cos(2\omega t)] + Q \sin(2\omega t)
\end{aligned}$$

The first term of the last line, $P[1 + \cos(2\omega t)]$, describes the unidirectional component of the instantaneous power with an average value P, this is called the real or active power in $[W]$. The second term $Q \sin(2\omega t)$ is a bidirectional (or oscillating) component, with an average value of 0. The amplitude Q is the reactive or imaginary power in $[var]$.

The active power and reactive power are expressed as:

$$P = |V||I| \cos(\phi) \quad \text{and} \quad Q = |V||I| \sin(\phi) \tag{2.4}$$

From the relations for active and reactive power, we see that P is the real part of the product of voltage and the complex conjugate of current, while Q is the imaginary part. The complex power S is the sum of active and reactive power. The apparent power $|S|$ is the magnitude of the complex power:

$$S = V\bar{I} = P + \iota Q \quad \text{and} \quad |S| = |V||I| \tag{2.5}$$

Note that we have thus far used the symbol ι as a complex unit in the computations. This, is to avoid any confusion with the character i which is used as an index value later on in the thesis.

2.2.3. Admittance

Electrical circuits exhibit impedance (Z). Impedance is the extension of resistance to current flow in alternating circuits. Impedance consists of resistance (R) and reactance (X). The inverse of impedance is admittance (Y) which consists of conductance (G) and susceptance (B). Admittance is often used to describe the power flow equations in electrical circuits. Z and Y are described by the following relations:

$$Y = \frac{I}{V} = G + \iota B \quad \text{and} \quad Z = \frac{1}{Y} = R + \iota X \tag{2.6}$$

2.2.4. Per Unit System

The power system is analysed as a per-unit system, having non-dimensional quantities. This has advantages because scaling leads to values within a narrow range, the voltage is close to unity (as the voltage is chosen as the base value) and it eliminates ideal transformers as circuit components [13]. This last derivation is shown in section 3.8.

The per-unit system is obtained using the following scaling equation:

$$\text{Per-unit value} = \frac{\text{actual value}}{\text{base value}}$$

As the actual value and the base value have the same units, the per-unit value is dimensionless. To set up the per-unit system, we need the base values for Voltage, Current, Impedance and Complex Power (V_{base}, I_{base}, Z_{base} and S_{base}, respectively). Two of them are chosen, and the third and fourth ones are deducted from the other two in the following manner:

$$S_{base} = V_{base} I_{base} \quad \text{and} \quad Z_{base} = \frac{V_{base}}{I_{base}}$$

As $Z = R + \iota X$ and $S = P + \iota Q$, there is no need for other base values, they can be defined accordingly:

$$Z_{base} = R_{base} = X_{base}$$
$$S_{base} = P_{base} = Q_{base}$$

The following equation shows that this holds:

$$Z_{pu} = \frac{R + \iota X}{Z_{base}} = \left(\frac{R}{Z_{base}} \right) + \iota \left(\frac{X}{Z_{base}} \right).$$

2.3. Network model of a general power system

An electrical power system is a network containing power generators, power consumers, electricity cables and other supplementary components necessary for the safe operation of the electrical grid, such as transformers, shunts, substations, and step-voltage regulators. The function and full mathematical description of these components are described in chapter 3.

2.3.1. Graph theory

We use a power system model to simulate what is going on in electricity networks. An electricity network model is presented on an undirected graph containing buses $i = 1, ..., N$, —also called nodes— and branches —also called edges. Branches represent the electricity cables and transformers, buses represent the generators, loads and shunts. Cables carry power over transmission and distribution lines. Transformers convert voltage and current to different levels [13]. Generators supply a symmetrical load and as a result, current and power are fed into the grid. Therefore, they are modelled as power injections. Loads convert the electrical energy into a usable form and are modelled as negative power injections. A detailed configuration of how all these elements are modelled is described in chapter 3.

2.3.2. Electrical Laws

The three most important laws to describe electrical circuits are Ohm's law and Kirchoff's Current and Voltage laws. The relation between current and voltage is described by Ohm's law:

$$I = YV \tag{2.7}$$

Kirchoff's Current Law (KCL) states that the current flowing to each bus is equal to the sum of currents flowing away from that bus:

$$\sum_k I_k = 0,$$

where I_k is the current entering or flowing away from bus k.

A similar law for voltages exists. Kirchoff's Voltage Law (KVL) states that the directed sum of voltages around a closed loop is zero:

$$\sum_j V_j = 0,$$

where V_j is the voltage across component j in the loop.

2.3.3. Network model

Load flow —or power flow— computations give insight into the steady-state behaviour of the power system. The network topology, parameters, and bus information are required as input. The topology is the description of the connected buses in the network. The following parameters are objects of study:

- the voltage magnitude $|V_i|$
- the voltage phase angle δ_i
- the injected active power P_i
- the injected reactive power Q_i

Next to these four parameters, we also need to specify the branch admittance Y_{ij}. Which is given for all the power cables. Every bus in the network has two known parameters and two to be computed. The bus type determines which of the parameters need to be computed.

The following three bus types can be distinguished:

- the load bus (PQ-bus);
- the generator bus (PV-bus);
- the slack bus;

Most of the bus types are load buses (PQ-buses) for which P and Q are known and $|V|$ and δ need to be computed. Load buses are modelled as constant power sinks, having a negative injected active and reactive power specified at the node. Most of the generators are modelled as PV-buses. Generators can control active power and voltage, therefore, P and $|V|$ are known at these buses and the other two need to be determined.

One generator, usually the first, is taken as the slack bus. This bus serves as a reference bus for the other buses. This is the only bus where the phase angle is specified [14]. The phase angles of the other nodes are measured with reference to the slack bus. The slack bus balances both the difference (the slack) between the total reactive power in- and output and between the total active power in- and output. There is always a slack bus in a power system. Table 2.1 presents the known parameters at each bus and the ones to be computed.

2.4. The power flow equation

The load flow problem is formulated as the determination of the flow of electrical power of a steady-state power system. This is done by computing the voltages (V_i, δ_i) such that the computed active and reactive power injected at each bus correspond with the specified values at each bus [14]. This problem is mathematically described using the power flow equation. The power flow equation is the assembly of the previously described information of parameters in an electrical circuit and computed using the network topology of the electrical power grid. The power flow equation is the following equation:

$$S_i = V_i \overline{I}_i = V_i (\overline{YV})_i = V_i \sum_{k=1}^{N} \overline{Y}_{ik} \overline{V}_k \qquad (2.8)$$

The S_i is the complex power injected at bus i, I_i is the current flowing into bus i, V_i is the voltage at bus i, Y_{ij} is the admittance of a branch between bus i and j and N is the total number of buses in the power system.

Table 2.1: Bus types in an electrical network

	Variables	
Bus type	known	unknown
PQ-bus	P_i, Q_i	$\delta_i, |V_i|$
PV-bus	$P_i, |V_i|$	Q_i, δ_i
slack bus	$\delta_i, |V_i|$	P_i, Q_i

2.5. Overview

Given a network of $i = \{1, .., N\}$ buses, we have the following nodal and branch parameters that are important for power system analysis:

$$\text{Voltage } V_i = |V|_i \exp(\iota \delta_{V_i})$$
$$\text{Current } I_i = |I|_i \exp(\iota \delta_{I_i})$$
$$\text{Active Power } P_i = |V||I| \cos(\phi)$$
$$\text{Reactive Power } Q_i = |V||I| \sin(\phi)$$
$$\text{Admittance } Y_{ij} = G_{ij} + \iota B_{ij}$$

Using the following power flow equation

$$S_i = V_i \bar{I}_i = V_i(\overline{YV})_i = V_i \sum_{k=1}^{N} \overline{Y}_{ik} \overline{V}_k,$$

the topology of the network, and bus information, we can determine the state of the network by computing the unknown quantities at each bus in the power system.

2

3

Transmission and Distribution Network analysis

3.1. Introduction

An electrical power system consists of a transmission and several distribution networks that transport power from generators to consumers. The previous chapter described the important parameters derived from electrical circuit theory when studying power systems. In this chapter, we describe the elements responsible for the safe operation of an electrical power grid and how the parameters in these elements differ, both physically and mathematically, per transmission and distribution network.

The transmission system is responsible for the transport of high-voltage power over large distances. The Dutch high-voltage grid is presented in figure 3.1. Usually, high-voltage power[1] has voltage levels between 220 and 380 kV [15]. It transports electricity from generators to substations and consumers. Most generators at the transmission level are large power plants, such as nuclear reactors, gas and coal turbines, and —nowadays— also wind farms and solar parks. Most of the consumers are connected at the distribution level, but some large ones —such as greenhouses— consume directly from the transmission grid.

The transmission grid transports power over the entire span of the country. At several locations, it is connected to distribution substations. These substations are large project sites containing multiple connected in-series transformers. They transform power to lower voltage levels and form the connection between transmission and distribution networks. Distribution networks are responsible for the transport of power to end-consumers, such as households and industrial consumers. The electrical power that is transported over the distribution network gets transformed multiple times to gradually decreasing lower levels until it can safely be consumed at the household level, using the power socket.

---

[1]We only regard high-voltage AC. HVDC cables can transport over voltage levels up to 800 kV.
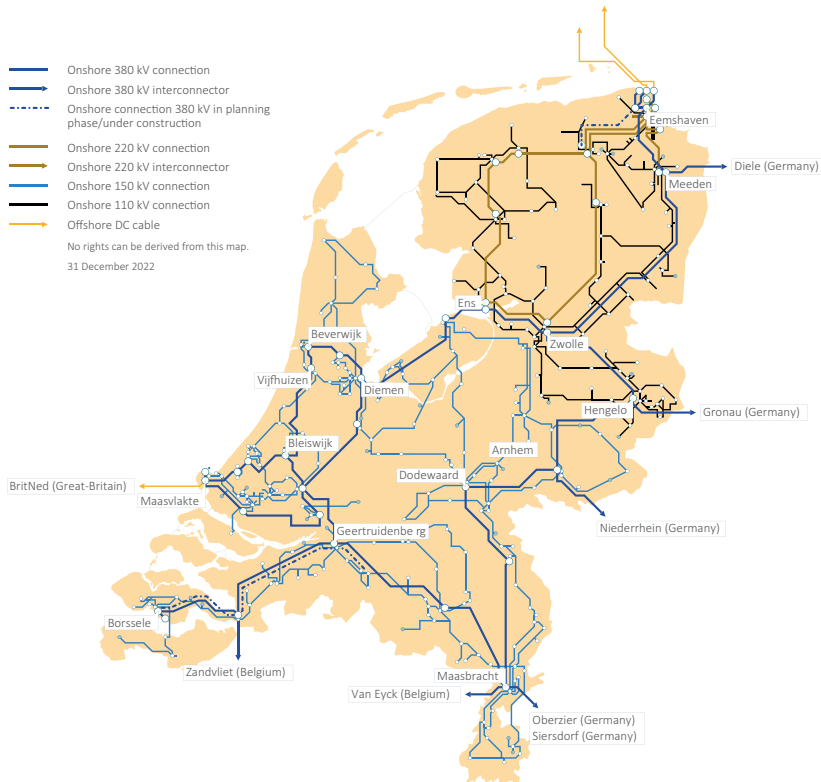
Figure 3.1: High-Voltage grid of Tennet adapted for design purposes from [16]

The design of transmission and distribution networks is different. The transmission network is a meshed network: All the buses are always connected by more than one branch. Distribution networks are originally radial: Power is supplied at one central bus and then transported to the rest of the network. As distribution networks are changing to decentralised systems where generation is also supplied at the distribution level, the networks are sometimes changing into weakly meshed designs, to properly connect these generators to the rest of the network. Figure 3.2 contains a radial and meshed network topology.

Power is supplied using three phases. The design of the transmission network uses transposed cables leading to a balanced transmission system: All phases are equal in magnitude and the phase difference between them is equal. Distribution cables are not transposed, and some distribution loads, such as household appliances, are connected to the network using a single-phase configuration, while industrial consumers are connected via three phases. The distribution network is therefore not balanced.

The conductor material and the much shorter length of distribution systems lead to higher R/X ratios on distribution lines compared to transmission networks, which affects the solvability and voltage control of the systems. For example, voltage regulation through reactive power control is mainly based on the reactance X of the line while the line resistance R is ignored [17]. Also, the original Fast-Decoupled Load
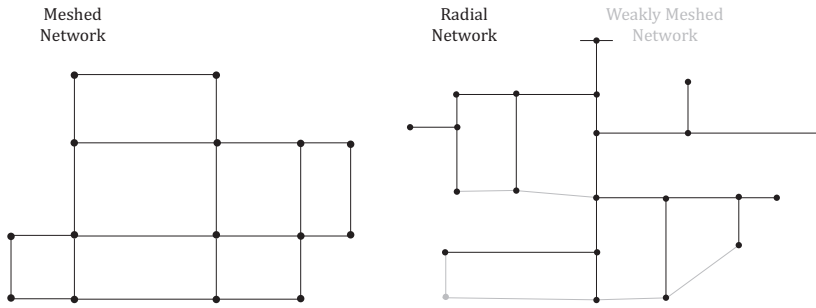
Figure 3.2: A meshed network (left) and a radial network (right) including in grey extra cables that change the network into a weakly meshed structure.

Flow (FDLF) method is based on decoupling of the parameters, which is not possible for high R/X ratios.

In summary, the distribution network differs from transmission networks on the following properties:

- a radial or weakly meshed structure compared to a meshed structure

- higher R/X ratio

- single-, double, and three-phase load connections

- unbalanced operation due to untransposed lines

- inclusion of Distributed Generation (DG)

- multilevel voltage (medium and low voltage distribution cables)

Due to these specifications, the transmission system and distribution systems are modelled and solved differently. The transmission system is modelled as a single-phase system while the distribution system is modelled as a three-phase system. Furthermore, the elements at the transmission and distribution level have different configurations and some elements, for example, regulators, only appear at the distribution level.

In this chapter, we provide a solid description of the electrical components and specification of parameters for single-phase transmission and three-phase distribution network analysis. We start by showing how the parameters and elements of general power systems described in the previous section relate to specific elements in transmission systems, which are provided using a single-phase description. These elements are extended to three-phase descriptions (with sometimes more complicated configurations) in distribution system analysis. Some elements are only encountered in distribution systems. All elements are described in such a way that we can perform a nodal analysis of our power system.

3.2. Voltage and current

The voltage and current in an electrical circuit were specified in section 2.2.1 using the effective phasor notation, stated in equation (2.2). In single-phase analysis, we choose a reference frame such that the voltage phase shift is zero. We express the current using the phase shift between the voltage and current phases (ϕ). The single-phase[2] voltage and current are:

$$V^a = |V^a|e^{\iota\delta_V^a},$$

$$I^a = |I^a|e^{\iota(\delta_V^a - \phi^a)}, \tag{3.1}$$

where $|\cdot|$ describes the effective phasor magnitude and δ_* the phase angle.

In a three-phase system, we have to specify all the three phases $\alpha_p = \{a, b, c\}$. Three-phase voltage and current are the following:

$$V^p = |V|^p e^{\iota\delta_V^p},$$

$$I^p = |I|^p e^{\iota(\delta_V^p - \phi^p)}, \quad p \in \alpha_p. \tag{3.2}$$

In a balanced system, the phasor magnitudes are equal and the difference between phases is equal. Therefore, only one phase needs to be specified, the other quantities can be found by rotating the corresponding phasors with respectively $2/3\pi$ and $4/3\pi$ rad.

3.3. Power flow Equations

We have derived the load flow equation in equation (2.8) of section 2.4. The single-phase load flow equation is expressed as:

$$S_i^a = V_i^a \overline{I_i^a} = V_i^a \overline{(YV^a)_i} = V_i^a \sum_{k=1}^N \overline{Y_{ik}V_k^a}. \tag{3.3}$$

The three-phase extension of the load flow equation looks as follows [18]:

$$S_i^p = V_i^p \overline{I_i^p} = V_i^p \sum_{k=1}^N \sum_{q=\alpha_p} \overline{Y_{ik}^{pq}V_k^q}, \quad p \in \alpha_p. \tag{3.4}$$

To solve the load flow equation for the voltage, we need to know the power and admittance in the network. Loads, generators, and shunts are nodal elements and are taken into account in the complex power vector S. Transformers, line elements, and regulators are accounted for in the nodal admittance matrix Y. The following sections in this chapter describe these elements and how they provide the required information. The way that load flow equations are solved is described in chapter 4.

---

[2]Note that transmission systems are often studied in the sequence frame, where the voltage and current are expressed only for the positive sequence. This does not change the phasor notation.

3.4. Generators

The bulk of electricity is generated by three-phase synchronous machines at the transmission level, which are modelled as power injectors. They have control of active power and voltage magnitude. Therefore, it is standard to model generators as PV buses in the network. Nowadays, more renewable resources that generate power can be found, such as Photo-Voltaic (PV) panels, wind turbines, and batteries. The latter is technically not a power generator, but in the context of power analysis, it does provide power. Generators that are connected at the distribution level often lack voltage control and therefore need to be specified differently. Most of the residential rooftop photo-voltaic installations are modelled as PQ-buses with negative power consumption. They do not supply reactive power, so, therefore, Q is set to 0 [19]. Generators that do have voltage control allowance are modelled as PV-buses. Lastly, generators can be modelled as PQ-buses, where Q depends on P by a predetermined polynomial function. These generators are called variable reactive power units [18].

3.5. Loads

Loads are modelled as buses where active and reactive power (P and Q) are specified. They are modelled as a function of the voltage in which the load-model type determines the relation between power and voltage. Three types exist: constant power (P), constant current (I), and constant impedance model (Z). Together called: ZIP-load models [18].

1. Constant Power models (P): power is independent of the change in voltage magnitude, which is expressed as

$$\frac{P}{P_0} = 1 \quad \text{and} \quad \frac{Q}{Q_0} = 1$$

   Constant power loads draw the same power from their source even if the source changes the voltage.

2. Constant Current models (I): power is related to the voltage magnitude as

$$\frac{P}{P_0} = \frac{|V|}{|V_0|} \quad \text{and} \quad \frac{Q}{Q_0} = \frac{|V|}{|V_0|}$$

   A constant current load varies its internal resistance according to the voltage which is being fed to it. This, is to achieve a constant current despite fluctuations in the source voltage.

3. Constant Impedance models (Z): power is related to the square of the voltage magnitude:

$$\frac{P}{P_0} = \left(\frac{|V|}{|V_0|}\right)^2 \quad \text{and} \quad \frac{Q}{Q_0} = \left(\frac{|V|}{|V_0|}\right)^2$$

   A constant impedance load presents the same impedance even when voltage is fluctuating.

The entities P_0 and Q_0 are the specified power ratings and $|V_0|$ is the nominal voltage magnitude.

Due to the voltage dependence of the loads, constant models are not always suitable [20] and a polynomial load model is introduced. The polynomial load model is a combination of the constant impedance model, the constant current model, and the constant power model and looks as follows [18]:

$$P = P_0(a_0 + a_1 V + a_2 V^2 + a_3 V^{1.38})$$
$$Q = Q_0(b_0 + b_1 V + b_2 V^2 + b_3 V^{3.22})$$
$$a_0 + a_1 + a_2 + a_3 = b_0 + b_1 + b_2 + b_3 = 1$$

These parameters are defined by experiments and empiric values.

V	p.u. value of the node voltage
P_0, Q_0	real and reactive power consumed under the reference voltage V_0
a_0, b_0	parameters for constant power load component
a_1, b_1	parameters for constant current load component
a_2, b_2	parameters for constant impedance load component
a_3, b_3	parameters for exponential load component

3.5.1. Three-phase configuration

Three-phase loads have the same models but then represented in three phases. As loads are physically connected in a Wye or Delta configuration, the models must be coherent to this configuration. In the Wye configuration, all three phases are connected to a single neutral point. This neutral point is connected to the ground by a fourth wire: the neutral conductor. The voltage is specified line-to-neutral. In a Delta configuration, the loads are connected phase-to-phase without a neutral conductor. Here, the voltage is specified phase-to-phase, also called line-to-line. The line-to-line voltages (V^{ab}, V^{bc}, and V^{ca}) and line-to-neutral voltages (V^a, V^b, and V^c) are related as follows:

$$V^{ab} = V^a - V^b,$$
$$V^{bc} = V^b - V^c,$$
$$V^{ca} = V^c - V^a.$$

The line-to-neutral currents are related to line-to-line currents according the following:

$$I^a = I^{ab} - I^{ca},$$
$$I^b = I^{bc} - I^{ab},$$
$$I^c = I^{ca} - I^{bc}.$$

In this section, we clarify the relationship of the ZIP-load models in a Wye and Delta configuration. Figure 3.3 represents a Wye and a Delta load model.
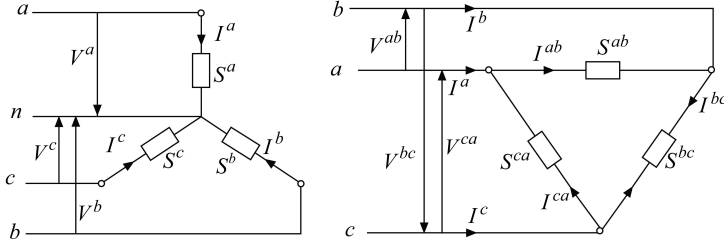
Figure 3.3: A Wye (left) and Delta (right) configuration for three-phase loads [21]. The voltages (and currents) in the left picture are the line-to-neutral voltages, while in the right they are line-to-line voltages.

Wye load models

Wye - P   We know that power is independent of voltage magnitude:

$$\frac{P}{P_0} = 1, \ \frac{Q}{Q_0} = 1 \ \Leftrightarrow \ S := P + \iota Q = P_0 + \iota Q_0$$

For phases a, b, and c this means that for each load bus i the active and reactive power are expressed as follows:

$$\begin{bmatrix} S^a \\ S^b \\ S^c \end{bmatrix}_i := \begin{bmatrix} P^a + \iota Q^a \\ P^b + \iota Q^b \\ P^c + \iota Q^c \end{bmatrix}_i = \begin{bmatrix} (P_0^a + \iota Q_0^a) \\ (P_0^b + \iota Q_0^b) \\ (P_0^c + \iota Q_0^c) \end{bmatrix}_i$$

Wye - I   Constant current load models vary their power S with voltage magnitude, leading to the following relationship:

$$\frac{P}{P_0} = \frac{|V|}{|V_0|}, \ \frac{Q}{Q_0} = \frac{|V|}{|V_0|} \ \Leftrightarrow \ S := P + \iota Q = (P_0 + \iota Q_0)\frac{|V|}{|V_0|}$$

For phases a, b, and c this means that for each load bus i the active and reactive power are expressed as follows:

$$\begin{bmatrix} S^a \\ S^b \\ S^c \end{bmatrix}_i := \begin{bmatrix} P^a + \iota Q^a \\ P^b + \iota Q^b \\ P^c + \iota Q^c \end{bmatrix}_i = \begin{bmatrix} (P_0^a + \iota Q_0^a)(\frac{|V^a|}{|V_0^a|}) \\ (P_0^b + \iota Q_0^b)(\frac{|V^b|}{|V_0^b|}) \\ (P_0^c + \iota Q_0^c)(\frac{|V^c|}{|V_0^c|}) \end{bmatrix}_i$$

Wye - Z   Constant impedance models vary their power with the square of voltage magnitude, leading to the following:

$$\frac{P}{P_0} = (\frac{|V|}{|V_0|})^2, \ \frac{Q}{Q_0} = (\frac{|V|}{|V_0|})^2 \ \Leftrightarrow \ S := P + \iota Q = (P_0 + \iota Q_0)(\frac{|V|}{|V_0|})^2$$

For phases a, b, and c this means that for each load bus i the active and reactive power are expressed as follows:

$$\begin{bmatrix} S^a \\ S^b \\ S^c \end{bmatrix}_i := \begin{bmatrix} P^a + \iota Q^a \\ P^b + \iota Q^b \\ P^c + \iota Q^c \end{bmatrix}_i = \begin{bmatrix} (P_0^a + \iota Q_0^a)(\frac{|V^a|}{|V_0^a|})^2 \\ (P_0^b + \iota Q_0^b)(\frac{|V^b|}{|V_0^b|})^2 \\ (P_0^c + \iota Q_0^c)(\frac{|V^c|}{|V_0^c|})^2 \end{bmatrix}_i$$

Table 3.1: Specified line-to-neutral current I_i^p of load bus i in Wye and Delta configuration, given for different load models (ZIP) and taken $V_0 = 1.0$pu to keep the notations clean.

	Configuration	
	Y	Δ
Load model	Wye	Delta
Z	$\begin{bmatrix} \overline{(P_0^a + \iota Q_0^a)}V^a \\ \overline{(P_0^b + \iota Q_0^b)}V^b \\ \overline{(P_0^c + \iota Q_0^c)}V^c \end{bmatrix}_i$	$\begin{bmatrix} \overline{(P_0^{ab} + \iota Q_0^{ab})}(V^a - V^b) - \overline{(P_0^{ca} + \iota Q_0^{ca})}(V^c - V^a) \\ \overline{(P_0^{bc} + \iota Q_0^{bc})}(V^b - V^c) - \overline{(P_0^{ab} + \iota Q_0^{ab})}(V^a - V^b) \\ \overline{(P_0^{ca} + \iota Q_0^{ca})}(V^c - V^a) - \overline{(P_0^{bc} + \iota Q_0^{bc})}(V^b - V^c) \end{bmatrix}_i$
I	$\begin{bmatrix} \overline{(P_0^a + \iota Q_0^a)}\frac{V^a}{|V^a|} \\ \overline{(P_0^b + \iota Q_0^b)}\frac{V^b}{|V^b|} \\ \overline{(P_0^c + \iota Q_0^c)}\frac{V^c}{|V^c|} \end{bmatrix}_i$	$\begin{bmatrix} \overline{(P_0^{ab} + \iota Q_0^{ab})}\frac{(V^a - V^b)}{|V^a - V^b|} - \overline{(P_0^{ca} + \iota Q_0^{ca})}\frac{(V^c - V^a)}{|V^c - V^a|} \\ \overline{(P_0^{bc} + \iota Q_0^{bc})}\frac{(V^b - V^c)}{|V^b - V^c|} - \overline{(P_0^{ab} + \iota Q_0^{ab})}\frac{(V^a - V^b)}{|V^a - V^b|} \\ \overline{(P_0^{ca} + \iota Q_0^{ca})}\frac{(V^c - V^a)}{|V^c - V^a|} - \overline{(P_0^{bc} + \iota Q_0^{bc})}\frac{(V^b - V^c)}{|V^b - V^c|} \end{bmatrix}_i$
P	$\begin{bmatrix} \overline{\left(\frac{P_0^a + \iota Q_0^a}{V^a}\right)} \\ \overline{\left(\frac{P_0^b + \iota Q_0^b}{V^b}\right)} \\ \overline{\left(\frac{P_0^c + \iota Q_0^c}{V^c}\right)} \end{bmatrix}_i$	$\begin{bmatrix} \overline{\left(\frac{P_0^{ab} + \iota Q_0^{ab}}{V^a - V^b}\right)} - \overline{\left(\frac{P_0^{ca} + \iota Q_0^{ca}}{V^c - V^a}\right)} \\ \overline{\left(\frac{P_0^{bc} + \iota Q_0^{bc}}{V^b - V^c}\right)} - \overline{\left(\frac{P_0^{ab} + \iota Q_0^{ab}}{V^a - V^b}\right)} \\ \overline{\left(\frac{P_0^{ca} + \iota Q_0^{ca}}{V^c - V^a}\right)} - \overline{\left(\frac{P_0^{bc} + \iota Q_0^{bc}}{V^b - V^c}\right)} \end{bmatrix}_i$

Delta load models   The Delta load description is specified using line-to-line relations.

Delta - P

$$\begin{bmatrix} S^{ab} \\ S^{bc} \\ S^{ca} \end{bmatrix}_i := \begin{bmatrix} P^{ab} + \iota Q^{ab} \\ P^{bc} + \iota Q^{bc} \\ P^{ca} + \iota Q^{ca} \end{bmatrix}_i = \begin{bmatrix} P_0^{ab} + \iota Q_0^{ab} \\ P_0^{bc} + \iota Q_0^{bc} \\ P_0^{ca} + \iota Q_0^{ca} \end{bmatrix}_i$$

Delta - I

$$\begin{bmatrix} S^{ab} \\ S^{bc} \\ S^{ca} \end{bmatrix}_i := \begin{bmatrix} P^{ab} + \iota Q^{ab} \\ P^{bc} + \iota Q^{bc} \\ P^{ca} + \iota Q^{ca} \end{bmatrix}_i = \begin{bmatrix} (P_0^{ab} + \iota Q_0^{ab})\left(\frac{V^{ab}}{V_0^{ab}}\right) \\ (P_0^{bc} + \iota Q_0^{bc})\left(\frac{V^{bc}}{V_0^{bc}}\right) \\ (P_0^{ca} + \iota Q_0^{ca})\left(\frac{V^{ca}}{V_0^{ca}}\right) \end{bmatrix}_i$$

Delta - Z

$$\begin{bmatrix} S^{ab} \\ S^{bc} \\ S^{ca} \end{bmatrix}_i := \begin{bmatrix} P^{ab} + \iota Q^{ab} \\ P^{bc} + \iota Q^{bc} \\ P^{ca} + \iota Q^{ca} \end{bmatrix}_i = \begin{bmatrix} (P_0^{ab} + \iota Q_0^{ab})\left(\frac{V^{ab}}{V_0^{ab}}\right)^2 \\ (P_0^{bc} + \iota Q_0^{bc})\left(\frac{V^{bc}}{V_0^{bc}}\right)^2 \\ (P_0^{ca} + \iota Q_0^{ca})\left(\frac{V^{ca}}{V_0^{ca}}\right)^2 \end{bmatrix}_i$$

It is common practice to not specify the three-phase power, but three-phase current in distribution system analysis [18], because of the solution method, see chapter 4. In table 3.1, we give an overview of these currents of the three static load models (P, I, and Z) in Wye and Delta configuration.

3.6. Shunts

Shunt capacitors are necessary for voltage regulation and reactive power support. They are placed along power system feeders at specific locations to provide support. A shunt connecting the bus and the ground is modelled as a reactance $z_s = \iota x_s$. Shunts are accounted for in the admittance matrix Y_{bus}. Shunt admittance y_s is derived as:

$$y_s = \frac{1}{z_s} = -\iota \frac{1}{x_s} = \iota b_s.$$

A three-phase description of a shunt looks as follows:

$$B_s^{abc} = \begin{bmatrix} b_s^{aa} & b_s^{ab} & b_s^{ac} \\ b_s^{ab} & b_s^{bb} & b_s^{bc} \\ b_s^{ac} & b_s^{bc} & b_s^{cc} \end{bmatrix}$$
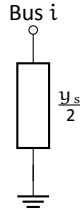
Figure 3.4: A shunt capacitor, located at bus i [18].

3.7. Electricity cables

Single-phase transmission cables are modelled by the per-unit admittance (y_{ij}) of a cable between nodes i and j. To form the nodal admittance matrix Y_{ij}, the branch admittance is converted to a nodal matrix in blocks. Admittance consists of branch admittance (self and mutual) and (optional) shunt admittance. The per-unit admittance and shunt admittance are as follows:

$$y_{ij} = \frac{1}{r_{ij} + \iota x_{ij}}$$
$$y_s = \iota b_s$$

The block admittance matrix is:

$$Y_{ij} = \left(y_{ij} \begin{bmatrix} 1 & -1 \\ -1 & 1 \end{bmatrix} + y_s \begin{bmatrix} \frac{1}{2} & 0 \\ 0 & \frac{1}{2} \end{bmatrix} \right)$$

Figure 3.5 shows a general transmission line and figure 3.6 shows a transmission line with shunts connected. The blocks are placed according to the nodal index of a matrix: In case a branch connects bus 1 with bus 3, the blocks are placed at (row, column): (1, 1), (1, 3), (3, 1) and (3, 3). This results in a sparse matrix.
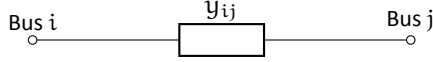
Figure 3.5: Transmission line model [18].
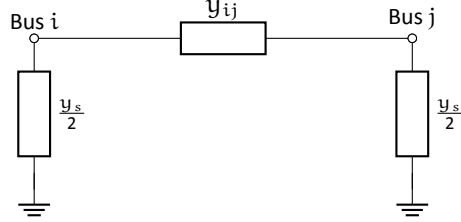
Figure 3.6: Transmission line model with a shunt [18].

Three-phase representation

The admittance matrix of a three-phase distribution branch between bus i and j consists of four 3 by 3 admittance blocks:

$$Y_{ij}^{abc} = \begin{bmatrix} Y_{ii}^{abc} & Y_{ij}^{abc} \\ Y_{ji}^{abc} & Y_{jj}^{abc} \end{bmatrix}.$$

A three-phase block y_{ij}^{abc} of the admittance matrix Y_{ij}^{abc} is represented by self and mutual admittance y^{pq}, where $p, q \in \alpha_p = \{a, b, c\}$. A block looks as follows:

$$Y_{ij}^{abc} = \begin{bmatrix} y^{aa} & y^{ab} & y^{ac} \\ y^{ab} & y^{bb} & y^{bc} \\ y^{ac} & y^{bc} & y^{cc} \end{bmatrix}_{ij} , \text{ where } y_{ij}^{pq} = \frac{1}{r_{ij}^{pq} + \iota x_{ij}^{pq}}, \quad p, q \in \alpha_p.$$

Distribution lines can contain two-phase or single-phase lines. In the case of a two-phase ab line, the matrix changes into:

$$Y_{ij}^{ab} = \begin{bmatrix} y_{aa} & y_{ab} & 0 \\ y_{ab} & y_{bb} & 0 \\ 0 & 0 & 0 \end{bmatrix}_{ij}$$

3.8. Transformers

Transformers are the elements that transform high voltage power to lower level voltage. Transformers are placed between two electrical circuits that have different voltage levels. The primary side (p) of the transformer is connected to the higher voltage network and the secondary side (s) is connected to the lower voltage level. The transformer in a power system is represented by two blocks:

- The leaking admittance matrix block, Y_{tr}, consisting of per-unit leakage admittance y_t, and

- A shunt block that models core losses. The shunt block can be represented by voltage-dependent loads and follow the representation in Table 3.1

The leakage admittance matrix block Y_{tr} depends on the transformer (or tap) ratio. If we define T as the transformer ratio, ie the change in voltage level from the primary side of the transformer to the secondary side. Then the modulus of T determines the change in voltage magnitude and the argument of T the change in voltage phase angle. Figure 3.7 shows a transformer connecting bus i and j, without shunt admittance. A transformer between bus i and j is modelled as a branch according to the following configuration, where the shunt block is optional:

$$Y_{tr} = y_t \begin{bmatrix} \frac{1}{|T|^2} & -\frac{1}{\bar{T}} \\ -\frac{1}{T} & 1 \end{bmatrix} + \begin{bmatrix} \frac{y_s}{2} & 0 \\ 0 & \frac{y_s}{2} \end{bmatrix}$$

Note that a transformer has the same admittance matrix as a transmission line when $T = 1$.
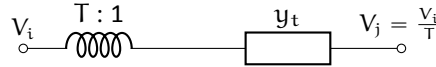
Figure 3.7: Transmission line model with a transformer [18].

3.8.1. Three-phase transformers

The primary and secondary sides of a three-phase transformer can be presented in a Delta or (grounded) Wye representation. They can be connected in the following combinations [18]:

- Grounded Wye - Grounded Wye
- Grounded Wye - Wye
- Grounded Wye - Delta
- Wye - Grounded Wye
- Wye - Wye

- Wye - Delta
- Delta - Grounded Wye
- Delta - Wye
- Delta - Delta

The admittance matrix block is given in a similar manner as the Y_{bus} matrix of a distribution cable, but now consisting of leakage admittance of the transformer:

$$Y_T^{abc} = \begin{bmatrix} Y_{pp}^{abc} & Y_{ps}^{abc} \\ Y_{sp}^{abc} & Y_{ss}^{abc} \end{bmatrix}.$$

Each block Y_{ij}^{abc}, $i, j \in \{p, s\}$ (where p stands for the primary side and s for the secondary side of the transformer) has a different configuration. This configuration depends on the connection of the transformer and is either one of the three following blocks:

$$Y_1 = \begin{bmatrix} y_t & 0 & 0 \\ 0 & y_t & 0 \\ 0 & 0 & y_t \end{bmatrix}, \quad Y_2 = \frac{1}{3} \begin{bmatrix} 2y_t & -y_t & -y_t \\ -y_t & 2y_t & -y_t \\ -y_t & -y_t & 2y_t \end{bmatrix}, \quad \text{and} \quad Y_3 = \frac{1}{\sqrt{3}} \begin{bmatrix} -y_t & y_t & 0 \\ 0 & -y_t & y_t \\ y_t & 0 & -y_t \end{bmatrix}. \quad (3.5)$$

Table 3.2: Matrix block for different three-phase transformer configurations.

Transformer model		Block matrix configuration			
Primary	Secondary	Y_{pp}^{abc}	Y_{ps}^{abc}	Y_{sp}^{abc}	Y_{ss}^{abc}
Wye-G	Wye-G	Y_1	$-Y_1$	$-Y_1$	Y_1
Wye-G	Wye	Y_2	$-Y_2$	$-Y_2$	Y_2
Wye-G	Delta	Y_1	Y_3	Y_3^T	Y_2
Wye	Wye-G	Y_2	$-Y_2$	$-Y_2$	Y_2
Wye	Wye	Y_2	$-Y_2$	$-Y_2$	Y_2
Wye	Delta	Y_2	Y_3	Y_3^T	Y_2
Delta	Wye-G	Y_2	Y_3^T	Y_3	Y_1
Delta	Wye	Y_2	Y_3^T	Y_3	Y_2
Delta	Delta	Y_2	$-Y_2$	$-Y_2$	Y_2

Table 3.2 represents the corresponding block per transformer configuration. The self admittance of the primary side (Y_{pp}^{abc}) should be divided by $|T|^2$ and the mutual admittance (Y_{ps}^{abc} an Y_{sp}^{abc}) by $\overline{T}$ and T respectively to account for the transformer tap ratio T.

3.9. Step-Voltage Regulators

Step-voltage regulators (SVRs) are installed along distribution feeders, often after the substation but also at other locations, to regulate the voltage along the feeder and to keep it within an acceptable range. As the voltages along a distribution feeder can vary, it is important to keep it within an acceptable range. An SVR consists of a sequence of autotransformers and load tap changing mechanisms [22]. The taps of the transformers are responsible for the voltage level at the secondary side, the output voltage. This voltage is measured: If it falls outside the safety region, the tap ratios are changed automatically to adjust this voltage level. Standard SVRs allow a total of $\pm 10\%$ voltage change, usually achieved in 32 steps. This means that each tap changes the voltage with 0.00625 per unit in an up or down direction [22]. In our load-flow computations, we are not implementing an SVR that changes its tap ratio automatically. Normally the tap ratio is determined using experimental analysis. We pre-determine the safe tap ratios based on earlier executed analyses, such as in OpenDSS [23].

An SVR is modelled as a series block that is placed between any connected pair of buses (n,m). The voltages and currents of the primary (bus n) and secondary side (bus m) of the SVR are related via matrices: A_V, A_I, and $Z_R \in \mathbb{C}^{6\times6}$. The first one represents voltage gain, the second current gain, and the last impedance. A_I and A_V consists of effective regulator ratio a_R and Z_R consists of pu series impedance z_R of the SVR [23]. The regulator ratio, a_R, is expressed as a function of the tap ratio:

$$a_R = 1 \pm 0.00625 tap,$$

where tap is the tap-ratio of the SVR. The minus sign in this equation applies for the raised position and the positive sign if a lower position is required.

Table 3.3: Matrix Block configurations for several Step Voltage Regulator connections.

	Matrix block configuration		
SVR connection	A_I	A_V	Z_R
Wye	$\begin{bmatrix} \frac{1}{a_{R_a}} & 0 & 0 \\ 0 & \frac{1}{a_{R_b}} & 0 \\ 0 & 0 & \frac{1}{a_{R_c}} \end{bmatrix}$	$\begin{bmatrix} a_{R_a} & 0 & 0 \\ 0 & a_{R_b} & 0 \\ 0 & 0 & a_{R_c} \end{bmatrix}$	$\begin{bmatrix} Z_{R_a} & 0 & 0 \\ 0 & Z_{R_b} & 0 \\ 0 & 0 & Z_{R_c} \end{bmatrix}$
Closed-Delta	$\begin{bmatrix} a_{R_{ab}} & 0 & 1-a_{R_{ca}} \\ 1-a_{R_{ab}} & a_{R_{bc}} & 0 \\ 0 & 1-a_{R_{bc}} & a_{R_{ca}} \end{bmatrix}^{-1}$	$\begin{bmatrix} a_{R_{ab}} & 1-a_{R_{ab}} & 0 \\ 0 & a_{R_{bc}} & 1-a_{R_{bc}} \\ 1-a_{R_{ca}} & 0 & a_{R_{ca}} \end{bmatrix}$	$\begin{bmatrix} Z_{R_{ab}} & 0 & 0 \\ 0 & Z_{R_{bc}} & 0 \\ 0 & 0 & Z_{R_{ca}} \end{bmatrix}$
Open-Delta	$\begin{bmatrix} \frac{1}{a_{R_{ab}}} & 0 & 0 \\ 1-\frac{1}{a_{R_{ab}}} & 1 & 1-\frac{1}{a_{R_{cb}}} \\ 0 & 0 & \frac{1}{a_{R_{cb}}} \end{bmatrix}$	$\begin{bmatrix} a_{R_{ab}} & 1-a_{R_{ab}} & 0 \\ 0 & 1 & 0 \\ 0 & 1-a_{R_{cb}} & a_{R_{cb}} \end{bmatrix}$	$\begin{bmatrix} Z_{R_{ab}} & 0 & 0 \\ 0 & 0 & 0 \\ 0 & 0 & Z_{R_{cb}} \end{bmatrix}$

Three-phase SVRs are commonly configured as Wye, closed-Delta, and open-Delta connections. Just like transformers, these configurations determine the entities of the three blocks A_I, A_V, and Z_R. Furthermore, it holds that:

$$A_V^{-1} = A_I^T.$$

These three blocks form the SVR-admittance matrix, Y_R^{abc}. The admittance matrix Y_R^{abc} looks as follows:

$$Y_R^{abc} = \begin{bmatrix} A_I F_R^{-1} Y_{ii}^{abc} A_I^T & -A_I F_R^{-1} Y_{ij}^{abc} \\ -Y_{ji}^{abc} F_R^{-T} A_I^T & Y_{jj}^{abc} - Y_{ji}^{abc} A_I^T Z_R A_I F_R^{-1} Y_{ij}^{abc} \end{bmatrix}$$

Y_{ij}^{abc}, $i,j \in \{n,m\}$ is the admittance of the distribution line along which the regulator is placed. F_R and F_R^{-T} are defined as follows:

$$F_R = \mathbb{I}_{3\times3} + Y_{ii}^{abc} A_I^T Z_R A_I,$$

$$F_R^{-T} = \mathbb{I}_{3\times3} - A_I^T Z_R A_I F_R^{-1} Y_{ii}^{abc}.$$

We list the entities of the blocks A_I, A_V, and Z_R, that depend on the SVR configuration, in Table 3.3. More information on how to derive these entities can be found in [23].

Ideal SVRs
If the auto-transformer of the SVR is ideal, the tap-ratio is equal to 0 and the impedance matrix Z_R is equal to 0. This results into F_R being the identity matrix: $\mathbb{I}_{3\times3}$. The admittance matrix of an ideal SVR becomes the following:

$$Y_{R,ideal}^{abc} = \begin{bmatrix} A_I Y_{ii}^{abc} A_I^T & -A_I Y_{ij}^{abc} \\ -Y_{ji}^{abc} A_I^T & Y_{jj}^{abc} \end{bmatrix}.$$

Table 3.4: Overview of elements in transmission and distribution networks

Elements	
Transmission network	Distribution Network
Generators	Generators
Loads	Wye and Delta Loads
Overhead Cables	Overhead and underground cables
Shunts	Shunts
Transformers	Transformers
	Step-Voltage Regulators

3.10. Overview

An electricity network model is represented as a graph consisting of buses $i = 1, ..., N$, representing generators, loads, and shunts and branches representing transformers and cables. The steady-state power flow problem of a network determines the voltages V_i of each bus given the power supply and demand S_i of each bus and admittance Y_{ij} of each branch [14]. Transmission and distribution networks have different designs, properties, and elements. The systems including their elements are therefore modelled differently.

The transmission network is the high-voltage network, responsible for the transportation of power over large distances. It is a balanced system which means that the three phases a, b, and c of the generated power are equal in magnitude and equal in phase-shift (ϕ). For a voltage V this means that $|V|_a = |V|_b = |V|_c$ and $\phi_{ab} = \phi_{bc} = \phi_{ca} = \frac{2}{3}\pi$. To simplify and speed up the computations in the transmission network, they only calculate V_a and deduct the other two phases from here. This changes (2.8) into the following:

$$S^p = V^p \overline{(YV)^p}, \quad p \in \{a, b, c\} \quad \Rightarrow \quad S^a = V^a \overline{(YV)^a}.$$

Distribution systems are unbalanced, therefore we model the distribution network using all three phases a, b, and c [18]. The power flow equation in three-phase is described by:

$$S_i^p = V_i^p \overline{I_i^p} = V_i^p \sum_{k=1}^{N} \sum_{q=a,b,c} \overline{Y_{ik}^{pq} V_k^q}, \quad p \in \{a, b, c\}.$$

Table 3.4 gives an overview of the elements per system. These differences will have an influence on how the power flow problem is solved, which is the topic of the next chapter.

4

Nonlinear Power flow solvers

4.1. Introduction

The power flow problem is a non-linear problem for which we use non-linear solvers such as Newton-Raphson and non-linear Gauss-Seidel. These solvers have been studied and widely applied to solve transmission networks. 20-30 Years ago, researchers realised that the changes between transmission and distribution networks require different solution methods [24] [25] [26]. Therefore, these networks have been studied separately and different solvers have been developed to analyse steady-state power flow simulations on distribution networks. Some of these solvers are adapted from transmission network solvers, while others evolved separately.

In this chapter, we explain the most important transmission and distribution network solvers, including the specific derivation to be applied to these separate networks.

4.2. Transmission networks

The widely used power flow solvers for transmission networks are Newton-Raphson, Gauss-Seidel, Fast Decoupled Load Flow, and DC Load Flow. The first two evaluate the full AC power flow equations, while the latter makes some assumptions to the full equations in the advantage of computational time but at the trade-off of accuracy. The DC Load Flow is a way of linearising the system such that it can be solved without iterations.

We focus in this thesis on Newton-Raphson methods as it is widely used by system operators, have good convergence characteristics, and are robust. Furthermore, experiments have shown that they work well together with Krylov solvers, which are necessary methods to solve large linear systems of equations [12]. We explain these methods in section 8.

4.2.1. The Newton-Raphson method

Newton-Raphson is a root-finding problem, which approximates the root of a function in several iterations. The method starts with an initial guess of the root of this function. Accordingly, the tangent line of the function is determined at this initial guess. By calculating the x-intercept of the tangent line, one will find a better approximation of the root which we use as the new guess to the function. This process is repeated until we are satisfied with the accuracy of the root. We define a tolerance value ε which the approximation must satisfy. If this is satisfied, we say that the method has converged. Note that Newton-Raphson only converges under certain conditions. Usually, this is the case when the initial guess is not too far from the root and the problem is well-posed. In the test cases we are considering, these conditions hold. In practice, this may not always be the case. Newton-Raphson can then be improved using line-search or other optimisation techniques [27]

A general nonlinear system of equations can be written as [28]:

$$\mathbf{F}(\mathbf{x}) = 0$$

where $\mathbf{x}$ is a vector of dimension N and $\mathbf{F}$ is a vector function of $\mathbf{x}$. Given an initial value $\mathbf{x}^0$, the Newton-Raphson method finds the roots of $\mathbf{F}$ by evaluating the following equation and updating the previous estimate accordingly:

$$\mathbf{J}(\mathbf{x}^\nu)\Delta\mathbf{x}^\nu = -\mathbf{F}(\mathbf{x}^\nu)$$
$$\mathbf{x}^{\nu+1} = \mathbf{x}^\nu + \Delta\mathbf{x}^\nu$$

(4.1)

The $\mathbf{J}(\mathbf{x}^\nu)$ is the Jacobian with elements $J_{ij} = \frac{\partial f_i}{\partial x_j}$.

Newton-Raphson for Power Flow equations

To apply the Newton-Raphson method for power flow computations the entities $\mathbf{x}$, $\mathbf{F}(\mathbf{x})$ and $\mathbf{J}(\mathbf{x})$ have to be determined in terms of power variables. We define $\mathbf{F}$ as the power mismatch vector, which is split into a real and imaginary part:

$$\mathbf{F}(\mathbf{x}) = \begin{bmatrix} \Delta\mathbf{P}(\mathbf{x}) \\ \Delta\mathbf{Q}(\mathbf{x}) \end{bmatrix}$$

(4.2)

The power mismatch vector (eq. (4.2)) represents the mismatch between injected (known) power at the buses and the computed power at these buses. The mismatch vector looks as follows:

$$\Delta\mathbf{P}(\mathbf{x}) = \mathbf{P}_s - \mathbf{P}(\mathbf{x}) \quad \text{and} \quad \Delta\mathbf{Q}(\mathbf{x}) = \mathbf{Q}_s - \mathbf{Q}(\mathbf{x}).$$

Where $\mathbf{P}_s$ (or $\mathbf{Q}_s$) is the known active (or reactive) *injected* power at the node and $\mathbf{P}(\mathbf{x})$ (or $\mathbf{Q}(\mathbf{x})$) is the computed active (reactive) power flow of the node and, which is determined by the power flow equation (2.8). The steps of the Newton-Raphson method are summarised in Algorithm 1.

Algorithm 1: Newton-Raphson method

---

1 The Newton-Raphson algorithm is as follows:
  1. Set $\nu = 0$ and choose appropriate starting value x^0;
  2. Compute $F(x^\nu)$;
  3. Test convergence:
     If $|F(x^\nu)| \leqslant \epsilon$ for then x^ν is the solution
     Otherwise, go to 4;
  4. Compute the Jacobian matrix $J(x^\nu)$;
  5. Update the solution:
     $$\Delta x^\nu = -J^{-1}(x^\nu)F(x^\nu)$$
     $$x^{\nu+1} = x^\nu + \Delta x^\nu$$
  6. Update iteration counter $\nu + 1 \rightarrow \nu$, go to step 2.

Solving this system using Newton-Raphson, we determine the state variables. As we use the phasor notation of V, $V_i = |V_i|e^{\iota\delta_i}$, we get two state variables: $|V_i|$ and δ_i. The vector x of state-variables is then written as:

$$x = \begin{bmatrix} \delta_2 \\ \vdots \\ \delta_N \\ |V_{N_{G+2}}| \\ \vdots \\ |V_N| \end{bmatrix}$$

Notice the subscript of the unknown quantities: the quantities δ_1 and $|V_1|$ (the phase angle and voltage magnitude of the slack bus) are known and can be left out of the vector. Furthermore, the voltage magnitude $|V_G|$ of all the generator buses can be dropped as we must make sure that the update for the known voltage is equal to 0. The size of the vector x remains: $2N - N_G - 2 = 2N_L + N_G$ (N_G number of generator buses, N_L number of load buses).

We determine the active and reactive *computed* power at each bus using the power flow equation (eq. (2.8)). We express it using the phasor notation of the voltage ($V_k = |V_k|e^{\iota\delta_k}$), its complex conjugate ($\overline{V_k} = |V_k|e^{-\iota\delta_k}$) and the admittance of electricity cables $Y_{ij} = G_{ij} + \iota B_{ij}$. We also use the difference between two phases, expressed as $\delta_{ij} = \delta_i - \delta_j$. The complex power expressed using these notations is the following:

$$S_i = V_i \overline{I}_i = V_i(\overline{YV})_i = V_i \sum_{k=1}^{N} \overline{Y}_{ik} \overline{V}_k$$

$$= \sum_{k=1}^{N} (G_{ik} - \iota B_{ik})|V_k||V_i|(\cos\delta_{ik} + \iota\sin\delta_{ik})$$

By splitting this equation into a real and imaginary part we can express P and Q. Note that $\delta_{ii} = \delta_i - \delta_i = 0$. We can then specify the active and reactive power at each bus i as follows [12]:

$$P_i = \sum_{k=1}^{N} |V_i||V_k|(G_{ik}\cos\delta_{ik} + B_{ik}\sin\delta_{ik})$$

$$= |V_i|^2 G_{ii} + \sum_{\substack{k=1 \\ k \neq i}}^{N} |V_i||V_k|(G_{ik}\cos\delta_{ik} + B_{ik}\sin\delta_{ik})$$

$$Q_i = \sum_{k=1}^{N} |V_i||V_k|(G_{ik}\sin\delta_{ik} - B_{ik}\cos\delta_{ik})$$

$$= -|V_i|^2 B_{ii} - \sum_{\substack{k=1 \\ k \neq i}}^{N} |V_i||V_k|(G_{ik}\sin\delta_{ik} - B_{ik}\cos\delta_{ik})$$

The iterative formula of Newton-Raphson requires the Jacobian J of the load-flow equations. The Jacobian consists of elements that are already evaluated in the assembly of the mismatch vector F, therefore the Jacobian is calculated at very little cost. The Jacobian looks as follows:

$$J(\boldsymbol{x}) = \begin{bmatrix} \frac{\partial P_2}{\partial \delta_2}(\boldsymbol{x}) & \cdots & \frac{\partial P_2}{\partial \delta_N}(\boldsymbol{x}) & \frac{\partial P_2}{\partial |V_{N_g+2}|}(\boldsymbol{x}) & \cdots & \frac{\partial P_2}{\partial |V_N|}(\boldsymbol{x}) \\ \vdots & \ddots & \vdots & \vdots & \ddots & \vdots \\ \frac{\partial P_N}{\partial \delta_2}(\boldsymbol{x}) & \cdots & \frac{\partial P_N}{\partial \delta_N}(\boldsymbol{x}) & \frac{\partial P_N}{\partial |V_{N_g+2}|}(\boldsymbol{x}) & \cdots & \frac{\partial P_N}{\partial |V_N|}(\boldsymbol{x}) \\ \frac{\partial Q_{N_g+2}}{\partial \delta_2}(\boldsymbol{x}) & \cdots & \frac{\partial Q_{N_g+2}}{\partial \delta_2}(\boldsymbol{x}) & \frac{\partial Q_{N_g+2}}{\partial |V_{N_g+2}|}(\boldsymbol{x}) & \cdots & \frac{\partial Q_{N_g+2}}{\partial |V_N|}(\boldsymbol{x}) \\ \vdots & \ddots & \vdots & \vdots & \ddots & \vdots \\ \frac{\partial Q_N}{\partial \delta_2}(\boldsymbol{x}) & \cdots & \frac{\partial Q_N}{\partial \delta_N}(\boldsymbol{x}) & \frac{\partial Q_N}{\partial |V_{N_g+2}|}(\boldsymbol{x}) & \cdots & \frac{\partial Q_N}{\partial |V_N|}(\boldsymbol{x}) \end{bmatrix}$$

The four blocks of the Jacobian are all square matrices and so is the entire Jacobian [28]. The values of the Jacobian entries are presented in table 4.1.

4.3. Distribution Networks

The special properties of the distribution network add complexity to the solvability of distribution power flow. Researchers have been investigating methods that are able to converge for distribution networks. Their starting point was the conventional transmission network methods: Newton-Raphson, Gauss-Seidel and Decoupled Load-flow algorithms, which have been adapted over the years for distribution networks. The branch-based Forward Backward Sweep method is specifically constructed for distribution networks [29].

For the same reason as transmission networks, we focus our work on Newton-Raphson methods. The eventual goal of this thesis is to solve integrated transmission-distribution systems efficiently. It is therefore also easier to study the same type of methods. Furthermore, in [30] it is shown that the modified Newton-Raphson method is advanced and robust: Its convergence behaviour does not change in case of different loading

Table 4.1: Overview of the derivatives in the Jacobian: The power mismatch with respect to voltage magnitude and angle

	bus	Derivative
P	$i = j$	$\frac{\partial P_i}{\partial \delta_i} = -Q_i - |V_i|^2 B_{ii}$
		$\frac{\partial P_i}{\partial |V_i|} = 2|V_i|G_{ii} + \sum_{\substack{k=1 \\ k \neq i}}^{N} |V_k|(G_{ik} \cos \delta_{ik} + B_{ik} \sin \delta_{ik}))$
	$i \neq j$	$\frac{\partial P_i}{\partial \delta_j} = |V_i||V_j|(G_{ij} \sin \delta_{ij} - B_{ij} \cos \delta_{ij})$
		$\frac{\partial P_i}{\partial |V_j|} = |V_i|(G_{ij} \cos \delta_{ij} + B_{ij} \sin \delta_{ij}))$
Q	$i = j$	$\frac{\partial Q_i}{\partial \delta_i} = P_i - |V_i|^2 G_{ii}$
		$\frac{\partial Q_i}{\partial |V_i|} = -2|V_i|B_{ii} + \sum_{\substack{k=1 \\ k \neq i}}^{N} |V_k|(-B_{ik} \cos \delta_{ik} + G_{ik} \sin \delta_{ik}))$
	$i \neq j$	$\frac{\partial Q_i}{\partial \delta_j} = |V_i||V_j|(-B_{ij} \sin \delta_{ij} - G_{ij} \cos \delta_{ij})$
		$\frac{\partial Q_i}{\partial |V_j|} = |V_i|(-B_{ij} \cos \delta_{ij} + G_{ij} \sin \delta_{ij}))$

conditions or high R/X ratios and also works on unbalanced systems. It can handle generation by modelling it as PV nodes. Furthermore, during test experiments where the method is applied on balanced and unbalanced systems, it converges in fewer iterations than the backward/forward method which is compared to [24].

In this section, we explain how the Newton-Raphson is modified for distribution networks.

4.3.1. The Newton-Raphson three-phase current injection method
Instead of using power mismatches as in the standard Newton-Raphson method, current mismatches are suggested as a better alternative for unbalanced distribution networks [24]. This method is called the Three-phase Current Injection Method (TCIM). Instead of applying the Newton-Raphson method to power mismatches (($\Delta \mathbf{P}, \Delta \mathbf{Q}$)), it is applied to Ohm's Law ($\mathbf{I} = \mathbf{Y}\mathbf{V}$) directly:

$$I_i = (\mathbf{Y}\mathbf{V})_i = \sum_{k=1}^{N} Y_{ik} V_k$$
$$\Delta I^{Re} = I_i^{Re} - I^{Re}(\mathbf{x})$$
$$\Delta I^{Im} = I_i^{Im} - I^{Im}(\mathbf{x})$$

We use the polar form of the current mismatch equation. As current is never specified, these values need to be determined from the specified power. We can derive current from the specified power as follows:

$$I_{sp} = \overline{\left(\frac{S_{sp}}{V}\right)}.$$

For a specific phase p in α_p, where $\alpha_p = \{a, b, c\}$, we express the current as:

$$I_{i,sp}^p = \overline{\left(\frac{P_{i,sp}^p + \iota Q_{i,sp}^p}{|V_i^p|(\cos(\delta_i^p) + \iota \sin(\delta_i^p))}\right)}, \quad p \in \alpha_p.$$

Likewise the power mismatch equation, we also split the current into real and imaginary parts:

$$Re(I_{i,sp}^p) = \frac{1}{|V_i^p|}(P_{i,sp}^p \cos(\delta_i^p) + Q_{i,sp}^p \sin(\delta_i^p))$$

$$Im(I_{i,sp}^p) = \frac{1}{|V_i^p|}(P_{i,sp}^p \sin(\delta_i^p) - Q_{i,sp}^p \cos(\delta_i^p))$$

The computed current is calculated directly from Ohm's Law and then specified per phase and expressed in polar form:

$$I_i^p(x) = \sum_{k=1}^{N} \sum_{q \in \alpha_p} Y_{ik}^{pq} V_k^q$$

$$= \sum_{q \in \alpha_p} (G_{ii}^{pq} + \iota B_{ii}^{pq})|V_i^q|e^{\iota \delta_i^q} + \sum_{k \in \Omega_i} \sum_{p,q \in \alpha_p} (G_{ik}^{pq} + \iota B_{ik}^{pq})|V_k^q|e^{\iota \delta_k^q}$$

$$Re(I_i^p(x)) = \sum_{q \in \alpha_p} \left(G_{ii}^{pq}|V_i^q|\cos(\delta_i^q) - B_{ii}^{pq}|V_i^q|\sin(\delta_i^q)\right)$$

$$+ \sum_{k \in \Omega_i} \sum_{q \in \alpha_p} \left(G_{ik}^{pq}|V_k^q|\cos(\delta_k^q) - B_{ik}^{pq}|V_k^q|\sin(\delta_k^q)\right)$$

$$Im(I_i^p(x)) = \sum_{q \in \alpha_p} \left(G_{ii}^{pq}|V_i^q|\sin(\delta_i^q) + B_{ii}^{pq}|V_i^q|\cos(\delta_i^q)\right)$$

$$+ \sum_{k \in \Omega_i} \sum_{q \in \alpha_p} \left(G_{ik}^{pq}|V_k^q|\sin(\delta_k^q) + B_{ik}^{pq}|V_k^q|\cos(\delta_k^q)\right)$$

where:

$$\begin{aligned}
p, q &\in & \alpha_p \\
\alpha_p &= & \{a, b, c\}, \text{ the three phases} \\
i &\in & \{1, ..., N\}, \text{ N total number of buses} \\
\Omega_i &= & \text{set of buses directly connected to bus } i
\end{aligned}$$

Power Mismatches Because distribution systems are sometimes solved using power mismatches — and because transmission systems are sometimes modelled in three phases (see chapter 5), we also describe the three-phase derivation for the power mismatch equation:

$$S_i^p(x) = V_i^p \sum_{k=1}^{N} \sum_{q \in \alpha_p} \overline{Y_{ik}^{pq} V_k^q}$$

$$= |V_i^p| e^{\iota \delta_i^p} \sum_{q \in \alpha_p} (G_{ii}^{pq} - \iota B_{ii}^{pq}) |V_i^q| e^{-\iota \delta_i^q}$$

$$+ |V_i^p| e^{\iota \delta_i^p} \sum_{k \in \Omega_i} \sum_{p,q \in \alpha_p} (G_{ik}^{pq} - \iota B_{ik}^{pq}) |V_k^q| e^{-\iota \delta_k^q}$$

$$P_i^p(x) = |V_i^p|^2 G_{ii}^{pp} + |V_i^p| \sum_{\substack{q \in \alpha_p \\ p \neq q}} |V_i^q| \left(G_{ii}^{pq} \cos(\delta_i^p - \delta_i^q) + B_{ii}^{pq} \sin(\delta_i^p - \delta_i^q) \right)$$

$$+ |V_i^p| \sum_{k \in \Omega_i} \sum_{q \in \alpha_p} |V_k^q| \left(G_{ik}^{pq} \cos(\delta_i^p - \delta_k^q) + B_{ik}^{pq} \sin(\delta_i^p - \delta_k^q) \right)$$

$$Q_i^p(x) = -|V_i^p|^2 B_{ii}^{pp} + |V_i^p| \sum_{\substack{q \in \alpha_p \\ p \neq q}} |V_i^q| \left(G_{ii}^{pq} \sin(\delta_i^p - \delta_i^q) - B_{ii}^{pq} \cos(\delta_i^p - \delta_i^q) \right)$$

$$+ |V_i^p| \sum_{k \in \Omega_i} \sum_{q \in \alpha_p} |V_k^q| \left(G_{ik}^{pq} \sin(\delta_i^p - \delta_k^q) - B_{ik}^{pq} \cos(\delta_i^p - \delta_k^q) \right)$$

The formulations of the Jacobian for current mismatches are presented in table 4.2 and the Jacobian for power mismatches in table 4.3 at the end of this chapter. The imaginary parts of the current are ordered first, to make sure that the Jacobian is diagonal dominant as $B_{ij} \gg G_{ij}$.

4.4. Overview

The eventual goal is to analyse integrated transmission and distribution systems efficiently. As transmission systems and distribution systems have different properties, they also use different solution methods. As Newton-Raphson is both efficient and robust for transmission as well as distribution power systems, and for ease of integration of the two methods, we will focus on Newton-Raphson methods only.

The Newton-Raphson power mismatch (NR-power) is used for transmission networks. It computes unknown quantities at each bus i. NR-power computes V_i using the following power mismatch formulation:

$$\Delta S_i = S_{s,i} - S(V_i) \approx 0.$$

S_s is the specified power, the known information at generator and load nodes: $S_s = S_g - S_d$, subscript g representing the generator buses and d the load buses. $S(x)$ is the injected power, $S(x) = V(YV)^*$.

The complex power S is split into an active and reactive part and combined to form

the power mismatch vector $\mathbf{F}$:

$$\mathbf{F}(\boldsymbol{x}) = \begin{bmatrix} \Delta \mathbf{P} \\ \Delta \mathbf{Q} \end{bmatrix} = \begin{bmatrix} \mathbf{P}_s - \mathbf{P}(x) \\ \mathbf{Q}_s - \mathbf{Q}(x) \end{bmatrix}.$$

The state variables are expressed by $x := V = \{|V|, \delta\}$. We compute $\boldsymbol{x}$ in an iterative manner using the Jacobian J of the power mismatch vector:

$$J(\boldsymbol{x}^\nu)\Delta\boldsymbol{x}^\nu = -\mathbf{F}(\boldsymbol{x}^\nu),$$
$$\boldsymbol{x}^{\nu+1} = \boldsymbol{x}^\nu + \Delta\boldsymbol{x}^\nu,$$

where the Jacobian contains the derivatives with respect to the voltage:

$$J = \begin{bmatrix} \frac{\partial P}{\partial \delta} & \frac{\partial P}{\partial |V|} \\[2mm] \frac{\partial Q}{\partial \delta} & \frac{\partial Q}{\partial |V|} \end{bmatrix}.$$

We repeat this until the norm of the power mismatch vector $||\mathbf{F}||_\infty$ is lower than a certain tolerance value ε.

We use the Newton-Raphson Three-Phase Current Injection Method (NR-TCIM) [24] to solve distribution networks. Instead of applying the standard Newton-Raphson method to power mismatches, Ohm's Law is directly used resulting in the current mismatch vector:

$$\mathbf{F}(\boldsymbol{x}) = \begin{bmatrix} \Delta\mathbf{I}^{Re,abc}(\boldsymbol{x}) \\ \Delta\mathbf{I}^{Im,abc}(\boldsymbol{x}) \end{bmatrix} = \begin{bmatrix} \mathbf{I}_s^{Re,abc} - \mathbf{I}^{Re,abc}(\boldsymbol{x}) \\ \mathbf{I}_s^{Im,abc} - \mathbf{I}^{Im,abc}(\boldsymbol{x}) \end{bmatrix}.$$

The specified current I_s and computed current $I(x)$ are calculated using the injected complex power and Ohm's Law:

$$I_{s,i} = \overline{\left(\frac{S_s}{V}\right)}_i \quad \text{and} \quad I(x)_i = \sum_{k=1}^{N} Y_{ik} V_k$$

The Jacobian is formed by taking the derivative of the real and imaginary current mismatch with respect to the real and imaginary voltage.

Table 4.2: Overview of the derivatives in the Jacobian of the current mismatch with respect to voltage magnitude and angle

<div style="text-align:center">

Real part

</div>

Bus	Phase	Derivative
$i = j$	$p = q$	$\dfrac{\partial I_i^{p,Re}}{\partial \delta_i^p} = -\lvert V_i^p \rvert \left(G_{ii}^{pp} \sin(\delta_i^p) + B_{ii}^{pp} \cos(\delta_i^p) \right)$ $\qquad + \dfrac{1}{\lvert V_i^p \rvert} \left(P_{i,sp}^p \sin(\delta_i^p) - Q_{i,sp}^p \cos(\delta_i^p) \right)$ $\dfrac{\partial I_i^{p,Re}}{\partial \lvert V_i^p \rvert} = G_{ii}^{pp} \cos(\delta_i^p) - B_{ii}^{pp} \sin(^p)$ $\qquad + \dfrac{1}{\lvert V_i^p \rvert^2} \left(P_{i,sp}^p \cos(\delta_i^p) + Q_{i,sp}^p \sin(\delta_i^p) \right)$
	$p \neq q$	$\dfrac{\partial I_i^{p,Re}}{\partial \delta_i^q} = -\lvert V_i^q \rvert \left(G_{ii}^{pq} \sin(\delta_i^q) + B_{ii}^{pq} \cos(\delta_i^q) \right)$ $\dfrac{\partial I_i^{p,Re}}{\partial \lvert V_i^q \rvert} = G_{ii}^{pq} \cos(\delta_i^q) - B_{ii}^{pq} \sin(\delta_i^q)$
$i \neq j$	$p = q$	$\dfrac{\partial I_i^{p,Re}}{\partial \delta_j^p} = -\lvert V_j^p \rvert \left(G_{ij}^{pp} \sin(\delta_j^p) + B_{ij}^{pp} \cos(\delta_j^p) \right)$ $\dfrac{\partial I_i^{p,Re}}{\partial \lvert V_j^p \rvert} = G_{ij}^{pp} \cos(\delta_j^p) - B_{ij}^{pp} \sin(\delta_j^p)$
	$p \neq q$	$\dfrac{\partial I_i^{p,Re}}{\partial \delta_j^q} = -\lvert V_j^q \rvert \left(G_{ij}^{pq} \sin(\delta_j^q) + B_{ij}^{pq} \cos(\delta_j^q) \right)$ $\dfrac{\partial I_i^{p,Re}}{\partial \lvert V_j^q \rvert} = G_{ij}^{pq} \cos(\delta_j^q) - B_{ij}^{pq} \sin(\delta_j^q)$

<div style="text-align:center">

Imaginary part

</div>

Bus	Phase	Derivative
$i = j$	$p = q$	$\dfrac{\partial I_i^{p,Im}}{\partial \delta_i^p} = \lvert V_i^p \rvert \left(G_{ii}^{pp} \cos(\delta_i^p) - B_{ii}^{pp} \sin(\delta_i^p) \right)$ $\qquad - \dfrac{1}{\lvert V_i^p \rvert} \left(P_i^{p,sp} \cos(\delta_i^p) + Q_i^{p,sp} \sin(\delta_i^p) \right)$ $\dfrac{\partial I_i^{p,Im}}{\partial \lvert V_i^p \rvert} = \left(G_{ii}^{pp} \sin(\delta_i^p) + B_{ii}^{pp} \cos(\delta_i^p) \right)$ $\qquad + \dfrac{1}{\lvert V_i^p \rvert^2} \left(P_i^{p,sp} \sin(\delta_i^p) - Q_i^{p,sp} \cos(\delta_i^p) \right)$
	$p \neq q$	$\dfrac{\partial I_i^{p,Im}}{\partial \delta_i^q} = \lvert V_i^q \rvert \left(G_{ii}^{pq} \cos(\delta_i^q) - B_{ii}^{pq} \sin(\delta_i^q) \right)$ $\dfrac{\partial I_i^{p,Im}}{\partial \lvert V_i^q \rvert} = G_{ii}^{pq} \sin(\delta_i^q) + B_{ii}^{pq} \cos(\delta_i^q)$
$i \neq j$	$p = q$	$\dfrac{\partial I_i^{p,Im}}{\partial \delta_j^q} = \lvert V_j^p \rvert \left(Gij^{pp} \cos(\delta_j^p) - B_{ij}^{pp} \sin(\delta_j^p) \right)$ $\dfrac{\partial I_i^{p,Im}}{\partial \lvert V_j^p \rvert} = G_{ij}^{pp} \sin(\delta_j^p) + B_{ij}^{pp} \cos(\delta_j^p)$
	$p \neq q$	$\dfrac{\partial I_i^{p,Im}}{\partial \delta_j^q} = \lvert V_j^q \rvert \left(Gij^{pq} \cos(\delta_j^q) - B_{ij}^{pq} \sin(\delta_j^q) \right)$ $\dfrac{\partial I_i^{p,Im}}{\partial \lvert V_j^q \rvert} = G_{ij}^{pq} \sin(\delta_j^q) + B_{ij}^{pq} \cos(\delta_j^q)$

Table 4.3: Overview of the derivatives in the Jacobian of the power mismatch with respect to voltage magnitude and angle

<table>
<tr><th colspan="3" align="center">Real part</th></tr>
<tr><th>Bus</th><th>Phase</th><th>Derivative</th></tr>
<tr>
<td rowspan="4">$i = j$</td>
<td rowspan="2">$p = q$</td>
<td>

$\dfrac{\partial P_i^p}{\partial \delta_i^p} = |V_i^p| \sum\limits_{\substack{r \in \alpha_p \\ p \neq i}} |V_i^r| \left(-G_{ii}^{pr} \sin(\delta_i^p - \delta_i^r) + B_{ii}^{pr} \cos(\delta_i^p - \delta_i^r)\right)$

$\qquad + |V_i^p| \sum\limits_{k \in \Omega_i} \sum\limits_{r \in \alpha_p} |V_k^r| \left(-G_{ik}^{pr} \sin(\delta_i^p - \delta_k^r) + B_{ik}^{pr} \cos(\delta_i^p - \delta_k^r)\right)$

</td>
</tr>
<tr>
<td>

$\dfrac{\partial P_i^p}{\partial |V_i^p|} = 2|V_i^p|G_{ii}^{pp} + \sum\limits_{\substack{r \in \alpha_p \\ p \neq r}} |V_i^r| \left(G_{ii}^{pr} \cos(\delta_i^p - \delta_i^r) + B_{ii}^{pr} \sin(\delta_i^p - \delta_i^r)\right)$

$\qquad + \sum\limits_{k \in \Omega_i} \sum\limits_{r \in \alpha_p} |V_k^r| \left(G_{ik}^{pr} \cos(\delta_i^p - \delta_k^r) + B_{ik}^{pr} \sin(\delta_i^p - \delta_k^r)\right)$

</td>
</tr>
<tr>
<td rowspan="2">$p \neq q$</td>
<td>

$\dfrac{\partial P_i^p}{\partial \delta_i^q} = |V_i^p||V_i^q| \left(G_{ii}^{pq} \sin(\delta_i^p - \delta_i^q) - B_{ii}^{pq} \cos(\delta_i^p - \delta_i^q)\right)$

</td>
</tr>
<tr>
<td>

$\dfrac{\partial P_i^p}{\partial |V_i^q|} = |V_i^p| \left(G_{ii}^{pq} \cos(\delta_i^p - \delta_i^q) + B_{ii}^{pq} \sin(\delta_i^p - \delta_i^q)\right)$

</td>
</tr>
<tr>
<td rowspan="4">$i \neq j$</td>
<td rowspan="2">$p = q$</td>
<td>

$\dfrac{\partial P_i^p}{\partial \delta_j^p} = |V_i^p||V_j^p| \left(G_{ij}^{pp} \sin(\delta_i^p - \delta_j^p) - B_{ij}^{pp} \cos(\delta_i^p - \delta_j^p)\right)$

</td>
</tr>
<tr>
<td>

$\dfrac{\partial P_i^p}{\partial |V_j^p|} = |V_i^p| \left(G_{ij}^{pp} \cos(\delta_i^p - \delta_j^p) + B_{ij}^{pp} \sin(\delta_i^p - \delta_j^p)\right)$

</td>
</tr>
<tr>
<td rowspan="2">$p \neq q$</td>
<td>

$\dfrac{\partial P_i^p}{\partial \delta_j^q} = |V_i^p||V_j^q| \left(G_{ij}^{pq} \sin(\delta_i^p - \delta_j^q) - B_{ij}^{pq} \cos(\delta_i^p - \delta_j^q)\right)$

</td>
</tr>
<tr>
<td>

$\dfrac{\partial P_i^p}{\partial |V_j^q|} = |V_i^p| \left(G_{ij}^{pq} \cos(\delta_i^p - \delta_j^q) + B_{ij}^{pq} \sin(\delta_i^p - \delta_j^q)\right)$

</td>
</tr>
<tr><th colspan="3" align="center">Imaginary part</th></tr>
<tr>
<td rowspan="4">$i = j$</td>
<td rowspan="2">$p = q$</td>
<td>

$\dfrac{\partial Q_i^p}{\partial \delta_i^p} = |V_i^p| \sum\limits_{\substack{r \in \alpha_p \\ p \neq r}} |V_i^r| \left(G_{ii}^{pr} \cos(\delta_i^p - \delta_i^r) + B_{ii}^{pr} \sin(\delta_i^p - \delta_i^r)\right)$

$\qquad + |V_i^p| \sum\limits_{k \in \Omega_i} \sum\limits_{r \in \alpha_p} |V_k^r| \left(G_{ik}^{pr} \cos(\delta_i^p - \delta_k^r) + B_{ik}^{pr} \sin(\delta_i^p - \delta_k^r)\right)$

</td>
</tr>
<tr>
<td>

$\dfrac{\partial Q_i^p}{\partial |V_i^p|} = -2|V_i^p|B_{ii}^{pp} + \sum\limits_{\substack{r \in \alpha_p \\ p \neq r}} |V_i^r| \left(G_{ii}^{pr} \sin(\delta_i^p - \delta_i^r) - B_{ii}^{pr} \cos(\delta_i^p - \delta_i^r)\right)$

$\qquad + \sum\limits_{k \in \Omega_i} \sum\limits_{r \in \alpha_p} |V_k^r| \left(G_{ik}^{pr} \sin(\delta_i^p - \delta_k^r) - B_{ik}^{pr} \cos(\delta_i^p - \delta_k^r)\right)$

</td>
</tr>
<tr>
<td rowspan="2">$p \neq q$</td>
<td>

$\dfrac{\partial Q_i^p}{\partial \delta_i^q} = |V_i^p||V_i^q| \left(-G_{ii}^{pq} \cos(\delta_i^p - \delta_i^q) - B_{ii}^{pq} \sin(\delta_i^p - \delta_i^r)\right)$

</td>
</tr>
<tr>
<td>

$\dfrac{\partial Q_i^p}{\partial |V_i^q|} = |V_i^p| \left(G_{ii}^{pq} \sin(\delta_i^p - \delta_i^q) - B_{ii}^{pq} \cos(\delta_i^p - \delta_i^q)\right)$

</td>
</tr>
<tr>
<td rowspan="4">$i \neq j$</td>
<td rowspan="2">$p = q$</td>
<td>

$\dfrac{\partial Q_i^p}{\partial \delta_j^q} = |V_i^p||V_k^p| \left(-G_{ik}^{pp} \cos(\delta_i^p - \delta_k^p) - B_{ik}^{pp} \sin(\delta_i^p - \delta_k^p)\right)$

</td>
</tr>
<tr>
<td>

$\dfrac{\partial Q_i^p}{\partial |V_i^p|} = |V_i^p| \left(G_{ik}^{pp} \sin(\delta_i^p - \delta_k^p) - B_{ik}^{pp} \cos(\delta_i^p - \delta_k^p)\right)$

</td>
</tr>
<tr>
<td rowspan="2">$p \neq q$</td>
<td>

$\dfrac{\partial Q_i^p}{\partial \delta_j^q} = |V_i^p||V_k^q| \left(-G_{ik}^{pq} \cos(\delta_i^p - \delta_k^q) - B_{ik}^{pq} \sin(\delta_i^p - \delta_k^q)\right)$

</td>
</tr>
<tr>
<td>

$\dfrac{\partial Q_i^p}{\partial |V_j^q|} = |V_i^p| \left(G_{ik}^{pq} \sin(\delta_i^p - \delta_k^q) - B_{ik}^{pq} \cos(\delta_i^p - \delta_k^q)\right)$

</td>
</tr>
</table>

II

Integrated Transmission and Distribution Networks

5

Integrated Networks

5.1. Introduction

As seen in the first part, transmission and distribution networks have different designs and properties. These differences impact how the network is modelled (1. Model), how the system is solved (2. Solver), and how the coupling between the networks is designed when the system is integrated (3. Coupling). We have to take the different designs and properties in these three aspects into consideration when we are developing the integration framework.

When creating a model (1.) of the integrated system, we have to consider that the transmission network is modelled in a single phase and the distribution network in three-phase. When selecting the solver (2.) for the integrated system, we have to consider that the Newton-Raphson three-phase current injection method (NR-TCIM) method works better for distribution networks due to the differences compared to transmission networks in topology (radial vs meshed), voltage level (medium and low vs high), power elements (distributed generation, regulators), and load models (Wye and Delta). Lastly, for coupling (3.), we have to consider that the distribution network operates in different voltage levels and base values, which should be taken into account. Besides these design challenges, some other challenges arise when integrating transmission and distribution systems [32]:

- Scale of the problem becomes very large (millions of buses): It should be solved in parallel to obtain results in a reasonable amount of time which increases the modelling complexity

- The models of transmission and distribution grids are built and maintained in geographically separated systems, which requires algorithms to support geographically distributed computation or other ways of data sharing

Parts of this chapter have been published [31]

The objective is to create a rationale that can solve the networks as an integrated system. In this chapter we:

1. Describe the outlook of the coupling mechanism

2. Give an overview of and describe and extend the methods that we have selected to handle the modelling and solving challenges

3. Review and assess these methods regarding modelling complexity, numerical performance, and accuracy

4. Discuss the challenges arising related to the size of integrated systems and the practical and legal issues that system operators may have.

5.1.1. Methodology

We have selected two different approaches to model the integrated system and two different methods that can solve the system, see the description in section 5.2.1. In total, we have four methods that are the object of our assessment study. We are going to test the methods on the following numerical criteria:

- Iteration number: does it scale independently of the number of unknowns

- Convergence rate: is quadratic convergence of Newton-Raphson still obtained for all methods

- Accuracy

- Parallel computing possibilities

In chapter 7, we will pay detailed attention to the influence of the increased amount of the influence of Photo-Voltaic generation (PV) on the different integrated system designs.

5.2. The substation

The transmission and distribution networks are connected via distribution substations. The substation is a series of tap-changing transformers that transform high voltage to low voltage power. This substation can be modelled as one transformer that connects the transmission network from the left and the distribution network from the right, as seen in Figure 5.1. In separate network analysis, this substation can be part of either of the networks. In integrated network analysis, the single-phase/three-phase connection results in a dimension mismatch at this substation.
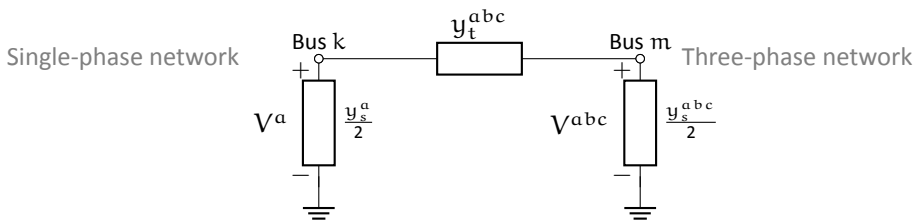

Figure 5.1: Substation transformer connecting a single-phase and three-phase network.

Table 5.1: Representation of single-phase and three-phase parameters in transmission and distribution network models respectively.

Network	Parameter		
	S_i	V_i	Y_{ij}
Transmission	$[S^a]_i$	$[V^a]_i$	$\begin{bmatrix} Y^a_{kk} \underset{1\times1}{} & Y^a_{km} \underset{1\times1}{} \\ Y^a_{mk} \underset{1\times1}{} & Y^a_{mm} \underset{1\times1}{} \end{bmatrix}_{ij}$
Distribution	$[S^a\ S^b\ S^c]_i^T$	$[V^a\ V^b\ V^c]_i^T$	$\begin{bmatrix} Y^{abc}_{kk} \underset{3\times3}{} & Y^{abc}_{km} \underset{3\times3}{} \\ Y^{abc}_{mk} \underset{3\times3}{} & Y^{abc}_{mm} \underset{3\times3}{} \end{bmatrix}_{ij}$

Table 5.1 shows the single-phase and three-phase representation of S, V, and Y in the network models. The explanation of how the dimension mismatch is resolved will be provided in the upcoming subsections during the discussion of the modelling and solution methods.

Besides the parameter dimension, there is also a difference in operating base conditions. The base parameters of a distribution network are defined in a different manner than in transmission networks. As the substation is modelled as a transformer, this transformer converts the networks to correct base values. The leakage admittance y_t of the substation consists of resistance r and reactance x. The equations should be scaled according to the correct base quantities to match the different pu-systems. The pu leakage admittance results in:

$$y_t = \frac{1}{z_t}, \quad \text{where } z_t = (r + \iota x)(\frac{V_{low}}{V_{base}})^2\frac{S_{base}}{S_t}, \tag{5.1}$$

where r and x are given in fractions. V_{low} is the voltage at the secondary level of the substation, and S_t is the apparent power of the substation, expressed in volt-ampere. V_{base} is always given in line-to-line and should be converted to line-to-neutral by dividing it by $\sqrt{3}$, in order to match the calculations.

5.2.1. Integrated system outlook

The model

We create network models that overcome the dimension mismatch between the two networks. We have identified two ways of doing so, either by modelling the integrated network as a homogeneous network or as a hybrid network. Homogeneous networks are networks where both the transmission and distribution networks are modelled in three phases. It requires a transformation of the transmission network[1]. Hybrid networks keep the transmission network as a single-phase model but require a transformation of the substation model.

The solver

Next to the modelling approaches, we classified the approaches to run stand-alone computations on integrated networks as unified and splitting methods: The unified method solves the integrated system as a whole [10]: The transmission network, substation, and distribution network are connected as one integrated network and then solved. The splitting method iterates between the two networks and at each iteration it solves the networks separately [11]. In the splitting method, the substation is part of the distribution network model. This method is similar to the co-simulation approach where the separate domains are solved on their own on distinct software platforms and coupled using an external iterative scheme [3].

We call the unified approach applied to homogeneous networks the Full three-phase (F3P) method and applied to hybrid networks the Interconnected (IC) method. We call all splitting methods manager-fellow splitting (MFS) methods. We define the MFS methods based on the network model they are applied to, eg: the splitting approach applied to hybrid networks is called the MFS-hybrid method. Figure 5.2 and Table 5.2 give an overview of the methods.
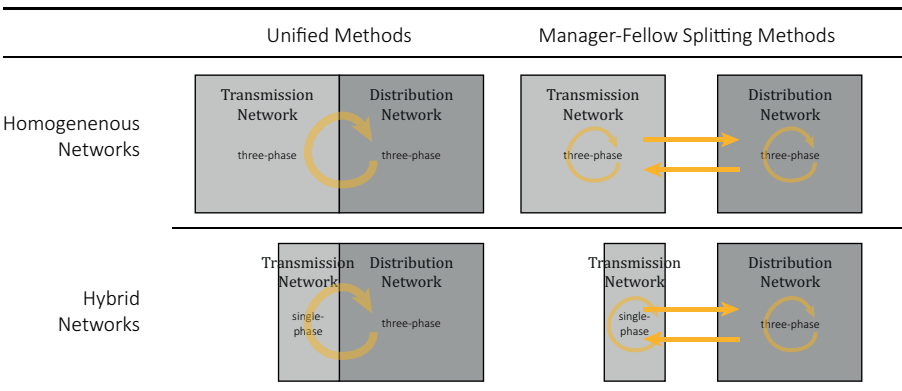
Figure 5.2: Overview of the Modelling (Hybrid and Homogeneous) and Solution (Unified and Splitting) Methods. The straight yellow arrows stand for the iterations between the networks. The curved arrow stands for a solver run. The size of the blocks indicates the size of the networks.

---

[1]Another option would be to model the distribution network in single-phase. But assuming the distribution network to be balanced would allow too many simplifications and result in useless solutions.

Table 5.2: Classification of numerical methods to solve integrated systems

	Integrated approach	
Network model	Unified	Splitting
Hybrid	*Interconnected (IC)* Transform substation Solve as a whole	*MFS-hybrid* Transform substation Extra iterative scheme
Homogeneous	*Full three-phase (F3P)* Transform Transmission Solve as a whole	*MFS-homogeneous* Transform Transmission Extra iterative scheme

5.3. Unified methods

Unified methods solve the integrated system using one iterative scheme applied to the entire integrated network. We put a substation model in between that connects the two networks. The original slack bus of the distribution network becomes a load bus that is connected to the right-hand side of the substation. Any load bus of the transmission network can be connected to the left-hand side of the substation. We solve the entire system using one algorithm.

5.3.1. The full three-phase method

The Full three-phase (F3P) method is the unified method applied to homogeneous networks. Unbalanced distribution networks are modelled in three-phase, the transmission networks require a transformation from a single phase to three phases. This transformation is based on the assumption that the transmission system is balanced: the phases b and c can be deducted from the first phase a and the voltage V^a, the complex power S^a, and the admittance Y_a of all the transmission buses $i = 1, ..., N$ are transformed to their three-phase equivalents. The following matrices are used to obtain this transformation:

$$T_1 = \begin{bmatrix} 1 & a^2 & a \end{bmatrix}^T \quad \text{and} \quad T_2 = \begin{bmatrix} 1 & 1 & 1 \end{bmatrix}^T, \quad a = e^{\frac{2}{3}\pi\iota},$$

and identity matrix $\mathbb{I}_{3\times3}$. This results in the following:

$$T_1 [V^a]_i = \begin{bmatrix} V^a & V^b & V^c \end{bmatrix}_i^T, \qquad (5.2)$$

$$T_2 \left[S^a \right]_i = \begin{bmatrix} S^a & S^b & S^c \end{bmatrix}_i^T, \qquad (5.3)$$

$$\begin{bmatrix} Y_{ij}^a \otimes \mathbb{I}_{3\times3} & Y_{ij}^a \otimes \mathbb{I}_{3\times3} \\ Y_{ji}^a \otimes \mathbb{I}_{3\times3} & Y_{jj}^a \otimes \mathbb{I}_{3\times3} \end{bmatrix}_{ij} = \begin{bmatrix} \overset{3}{Y_{ij}^{abc}} & \overset{3}{Y_{ij}^{abc}} \\ \underset{3}{Y_{ji}^{abc}} & \underset{3}{Y_{jj}^{abc}} \end{bmatrix}_{ij}. \qquad (5.4)$$

5.3.2. The interconnected method

The Interconnected method (IC) is the unified method applied to hybrid networks. The substation handles the dimension transformation by coupling the single-phase quantities of bus k at the transmission side to the three-phase quantities at bus m at the distribution side. The π-element model of the connecting substation is depicted in Figure 5.1. The concept of transformation such that single-phase quantities can be connected to three-phase quantities is called the MonoTri formulation by the authors that originally described this concept [10]. This formulation is based on the transformation of the nodal admittance matrix Y_{km}. To obtain this transformation, the following four matrices are used:

$$\mathbf{T_1},\ \mathbf{T_3} = \frac{1}{3}[1\ \mathbf{a}\ \mathbf{a^2}],\ \mathbf{T_4} = \frac{1}{3}\left[1\ 1\ 1\right],\ \mathbf{T_5} = \frac{1}{3}\left[1\ \mathbf{a^2}\ \mathbf{a}\right],$$

where $\mathbf{a} = e^{\frac{2}{3}\pi\iota}$, to establish the connection of bus k and m via the admittance matrix Y_{km}. This transformation is based on the assumption that the connecting bus k is perfectly balanced. This means that the single-phase and three-phase quantities are related as follows:

$$\mathbf{V_k^{abc}} = \begin{bmatrix} V^a & V^b & V^c \end{bmatrix}_k^T = \mathbf{T_1}V_k^a, \tag{5.5}$$

$$I_k^a = \mathbf{T_3}\begin{bmatrix} I^a & I^b & I^c \end{bmatrix}_k^T = \mathbf{T_3}\mathbf{I_k^{abc}}, \tag{5.6}$$

$$S_k^a = \mathbf{T_4}\begin{bmatrix} S^a & S^b & S^c \end{bmatrix}_k^T = \mathbf{T_4}\mathbf{S_k^{abc}}. \tag{5.7}$$

The change of the transformer substation depends on whether the unified system is solved with Newton-Raphson using power injections (NR-Power) or using current injections (NR-TCIM).

Using power injections

The deduction of the transformed admittance matrix Y_{km} starting from the power equations, $S_i = V_i\overline{(YV)}_i$, is done in a similar way [10]:

$$\mathbf{S} = \mathbf{V}\overline{\mathbf{I}} \quad \Leftrightarrow \quad \begin{bmatrix} S_k \\ S_m \end{bmatrix} = \begin{bmatrix} V_k \\ V_m \end{bmatrix}\overline{\begin{bmatrix} I_k \\ I_m \end{bmatrix}}$$

In the same manner as current injections, we can write this relation in three-phase:

$$\mathbf{S_k^{abc}} = \mathrm{diag}(\mathbf{V_k^{abc}})\overline{\mathbf{I_k^{abc}}} + \mathrm{diag}(\mathbf{V_k^{abc}})\overline{\mathbf{I_m^{abc}}},$$

$$\mathbf{S_m^{abc}} = \mathrm{diag}(\mathbf{V_m^{abc}})\overline{\mathbf{I_k^{abc}}} + \mathrm{diag}(\mathbf{V_m^{abc}})\overline{\mathbf{I_m^{abc}}}.$$

$$\Leftrightarrow$$

$$\mathbf{S_k^{abc}} = \mathrm{diag}(\mathbf{V_k^{abc}})\overline{(\mathbf{Y_{kk}^{abc}}\mathbf{V_k^{abc}})} + \mathrm{diag}(\mathbf{V_k^{abc}})\overline{(\mathbf{Y_{km}^{abc}}\mathbf{V_k^{abc}})}, \tag{5.8}$$

$$\mathbf{S_m^{abc}} = \mathrm{diag}(\mathbf{V_m^{abc}})\overline{(\mathbf{Y_{mk}^{abc}}\mathbf{V_k^{abc}})} + \mathrm{diag}(\mathbf{V_m^{abc}})\overline{(\mathbf{Y_{mm}^{abc}}\mathbf{V_m^{abc}})}. \tag{5.9}$$

We multiply equation (5.8) from the left by $\mathbf{T_4}$ to obtain the single-phase S_k^a:

$$S_k^a = \mathbf{T_4}\mathbf{S_k^{abc}} = \mathbf{T_4}\mathrm{diag}(\mathbf{V_k^{abc}})\overline{(\mathbf{Y_{kk}^{abc}}\mathbf{V_k^{abc}})} + \mathbf{T_4}\mathrm{diag}(\mathbf{V_k^{abc}})\overline{(\mathbf{Y_{km}^{abc}}\mathbf{V_m^{abc}})}. \tag{5.10}$$

Then, we substitute $\mathbf{V}_k^{abc} = \mathbf{T}_1 V_k^a$ (equation (5.5)) in equations (5.10) and (5.9) and obtain the following:

$$S_k^a = \mathbf{T}_4 \mathrm{diag}(\mathbf{T}_1 V_k^a)\overline{(\mathbf{Y}_{kk}^{abc}\mathbf{T}_1 V_k^a)} + \mathbf{T}_4 \mathrm{diag}(\mathbf{T}_1 V_k^a)\overline{(\mathbf{Y}_{km}^{abc}\mathbf{V}_m^{abc})}, \qquad (5.11)$$

$$S_m^{abc} = \mathrm{diag}(\mathbf{V}_m^{abc})\overline{(\mathbf{Y}_{mk}^{abc}\mathbf{T}_1 V_k^a)} + \mathrm{diag}(\mathbf{V}_m^{abc})\overline{(\mathbf{Y}_{mm}^{abc}\mathbf{V}_m^{abc})}. \qquad (5.12)$$

We can rewrite $\mathbf{T}_4 \mathrm{diag}(\mathbf{T}_1 V_k^a)$, the first part of the rhs in (5.11), as:

$$\mathbf{T}_4 \mathrm{diag}(\mathbf{T}_1 V_k^a) \Leftrightarrow \mathbf{T}_4 \mathrm{diag}(\mathbf{T}_1)\mathrm{diag}(V_k^a)$$

$$\Leftrightarrow \frac{1}{3}\begin{bmatrix} 1 & 1 & 1 \end{bmatrix}\begin{bmatrix} 1 & 0 & 0 \\ 0 & a^2 & 0 \\ 0 & 0 & a \end{bmatrix}\begin{bmatrix} V_k^a & 0 & 0 \\ 0 & V_k^a & 0 \\ 0 & 0 & V_k^a \end{bmatrix}$$

$$\Leftrightarrow \underbrace{\frac{1}{3}\begin{bmatrix} 1 & a^2 & a \end{bmatrix}}_{\mathbf{T}_5} V_k^a$$

$$\Leftrightarrow V_k^a \mathbf{T}_5.$$

This results in the following relations for single-phase and three-phase power:

$$S_k^a = V_k^a\overline{(\mathbf{T}_5\mathbf{Y}_{kk}^{abc}\mathbf{T}_1 V_k^a)} + V_k^a\overline{(\mathbf{T}_5\mathbf{Y}_{km}^{abc}\mathbf{V}_m^{abc})}, \qquad (5.13)$$

$$\mathbf{S}_m^{abc} = \mathrm{diag}(\mathbf{V}_m^{abc})\overline{(\mathbf{Y}_{mk}^{abc}\mathbf{T}_1 V_k^a)} + \mathrm{diag}(\mathbf{V}_m^{abc})\overline{(\mathbf{Y}_{mm}^{abc}\mathbf{V}_m^{abc})}. \qquad (5.14)$$

Equations (5.13), (5.14) yield the following transformed admittance matrix Y_{km}:

$$Y_{km} = \begin{array}{c} \\ 1 \\ 3 \end{array}\begin{array}{cc} 1 & 3 \\ \left[\begin{array}{cc} \mathbf{T}_5[Y_{kk}^{abc}]\mathbf{T}_1 & \mathbf{T}_5[Y_{km}^{abc}] \\ [Y_{mk}^{abc}]\mathbf{T}_1 & Y_{mm}^{abc} \end{array}\right]_{km} \end{array}$$

This is the new nodal admittance matrix, deducted from power equations.

Using Power Polar coordinates   Not all software packages can work with complex matrix-vector equations directly. Therefore, a similar derivation has to be made for power (or current) injections expressed in polar coordinates. The derivation for both power and current polar coordinates is explained in Appendix A of which A.1 contains the derivation for power coordinates.

Using current injections

The NR-TCIM method uses Ohm's law directly. The relation between node k and m is expressed as follows [10]:

$$\mathbf{I} = \mathbf{Y}\mathbf{V} \quad \Leftrightarrow \quad \begin{bmatrix} I_k \\ I_m \end{bmatrix} = \begin{bmatrix} Y_{kk} & Y_{km} \\ Y_{mk} & Y_{mm} \end{bmatrix} \begin{bmatrix} V_k \\ V_m \end{bmatrix}$$

If node k and m are both modelled in three-phase, the following holds:

$$I_k^{abc} = Y_{kk}^{abc}\mathbf{V}_k^{abc} + Y_{km}^{abc}\mathbf{V}_m^{abc}, \tag{5.15}$$

$$I_m^{abc} = Y_{mk}^{abc}\mathbf{V}_k^{abc} + Y_{mm}^{abc}\mathbf{V}_m^{abc}. \tag{5.16}$$

Equation (5.15) is multiplied by $\mathbf{T_3}$ to obtain the single-phase I_k^a:

$$I_k^a = \mathbf{T_3}I_k^{abc} = \mathbf{T_3}Y_{kk}^{abc}\mathbf{V}_k^{abc} + \mathbf{T_3}Y_{km}^{abc}\mathbf{V}_m^{abc}. \tag{5.17}$$

Accordingly, $\mathbf{V}_k^{abc}$ is substituted into equations (5.17) and (5.16) by $\mathbf{T_1}V_k^a$ (equation (5.5)):

$$I_k^a = \mathbf{T_3}I_k^{abc} = \mathbf{T_3}Y_{kk}^{abc}\mathbf{T_1}V_k^a + \mathbf{T_3}Y_{km}^{abc}\mathbf{V}_m^{abc}, \tag{5.18}$$

$$\mathbf{I}_m^{abc} = Y_{mk}^{abc}\mathbf{T_1}V_k^a + Y_{mm}^{abc}\mathbf{V}_m^{abc}. \tag{5.19}$$

Equations (5.18) and (5.19) result into this new admittance matrix:

$$Y_{km} = \begin{array}{c} \\ 1 \\ 3 \end{array} \begin{array}{c} 1 \qquad\qquad 3 \\ \begin{bmatrix} \mathbf{T_3}[Y_{kk}^{abc}]\mathbf{T_1} & \mathbf{T_3}[Y_{km}^{abc}] \\ [Y_{mk}^{abc}]\mathbf{T_1} & Y_{mm}^{abc} \end{bmatrix}_{km} \end{array}$$

Using Current Polar coordinates   Like power polar coordinates, the current polar coordinate derivation can be found in the appendix A.2.

Jacobian Interconnected Method

The Jacobian of the Interconnected method is derived by differentiating the transformed complex power or current to the voltage. The results for both the power and current injections are summarised in tables B.1, B.2, B.3, and B.4 respectively of Appendix B.

5.4. Manager-Fellow splitting methods

In contrast to the unified methods, the MFS methods keep two separate domains, the manager and the fellow and introduce an extra iterative scheme on top of them [11], see Figure 5.3. The fellow represents the distribution network including the substation. The manager represents the transmission network. The left bus of the substation is called the boundary bus B [33]. This bus is part of the manager *and* of the fellow. It can be any load bus of the transmission network and is the reference bus of the distribution network. We assume that this boundary bus is balanced and that the total
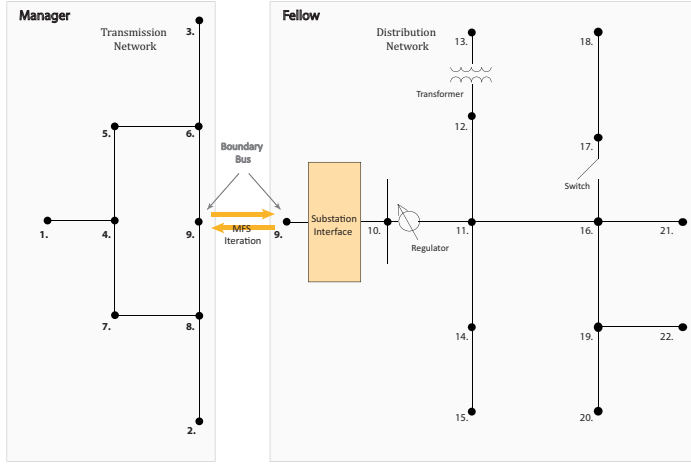
Figure 5.3: MFS iterative scheme put on top of transmission and distribution network model. Boundary Bus indicated with the grey arrow. Substation part of the Fellow.

nodal load of the transmission grid is equal to the total three-phase power injected into the distribution grid.

As the boundary bus is the slack bus of the distribution system, it requires the voltage $V_B = |V|e^{\iota \delta_B}$ as known information. In the first iteration, we initialise the boundary voltage with a flat profile. The boundary bus is a load bus for the transmission system and thus requires the complex power known. By solving the fellow, we get the complex power at the boundary bus (S_B) and use this as input for the manager. Then we can solve the manager and obtain the voltage at the boundary bus (V_B). We can continue the iteration cycle until we are satisfied with the result. This is when both systems have converged and the difference between the voltage of the boundary bus of two subsequent iterations is lower than a certain tolerance value ε_{MFS}. The iterative steps are summarised in Alg. 2. Note that as the MFS method is an extra scheme that is put on top of the separate system, it allows for solving the separate systems using their preferred Newton-Raphson method.

As the manager and fellow are modelled in different dimensions, the network models require some transformation. Also here, the Manager Fellow Splitting method can be applied to homogeneous networks and hybrid networks [34]. The first one requires a transformation of the entire manager domain, the latter requiring a transformation of the boundary bus output only.

5.4.1. The MFS-homogeneous method
The MFS method applied to homogeneous networks requires a transformation of the single-phase transmission system. The balanced transmission system is transformed in the same way as in the F3P method. The voltage, power, and admittance of all buses $i = 1, .., N$ are transformed into three-phase equivalents. This idea is already explained in equations (5.2) - (5.4) of section 5.3.1. The output of the distribution system can directly be used as input for the three-phase transmission system and vice-versa.

Algorithm 2: Manager-Fellow Splitting methods

1. Initialisation: set iteration counter $\nu = 0$ and initialise the voltage of the boundary bus with a flat profile
2. initialise the rest of the fellow with a flat voltage profile and solve as a separate system. Output: S_B^ν.
3. Inject S_B^ν into the transmission system.
4. initialise the rest of the manager with a flat voltage profile and solve as a separate system. Output: $V_B^{\nu+1}$.
5. Is $||x_B^{\nu-1} - x_B^\nu|| > \varepsilon_{MFS}$? Set $\nu = \nu + 1$ and repeat step 2 till 5.

5.4.2. The MFS-hybrid method

The MFS method applied to hybrid systems keeps the transmission system in single-phase. Following the original design of the splitting method [11], we transform the complex power and voltage of the boundary bus after one run of the fellow and the manager, respectively. First, the three-phase complex power S_B is transformed into a single-phase quantity. Once the Manager system is solved, the voltage V_B is transformed to a three-phase quantity. Here again, the transformation is based on the assumption that the boundary bus is completely balanced. Balanced three-phase power in pu is related to single-phase power in (5.7) according to the following relation:

$$[S^a] = T_4 \begin{bmatrix} S^a & S^b & S^c \end{bmatrix}^T, \tag{5.20}$$

where $T_4 = \frac{1}{3} \begin{bmatrix} 1 & 1 & 1 \end{bmatrix}$, and $\mathbf{a} = e^{\frac{2}{3}\pi\iota}$. The voltage of the boundary bus has the same relation as in (5.5), using :

$$\begin{bmatrix} V^a & V^b & V^c \end{bmatrix}_B^T = T_1 \begin{bmatrix} V^a \end{bmatrix}_B, \tag{5.21}$$

where $T_1 = \begin{bmatrix} 1 & \mathbf{a}^2 & \mathbf{a} \end{bmatrix}^T$, and $\mathbf{a} = e^{\frac{2}{3}\pi\iota}$.

Algorithm 2 requires two extra lines: Transformation (5.20) is added after step 2 and (5.21) after step 4 of algorithm 2. These steps are similar to transforming the nodal admittance matrix of the substation, which is connected to the fellow, directly, in the same manner as explained in section 5.3.2. In this way, the splitting approach does not require the addition of the two extra lines after steps 2 and 4 anymore. Furthermore, it makes the description of methods applied to hybrid networks generic.

The MFS methods reach convergence if both the separated systems and the MFS scheme have reached convergence, based on a defined tolerance value for the fellow, ε_F, for the manager, ε_M, and the MFS algorithm, ε_{MFS} is met. A summary of the solution approach of the unified and splitting methods applied to homogeneous and hybrid networks is described in the flowchart of Figure 5.4 at the end of the chapter.

Algorithm 3: Improved Manager-Fellow Splitting methods with the modifications in bold.

---

1. Initialisation: set iteration counter $\nu = 0$ and initialise the voltage of the boundary bus with a flat profile
2. IF $\nu = 0$: **initialise the rest of the fellow with a flat voltage profile.**
   ELSE: initialise the fellow with the voltage profile obtained at $\nu = \nu - 1$. and solve as a separate system. Output: S_B^ν.
   IF $\nu \neq 0$: **Store voltage profile of the fellow.**
3. Inject S_B^ν into the transmission system.
4. initialise the rest of the manager with a flat voltage profile and solve as a separate system. Output: $V_B^{\nu+1}$.
5. Is $||x_B^{\nu-1} - x_B^\nu|| > \varepsilon_{MFS}$? Set $\nu = \nu + 1$ and repeat step 2 till 5.

5.4.3. The manager-fellow iterative schemes

In earlier work of the research group of [35], two iterative schemes of the manager-fellow splitting are proposed. The first is the Convergence Alternating Iterative (CAI) scheme and the second is the Multistep Alternating Iterative (MAI) scheme. The MAI scheme is probably disregarded later as it is not mentioned in recent work [11] [33] [36]. We explain both schemes, but decided to only include the results of the CAI-scheme in our comparison[2].

In the CAI scheme, an explicit convergence condition is defined for the fellow and the manager. The fellow is solved with NR-TCIM, for which we define a tolerance value ε_D. Once this system has converged, its boundary output is injected into the manager. The manager is solved using NR-power, for which a (not necessarily) different tolerance value ε_T is defined. Once the manager has converged, its boundary output is injected into the fellow. The integrated network is converged once the convergence condition of the MFS algorithm is met. In the MAI scheme, first, a maximum number of iterations per separate system is defined, ie: $I_{max,D}$ and $I_{max,T}$. Then, the output of one system is injected into the other as soon as this maximum number of iterations has been reached. The convergence of the integrated network is based on the convergence condition of the MFS algorithm.

Speeding up the MFS iterative scheme

The convergence of the manager can be improved by making use of information from the previous MFS iteration. Note that this only works for the manager, as the voltage of the fellow is related to the voltage of the boundary bus as this is the slack bus, which is updated by the manager. In the current suggested scheme, at every MFS iteration, all the buses —except the boundary bus B— are initialised with a flat profile. We can reduce the number of required iterations for the separate systems if we initialise the voltages to its last obtained solution in the previous MFS iteration, ie: $V_{0,D}^{\nu+1} = V_{I,D}^\nu$ and $V_{0,T}^{\nu+1} = V_{I,T}^\nu$. See Alg. 3.

---

[2]We did implement the MAI-scheme, but these tests showed us that MAI was not beneficial compared to the CAI-scheme and only leads to extra work.

5.5. Advantages and disadvantages

Based on the theoretical study of the unified and splitting methods and hybrid and homogeneous networks, we list the advantages of one method over another based on the expected numerical performance, physical details, and applicability.

In terms of numerical performance, we first expect that the methods applied to hybrid networks perform better in terms of CPU time. Homogeneous networks represent the transmission network in three-phase, thus have to process a larger Jacobian matrix: The three-phase Jacobian matrix of a transmission system with N buses will have size 6N x 6N compared to a single-phase Jacobian matrix of size 2N x 2N. This is an advantage for the hybrid networks. In general, transmission systems are much smaller than distribution systems, so in practice, this difference is not that substantial.

Secondly, we may observe a higher number of iterations for the methods applied to hybrid networks. The reasoning behind this expectation is that the substation is modelled as a balanced bus, while it might be unbalanced, as it is directly connected to the unbalanced distribution network.

Thirdly, we expect to see an advantage in speed for the unified methods as they solve the integrated system at once.

An advantage of the splitting methods is that the developments in solving the separate systems continue. It is possible that the current solvers of distribution systems are not as efficient, as this is a relatively new research field. As the MFS method is an iterative scheme that is put on top of the separate systems, these improvements can easily be integrated. For the unified methods, this analysis should be carried out for the systems as a whole.

In terms of physical details, the homogeneous networks are a better representation of what is physically happening as power is generated and transported in three-phase over the entire electricity grid. Furthermore, due to new load types and intermittent renewable generation at the distribution level, imbalance can arise at the transmission level which would not be captured by hybrid network models.

Lastly, we consider the usability for system operators. Although it seems that unified methods have a clear advantage in terms of numerical performance, one should be aware of the fact that in many countries it is currently not allowed to exchange complete network information between different system operators. Therefore, the splitting methods are advantageous as only a minimum amount of data sharing is necessary to do load flow computations. Also in the unified methods improvements have been made by the use of domain-decomposition methods [9], which allow different system operators to a minimum amount of data sharing as well. Despite these improvements, there is still a clear distinction between these two, because computations in the unified methods need to be made on the same computer (and require a new entity in the role of an independent system operator). In the case of the manager-fellow splitting methods, system operators can be in geographically distinct locations and each run their computations. A disadvantage that arises then, is that it takes more communication time to distribute the data among different computer systems. The findings are summarised in Table 5.3.

Table 5.3: Advantages and Disadvantages of the network models and integration methods

	Properties	
Network Design	Advantages	Disadvantages
Hybrid	Smaller Jacobian In line with current operational models	Balanced substation bus
Homogeneous	Intuitive physical approach Suitable for unbalanced transmission conditions	Larger system
Method	Advantages	Disadvantages
Unified	One outer iteration	Same solver (NR) must be used for complete system
Splitting	Limited data sharing between system operators Allows for continuation of separate developments	Extra iterative scheme

5.6. Overview

Transmission and distribution networks have different designs and properties and care should be taken when integrating these models: a correct coupling framework should be placed between the two systems to handle the different operating base conditions, the networks should be modelled in such a way that the dimensions of the networks will match, and care should be taken to solve integrated networks: can we allow preferred separate solvers or do we have to stick to one solution method for the entire system.

These considerations were taken into account when we were selecting different methods that can model and solve integrated networks. We have evaluated two ways of creating an integrating network model: homogeneous versus hybrid, and two ways of solving stand-alone integrated systems: in a unified approach, or using a splitting method. This resulted in four different methods that are the object of study. The flowchart in figure 5.4 gives an overview of the methods and how they model and solve integrated systems. We will assess and compare these methods based on their numerical performance, accuracy, and physical conditions. The results are described in chapter 6. We already described what to expect from these methods based on the theoretical study. Unified, hybrid methods are preferred in terms of numerical performances, homogeneous networks are a better representation of the physical network, and splitting methods are better for respecting the legal and privacy concerns of system operators and easier to perform parallel computing studies.
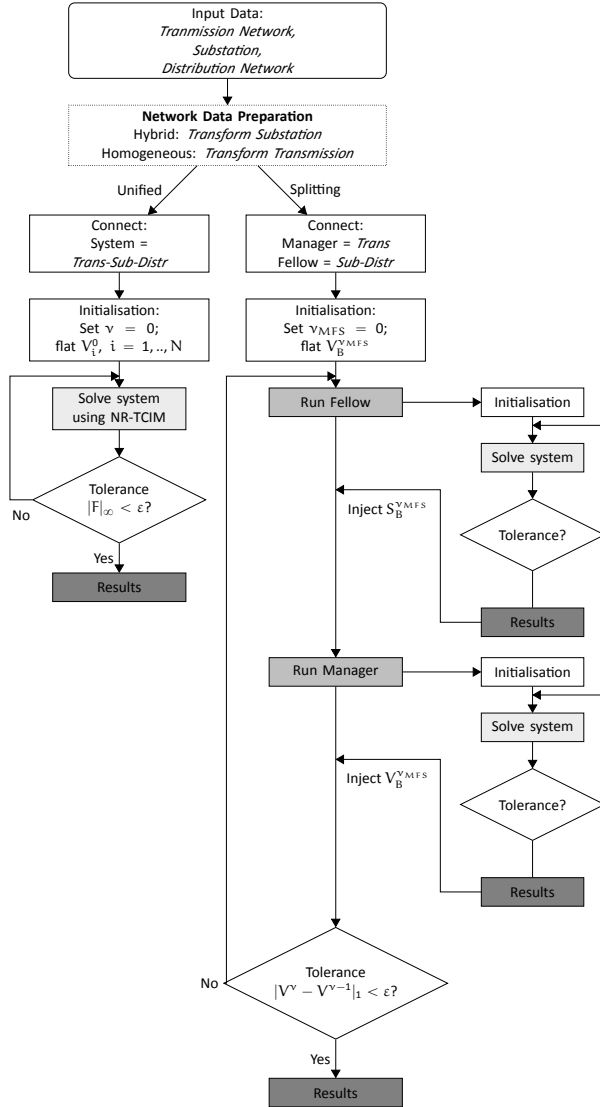
5

Figure 5.4: Algorithmic process of the Unified and Splitting methods.

6

Numerical Results

6.1. Introduction

This thesis provides insight into robust methods that can solve integrated power systems efficiently. So far, we have given the theoretical background of models and methods to simulate power flow in (integrated) electric power systems. In this chapter, we provide a first insight into the numerical performance of the evaluated integration methods, as described in chapter 5, to test the feasibility of the methods using small test networks.

We focus our performance analysis on numerical properties, which are the number of iterations and CPU time, such that we can predict how these methods would perform on larger cases. The methods that we assess in this study are unified and splitting methods that are applied to homogeneous and hybrid network representations. In total this leads to four methods that are the object of study: two unified methods; the Interconnected method (IC) and the Full 3Phase method (F3P), and two Manager-Fellow Splitting (MFS) methods; the MFS-hybrid and the MFS-homo method.

We test these methods on small-size test cases, which are simplified versions of real-world data of several worldwide power systems, and use a low-level programming language. This allows us extra flexibility to test the methods' performance on additional conditions that are encountered in real-life applications. These conditions are simulated by making use of power systems containing multiple distribution networks and systems with a higher number of (renewable) distributed generation.

Besides that, we try to give an insight into the accuracy of the methods. However, as the results of integrated system analysis differ from the separate analysis [37] and we do not have access to any physical data, we restrict ourselves to accuracy comparison between the results of the four integration methods themselves.

Parts of this chapter have been published [31]

We perform our simulations in Matlab using the Matpower[1] library. A single-core machine with an Intel Core i7-7600 processor, 2.80 GHz CPU and 8.00 GB memory is used. All problems are solved using the power or current mismatch formulation of Newton-Raphson. The size of the test cases allows us to solve the linear step (equation (4.1)) of Newton-Raphson with a direct method and a sequential implementation. We use an LU factorisation as a direct method. The unified methods are all solved using the Newton-Raphson with Current Mismatches (NR-TCIM); the transmission system in an MFS method is solved using Newton-Raphson with Power Mismatches (NR-P) and the distribution system using NR-TCIM.

To summarise, this chapter is structured as follows: we start with a description of the test cases that we created from existing test data, and we assess the numerical performances of the integration methods where we pay attention to the number of iterations and CPU time. We continue our assessment by applying these methods in simulated physical conditions and testing again its numerical performances.

6.2. Test-case description

Integrated test cases are created from the existing transmission and distribution test cases from the Matpower library and resources page of IEEE Power & Energy Society (P&ES) [39]. The 9-bus, 118-bus, and 3120-bus networks from Matpower are used as balanced network test cases. All these test cases are transmission networks. The IEEE 13-bus, 123-bus, and 8500-bus data from IEEE P&ES are used as unbalanced distribution test cases. The following integrated test cases are created by integrating a balanced network into an unbalanced network:

  1: Test case T9-D13

  2: Test case T118-D123

  3: Test case T3120-D8500

The loads of the IEEE test-networks are connected according to their given configuration – Wye or Delta – and load model – Z, I, or P –, see chapter 3 for the details of these configurations. The loads in the balanced transmission test networks are originally single-phase loads. In the homogeneous networks, they are modelled as Wye-P loads. The transformers in these networks are modelled in a Wye-Wye configuration.

The test cases are connected via a substation, which is modelled as a transformer connecting the distribution network (on the right-hand side of the transformer) and the transmission network (on the left-hand side). The bus in the transmission network connected to the substation on the left and the bus in the distribution network connected to the substation on the right are called connection buses. The following load buses of the transmission networks are selected as the connection bus in the integrated networks: Bus 7 in the 9-bus network, Bus 108 in the 118-bus network, and Bus 2700 in the 3120-bus network. The original reference bus in the distribution network becomes the connection bus.

---

[1]MATPOWER is a package of free, open-source Matlab-language M-files for solving steady-state power system simulation and optimization problems [38].

(a) Separate Models

(b) Unified Model   (c) Manager and Fellow model
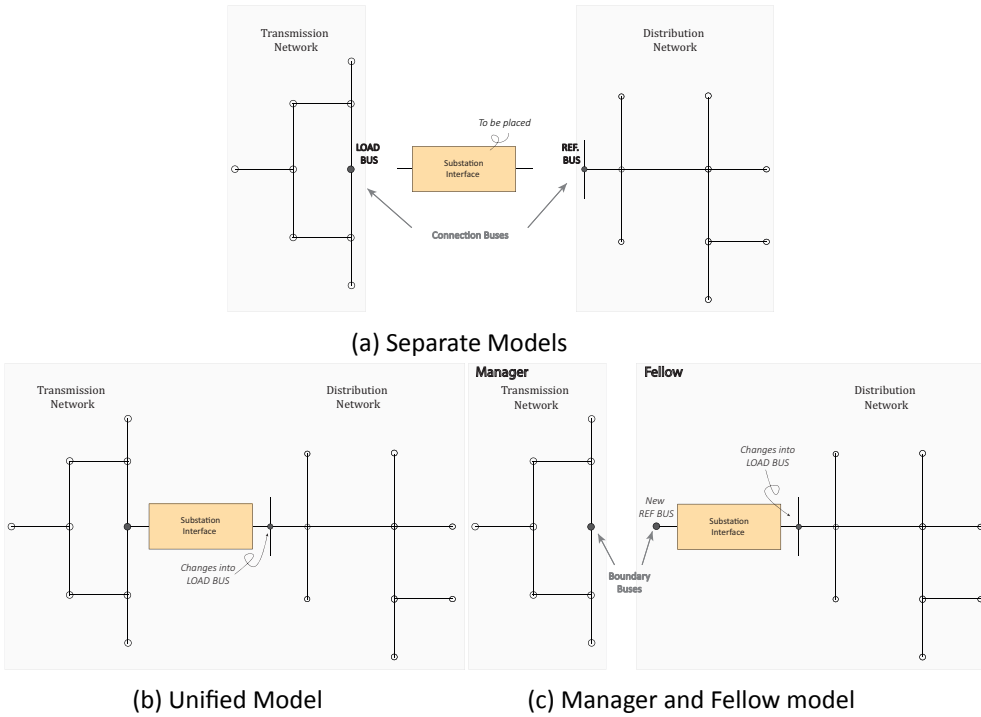
Figure 6.1: Clarification of the connection buses and boundary buses in integrated networks when running separate, unified, or splitting simulations. The relevant buses in transmission and distribution networks are indicated: connection bus, boundary bus, original load and reference (ref.) buses. The pictures show how the naming changes when a certain method is applied.

In the unified methods, the former distribution reference bus must be changed to a load bus. In the MFS methods, one talks about the boundary bus [11]. The boundary bus is the bus on the left-hand side of the substation. The connection bus of the transmission network is the same as the boundary bus when analysing the Manager and acts as a load bus. When analysing the fellow, this boundary bus is connected to the connection bus of the distribution network. See Figure 6.1 for a visualisation. This boundary bus acts as a reference bus for the fellow and is initialised by the output it receives from the transmission network.

6.3. Performance Assessment

The performance assessment is divided into numerical performance assessment, accuracy comparison, and assessment of real-life physical conditions.

6.3.1. Numerical Performance

We run power flow simulations on the integrated test cases and compare the numerical performance of the methods. We initialise the voltage of the unified methods, the voltage of the boundary bus of the MFS method, and the voltage of the manager and fellow with a flat start. The tolerance value of the unified methods, the manager, the fellow, and the MFS method are defined as $\varepsilon_U = \varepsilon_M = \varepsilon_F = \varepsilon_{MFS} = 10^{-5}$. To compare the numerical performance, the number of iterations and CPU time are listed in Table 6.1. Figures 6.2 and 6.3 show the relative norms per iteration.

Table 6.1: Comparison on the number of iterations (for the MFS-method: $\mathcal{I}_{MFS}$ of the MFS-scheme and $\mathcal{I}_M$ and I_D, the average number of iterations per subdomain), and CPU-time of the integration methods, of three test cases. The top table displays methods applied to hybrid- and the bottom one to homogeneous networks. The slowest CPU times are printed in bold.

Hybrid Network

	Method				
	IC		MFS-hybrid		
	$\mathcal{I}_U$	CPU	$\mathcal{I}_{MFS}$	$\mathcal{I}_M$	$\mathcal{I}_F$	CPU
Test case	#	sec	#	#	#	sec
T9-D13	3	0.016	3	4	4	0.901
T118-D123	4	0.025	3	7	5	0.807
T3120-D8500	4	0.367	3	6	5	2.569

Homogeneous Network

	Method				
	F3P		MFS-homo		
	$\mathcal{I}_U$	CPU	$\mathcal{I}_{MFS}$	$\mathcal{I}_M$	$\mathcal{I}_F$	CPU
Test case	#	sec	#	#	#	sec
T9-D13	3	0.015	3	4	4	**1.071**
T118-D123	4	0.039	3	4	5	**1.173**
T3120-D8500	4	0.612	3	6	5	**3.697**
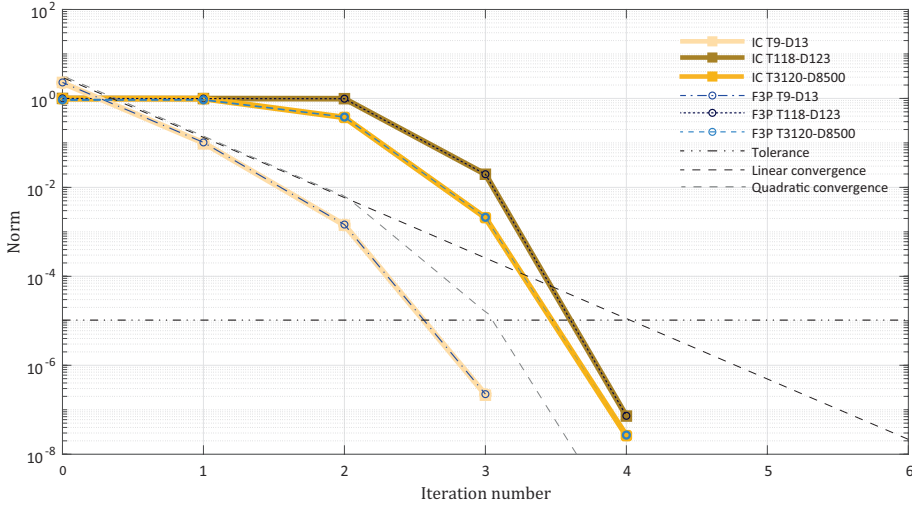
Figure 6.2: Representation of the relative norms of $|F|_\infty$, per iteration, of the interconnected and full three-phase methods for three test cases. Linear and quadratic convergence are shown in the figure. The horizontal black dotted line is the tolerance value. Note that the results of the IC and F3P methods are on top of each other as they exhibit the same convergence pattern.

6
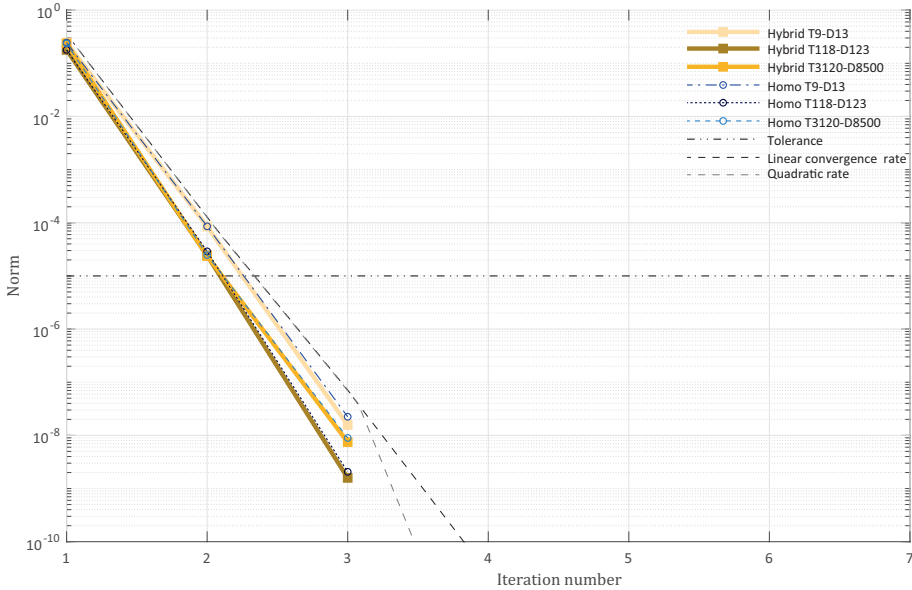

Figure 6.3: Representation of the relative norms of $|V_B^{\gamma+1} - V_B^\gamma|_1$, per iteration, of the splitting methods for three different test cases. Linear and quadratic convergence are shown in the figure. The horizontal black dotted line is the tolerance value. The results of the hybrid methods are below the results of the homogeneous methods.

The results between the unified and splitting methods are firstly analysed. Table 6.1 shows that the unified methods require more CPU time than the splitting method. The splitting methods require, on average, three MFS iterations and during one iteration, two systems are solved. The expected difference in CPU time is visible in the results: The splitting methods are around six times slower than the unified methods. The difference between hybrid and homogeneous network models is visible but less significant; the small test cases are even comparable in speed. Overall, the MFS-homo methods perform the least and the IC methods perform the best, in line with the expectations. In the figures, we have shown the linear and quadratic convergence rates which the methods are approaching. Nevertheless, it is difficult to say anything reasonable about the convergence pattern with so few iterations.

Speeding up the Manager-Fellow iterative scheme

In the iterative scheme outlined in the preceding paragraph, the MFS manager is initialised to a flat voltage profile at the start of every MFS iteration, which is not efficient. Instead, the solution of the manager at every MFS iteration can be stored and used as an initial guess for the next iteration. See the subparagraph in section 5.4.3 of chapter 5 for more details on this matter. This should lead to additional speed up.

Table 6.2: The number of manager iterations per MFS iteration and the CPU-time of the three different test cases when the idea of speeding up the splitting methods is applied.

Hybrid Network

	MFS-hybrid				
	$\mathcal{I}_{\mathrm{MFS}}$	$\mathcal{I}_{\mathrm{M}}^1$	$\mathcal{I}_{\mathrm{M}}^2$	$\mathcal{I}_{\mathrm{M}}^3$	$\mathcal{I}_{\mathrm{F}}$	*CPU*
Test case	#	#	#	#	#	*sec*
T9-D13	3	4	2	1	5	0.785
T118-D123	3	7	1	1	5	0.831
T3120-D8500	3	6	2	1	5	2.227

Homogeneous Network

	MFS-homo				
	$\mathcal{I}_{\mathrm{MFS}}$	$\mathcal{I}_{\mathrm{M}}^1$	$\mathcal{I}_{\mathrm{M}}^2$	$\mathcal{I}_{\mathrm{M}}^3$	$\mathcal{I}_{\mathrm{F}}$	*CPU*
Test case	#	#	#	#	#	*sec*
T9-D13	3	4	2	1	5	1.028
T118-D123	3	4	2	1	5	1.118
T3120-D8500	3	6	2	1	5	3.651

Table 6.2 shows that the idea works: the number of manager iterations decreases as the MFS iterations increase. It is noteworthy that the impact on the total elapsed CPU time is not very significant as the solution time of the distribution system is the dominant factor.

6.3.2. Accuracy

For the accuracy assessment, we compare the relative difference of the per-unit volt-age magnitude and voltage angle of the connection buses of the three test cases. These values and their differences are presented in table 6.3. Additionally, we show the full voltage magnitude profile of test-case T9-D12 in figures 6.4 and 6.5.

Table 6.3: Accuracy comparison. The per-unit voltage magnitudes of the connection bus in different integrated test cases of the four methods (IC, F3P, Hybrid-MFS, and Homogeneous MFS). The *Diff.* column shows the absolute difference of this voltage between hybrid and homogeneous network models. The difference between the two methods is small, so the various methods produce similar results.

		Method					
		Unified			Splitting		
		IC	F3P	Diff.	Hybrid	Homo	Diff.
Test-case	Phase	$|V|$	$|V|$	$|V|_{IC} - |V|_{F3P}$	$|V|$	$|V|$	$|V|_{Hy} - |V|_{Ho}$
T9-D13	A	1,0075	1,0076	1,00e-04	1,0074	1,0073	-1,00e-04
	B	1,0075	1,0076	1,00e-04	1,0074	1,0073	-1,00e-04
	C	1,0075	1,0074	-1,00e-04	1,0074	1,0075	1,00e-04
T118-D123	A	0,9651	0,9651	0,00e+00	0,9662	0,9662	0,00e+00
	B	0,9651	0,9652	1,00e-04	0,9662	0,9661	-1,00e-04
	C	0,9651	0,9651	0,00e+00	0,9662	0,9661	-1,00e-04
T3120-D8500	A	1,0716	1,0716	0,00e+00	1,0722	1,0722	0,00e+00
	B	1,0716	1,0715	-1,00e-04	1,0722	1,0722	0,00e+00
	C	1,0716	1,0716	0,00e+00	1,0722	1,0722	0,00e+00

The comparison of the full voltage profiles, shown in figures 6.4 and 6.5, shows that phases a, b, and c are similar in the T9-D13 case. Table 6.3 shows the per-unit values of the connecting bus voltage and the differences, from which can be observed that the solutions closely match.
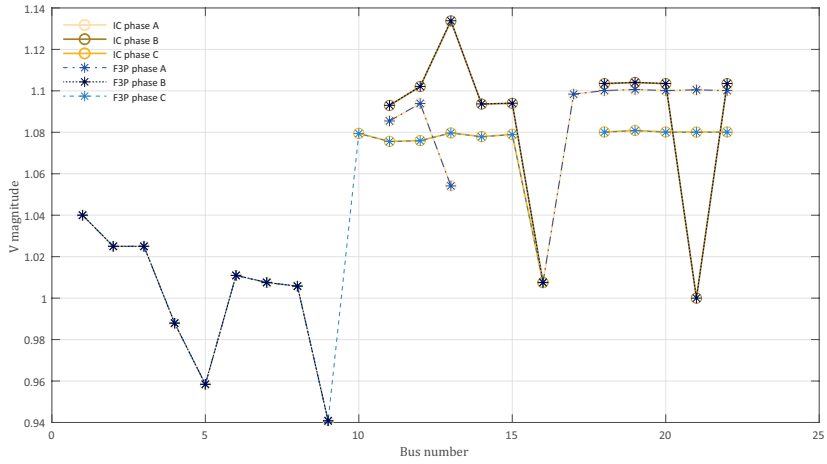
Figure 6.4: Per unit voltage magnitude profile of the three phases of the Interconnected and Full Three-Phase method. The represented network is the T9-D13 network. Distribution networks can contain single-phase and double-phase loads. Therefore some phases are missing at the distribution buses.
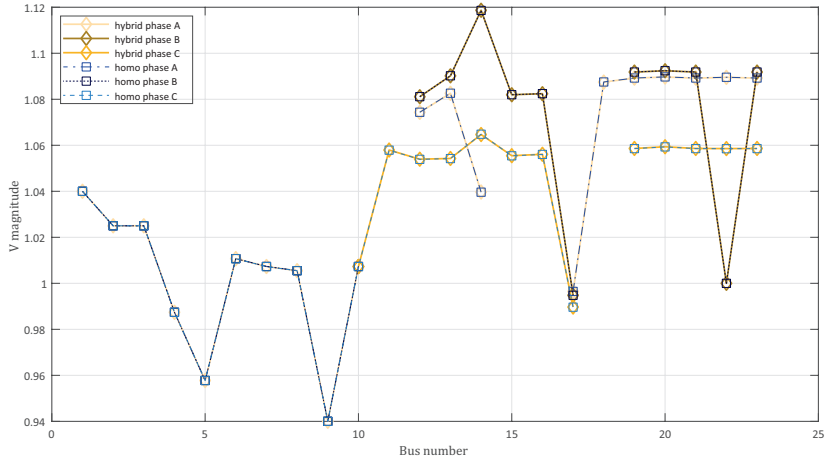
6

Figure 6.5: Per unit voltage magnitude profile of the three phases of the Manager-Fellow Hybrid and Homo Splitting methods. The represented network is the T9-D13 network. Distribution networks can contain single-phase and double-phase loads. Therefore some phases are missing at the distribution buses.

6.4. Physical Conditions

We want to know how the methods would perform in realistic conditions. Therefore, the numerical performance assessment is continued on integrated networks containing multiple distribution feeders and on those containing an increased amount of distributed generation.

6.4.1. Multiple Distribution Networks

For the numerical assessment of multiple distribution feeders connected to one transmission feeder, the same basis test cases are used, but 3, 5, and 10 distribution networks have been added to the transmission network, respectively. They are connected to the same connection bus and its respective number of consecutive buses. Table 6.4 shows the number of iterations and CPU time.

Table 6.4: Comparison of number of iterations and CPU-time of the integration methods, applied to the test cases having multiple distribution feeders connected. The changes in iteration number, compared to the original networks from table 6.1, are bold.

Hybrid Network

	Method				
	IC		MFS-hybrid		
	$\mathcal{I}_\mathrm{U}$	CPU	$\mathcal{I}_\mathrm{MFS}$	$\mathcal{I}_\mathrm{M}$	$\mathcal{I}_\mathrm{F}$	CPU
Test case	#	sec	#	#	#	sec
T9-3D13 *(7-9)*	3	0.020	3	4	**5**	1.494
T118-5D123 *(108-112)*	4	0.060	3	**7**	**4**	1.691
T3120-10D8500 *(2700-2709)*	**5**	3.015	3	6	**4**	12.51

Homogeneous Network

	Method				
	F3P		MFS-homo		
	$\mathcal{I}_\mathrm{U}$	CPU	$\mathcal{I}_\mathrm{MFS}$	$\mathcal{I}_\mathrm{M}$	$\mathcal{I}_\mathrm{F}$	CPU
Test case	#	sec	#	#	#	sec
T9-3D13 *(7-9)*	3	0.017	3	4	**5**	1.791
T118-5D123 *(108-112)*	4	0.073	3	4	**4**	1.973
T3120-10D8500 *(2700-2709)*	4	3.675	3	6	**4**	14.53

A comparison of table 6.1 with 6.4, does not show an increase of iterations when multiple distribution networks are connected. Therefore, it can be concluded that in general none of the methods is sensitive to the number of distribution networks, which makes them applicable to realistic electricity networks. Furthermore, there is almost a linear correlation between the CPU time of the network and the number of distribution networks.

6.4.2. Distributed generation

The second part of this assessment tests its sensitivity towards the increase of distributed generation. To test this, we added 4 to 5 PV buses to the original distribution feeders by changing the original three-phase load buses to PV buses. We compare the number of iterations of these new networks. These results are shown in table 6.5.

Table 6.5: Influence of PV buses on number of iterations. The changes in iteration number compared to the original network are bold.

Hybrid Network

| | | Original | | | | | Extra Distr. Generation | | | |
| | | IC | MFS-hybrid | | | | IC | MFS-hybrid | | |
Test case	PV buses	$\mathcal{I}_U$ #	$\mathcal{I}_{MFS}$ #	$\mathcal{I}_M$ #	$\mathcal{I}_F$ #	PV buses	$\mathcal{I}_U$ #	$\mathcal{I}_{MFS}$ #	$\mathcal{I}_M$ #	$\mathcal{I}_F$ #
T9-D13	0	3	3	4	4	4	3	**5**	4	**5**
T118-D123	0	4	3	7	5	5	4	**6**	7	5
T3120-D8500	0	4	3	6	5	5	4	3	6	**4**

Homogeneous Network

| | | Original | | | | | Extra Distr. Generation | | | |
| | | F3P | MFS-homo | | | | F3P | MFS-homo | | |
Test case	PV buses	$\mathcal{I}_U$ #	$\mathcal{I}_{MFS}$ #	$\mathcal{I}_M$ #	$\mathcal{I}_F$ #	PV buses	$\mathcal{I}_U$ #	$\mathcal{I}_{MFS}$ #	$\mathcal{I}_M$ #	$\mathcal{I}_F$ #
T9-D13	0	3	3	4	4	4	3	**6**	4	**5**
T118-D123	0	4	3	4	5	5	4	**6**	4	5
T3120-D8500	0	4	3	6	5	5	4	3	6	**4**

We can conclude that the unified methods are not sensitive to the amount of extra PV buses. The separate manager and fellow itself show little sensitivity to the increase of distributed generation, but we do observe a slight increase in iteration count within the MFS-iterative scheme.

6.5. Overview and conclusion

We compared and assessed two types of stand-alone integration methods to solve the power flow problem. We classified them as unified and splitting methods and applied them to hybrid and homogeneous networks. This resulted in four different methods as the starting point of our comparison study and numerical assessment. We analysed their accuracy and numerical performance — CPU time and the number of iterations — using a Newton-Raphson solver together with an LU factorisation.

The numerical assessment shows that the unified methods are most favourable, which is in line with the expectations, stated in section 5.5. As soon as the test cases get larger, the difference becomes more significant. Furthermore, it can be concluded that the methods applied to homogeneous networks require more CPU time than the methods applied to hybrid networks (on average 1.5 times as much in the simulations on these test cases). The analysis on the addition of distributed generation and multiple distribution feeder shows that all methods are robust as they are not influenced by physical conditions.

Overall, it can be concluded that the interconnected method is the most favourable method at this moment. Realistically sized networks have often multiple and larger distribution networks. The results between hybrid and homogeneous networks become then less significant. On top of that, these large networks require high-performance computing techniques such as Newton-Krylov methods and domain-decomposition techniques in a parallel or GPU environment. This makes the MFS methods more advantageous as they are by design a domain-decomposition method, although recent developments show how unified methods can be solved efficiently in parallel as well. The results in chapter 9 will show how these methods will perform using additional numerical methods, such as preconditioners and Newton-Krylov methods.

6

7

The influence of additional Photo-voltaic generation

7.1. Introduction

The goal of this thesis is to design a framework to model and solve large integrated electricity systems efficiently, taking into account the physical conditions and privacy issues of system operators. One reason to analyse the computations on these integrated networks is to simulate the effects that distribution networks can have on transmission networks which are evoked by the energy transition, mainly due to the increasing amount of generation at the distribution level. In chapter 6 we showed that both homogeneous and hybrid networks can be used as frameworks to model an integrated network. A homogeneous network contains a three-phase representation of the transmission network. This representation is necessary when a network is unbalanced. The increasing amount of distribution generation can cause this imbalance on the transmission network [4].

Homogeneous networks are not as efficient in simulating power flow on them as hybrid networks are and therefore large power flow studies are not preferred on these networks. Therefore, we want to study whether hybrid networks are sufficient to analyse integrated power systems whilst studying the effects of distribution generation on integrated systems. The objective of this chapter is thus two-fold:

1. To analyse the effects of increased distribution on power systems, focusing on the increasing amount of residential Photo-Voltaic (PV) generation,

2. To study whether hybrid networks are sufficient to analyse integrated networks. We study this by analysing the amount of imbalance created on transmission networks when using a homogeneous network representation. If this imbalance is minor, then hybrid networks are sufficient.

This chapter is part of the book [40]

The main driver for the increase in distribution generation is the high level of PV power penetration in urban residential areas. The increase of PV power is one of the biggest challenges related to the energy transition: High levels of distribution induce bi-directional power flow between transmission and distribution networks and increased imbalance on the electrical power system [4] [41] [42]. More and more households are motivated to place PV panels on their rooftop, out of care for the planet, out of financial incentives, and/or because of lowering purchase and installation costs [43]. Governments may support this trend as it is in line with the global sustainable development goals, but it puts extra pressure on the electricity grid: As residential rooftops only supply active power, it might lead to an insufficient supply of reactive power to the loads [19]. This can cause the voltage to drop. This will not only lead to voltage variations outside the safe operating limits but also to individual phase variations as the distribution network is unbalanced. This leads to increasing imbalance, which is harmful to the entire electrical power system [44].

There is a need for power flow simulations that can show the effects of the energy transition, hence integrated network analysis. In the previous chapter, we have shown the numerical performance of integration methods. In this chapter, we focus on the effects of increased PV integration when using a Unified solution framework. We use it to study the sensitivies of an electrical power system towards PV power penetration such as steady-state voltage stability, induced imbalance, and reduced power losses. The MFS methods are not part of this study as the split between the two networks does not allow transmission systems to exhibit imbalance [35], so effects on these networks cannot be captured.

7

We have seen in the previous chapter that power flow computations that run on hybrid network models are faster than computations that run on full three-phase network models. Nevertheless, hybrid network models are not capable of showing the amount of induced imbalance on transmission networks. To investigate whether the hybrid network model is a sufficient way to analyse the effects of PV penetration on transmission networks, we compare the results with a homogeneous representation of the integrated network. Using the names introduced in chapter 5, we can say that we compare the outcome of the Interconnected (IC) methods with the Full Three-Phase (F3P) method.

In summary, this chapter contains the following objectives:

1. We give an introduction to photo-voltaic rooftop panels and their consequences for the steady-state operation of electrical power systems;

2. We define four PV penetration challenges, which we use to study their main consequences on steady-state operation: exceeding voltage levels and high amount of imbalance on both distribution and transmission systems;

3. We compare the results of the interconnected method with the full three-phase method and test whether the IC method is sufficient for integrated network analysis or whether it is 'hiding' the effects of extra imbalance on transmission networks;

4. We test these effects using three different integrated test cases.

7.2. Photo-voltaic panels

PV panels connected to an electrical power system can be categorised into two categories: 1) residential rooftop PV systems and 2) utility-scale PV panels. As the name implies, residential rooftop systems can be found on rooftops of households and other residential buildings. This means that these systems are connected at the distribution level, closely located to the loads. Utility-scale panels are often installed at the transmission level and —due to the size of these installations—could be used to replace conventional bulk power plants [19].

The rise in residential PV panels is associated with certain challenges. These panels produce only active power as voltage regulatory purposes do not allow them to produce reactive power [43]. The lack of reactive power might result in a voltage drop to an undesirable level as reactive power is required to convert the flow of electrons into useful work [45]. On top of that, as distribution networks are unbalanced networks, a voltage drop can result in different phase variations [44]. This can evoke an extra degree of imbalance that is harmful to the network [44]. DSOs operate their system between a certain bandwidth of allowed voltage levels and degree of imbalance [7]. Likewise DSOs, it might become difficult for TSOs to maintain safe voltage levels [46]: A high amount of imbalance and out-of-bound voltage levels in distribution systems might affect transmission networks as well. These networks are designed for balanced operating conditions only and imbalance can cause extra harmful effects.

The focus of this study is on residential rooftop systems closely connected to loads along the distribution feeder. The location close to the loads has a positive effect: It might limit the power losses that arise due to the distances that electrical power conventionally has to bridge to get from a transmission power plant towards end-consumers at the distribution level. On the other hand, it also leads to the effects of extra imbalance and phase variations which are harmful to the entire network. These effects are studied using different PV penetration scenarios.

7.2.1. Photo-voltaic power models

Most residential PV systems provide active power only. Therefore, we model them as load buses with only negative active power provision. We analyse the steady-state behaviour of the integrated network by running simulations with various levels of PV penetration at the distribution level. Several methods exist to define the amount of PV penetration. We use the definition based on the total available generation in the base case (so before adding extra PV) [19], defined as follows:

$$\text{PV penetration}(\%) = \frac{\text{total PV generation}}{\text{total base generation}} \cdot 100\% \qquad (7.1)$$

We use varying penetration levels between 10% and 50% and an extreme level of 200%. Based on the data analysis of [42], we see that the peak irradiation[1] of residential PV systems is 7 kW/m^2 and that an individual panel with this level of irradiation produces a maximum power of 105 W. In this way, we can calculate how many panels are necessary to obtain the desired amount of PV penetration and whether this number of panels is a realistic amount for a certain neighbourhood or residential area.

---

[1]Irradiance is an instantaneous measurement of solar power over some area [47]

In summary, we are defining five scenarios with varying levels of PV penetration which we are going to assess:

0. The base case: No PV penetration

I. 10% PV penetration

II. 20% PV penetration

III. 50% PV penetration

IV. An extreme scenario of 200% PV penetration, only supplied via phase A, to intensify its effects.

7.3. Simulation Results

In this section, we analyse the steady-state voltage stability and amount of transmission and distribution imbalance on three test cases using the five different scenarios. We use the first two test cases from the previous chapter (T9-D13 and T118-D123), and we create a third test case with the 118-bus transmission network and ten 123-bus distribution networks. This one is created because the electrical power systems of countries consist of one transmission network and multiple distribution networks. We model the connecting substations in these networks using a Delta-Grounded Wye configuration.

The focus of this study is to simulate the effects of increasing PV penetration on steady-state voltage stability and the amount of imbalance in both distribution and transmission networks. We start with steady-state voltage stability.

Figure 7.2 shows such an integrated network. This is the visualisation of the T9-D13 network, where the PV panels are connected to bus 21 of the integrated network.

7.3.1. Steady-state voltage stability

The steady-state voltage of distribution networks should not exceed certain predefined limits. These limits are defined by system operators per network and are drawn in the figures 7.1a - 7.1c. For the 13-bus distribution network, for example, this limit is defined as 10%. The amount of PV penetration, modelled as a negative PQ-load only supplying active power might lead to an insufficient supply of reactive power to the loads, which can cause the voltage to drop. We investigate whether this is happening for the different scenarios.

Figures 7.1a - 7.1c show the new steady-state voltages magnitudes of the T9-D13 test-case under varying PV penetration levels. One can see that during normal PV penetration levels, the voltages of the T9-D13 test case never exceed its limits. Furthermore, they show that the voltage profile stays close to its original base profile (without any PV penetration). Only in the extreme scenario, do we see that the levels drop significantly.

The results of the bigger test cases, T118-D123 and T118-10D123, are summarised in tables 7.1 and 7.2. These tables show the minimum and maximum voltage magnitudes of the three separate phases. In normal operation levels, the voltage magnitudes of the T118-D123 test case do not decrease to a certain extent that it exceeds the prescribed operating limits.

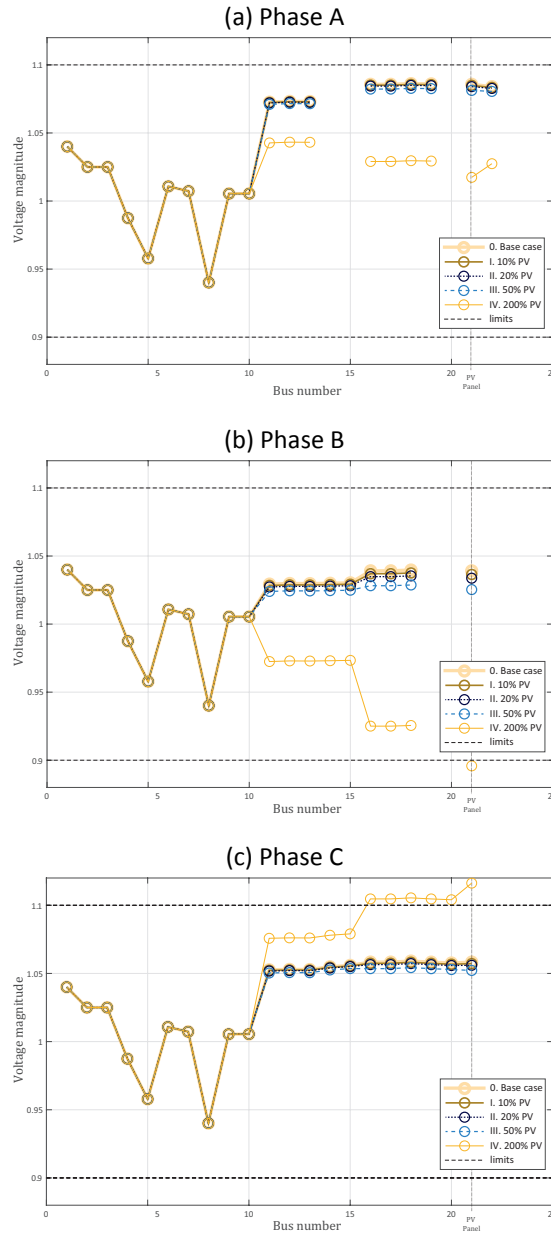Figure 7.1: Steady-state voltage profile of the three phases of the T9-D13 Network having different levels of PV penetration. The operating limits, which the voltages should note exceed, are given. The vertical line shows the location of the bus to which the PV panels are connected. The missing information on certain buses is because the distribution feeder contains single, double and three-phase laterals.

Table 7.1: The minimum and maximum voltage magnitudes of phases a, b, and c. Test cases T118-D123 and T118-10D123 are shown. Almost all the voltage magnitudes are within the safe operating range. The ones that fall outside the range are in bold.

Test-case T118-D123

Scenario	Voltage levels					
	V_{min}^a	V_{max}^a	V_{min}^b	V_{max}^b	V_{min}^c	V_{max}^c
0.	0.97	1.08	0.96	1.03	0.97	1.06
I.	0.97	1.08	0.97	1.03	0.97	1.05
II.	0.97	1.08	0.97	1.03	0.97	1.05
III.	0.97	1.07	0.97	1.03	0.97	1.05
IV.	0.97	1.04	**0.91**	1.01	0.97	**1.13**

Table 7.2: The minimum and maximum voltage magnitudes of phases a, b, and c. Test cases T118-D123 and T118-10D123 are shown. The boldface printed magnitudes exceed the voltage magnitude limits of distribution test cases.

Test-case T118-10D123

Scenario	Voltage levels					
	V_{min}^a	V_{max}^a	V_{min}^b	V_{max}^b	V_{min}^c	V_{max}^c
0.	0.96	**1.12**	0.96	1.07	0.96	**1.10**
I.	0.96	**1.12**	0.96	1.07	0.96	**1.10**
II.	0.96	**1.12**	0.96	1.07	0.96	1.09
III.	0.96	**1.12**	0.96	1.07	0.96	1.09
IV.	0.96	1.08	**0.90**	1.05	0.96	**1.17**

The test case including multiple distribution networks, the T118-10D123 test case, is exceeding its maximum safe operating limit. But, this is already happening during the zero PV penetration level. This is rather caused by the number of distribution networks than the amount of PV penetration.

The authors of [42] studied the effects of several levels of PV penetration on distribution networks only. They also conclude that the effects on voltage levels are limited. Our results are in line with their findings.
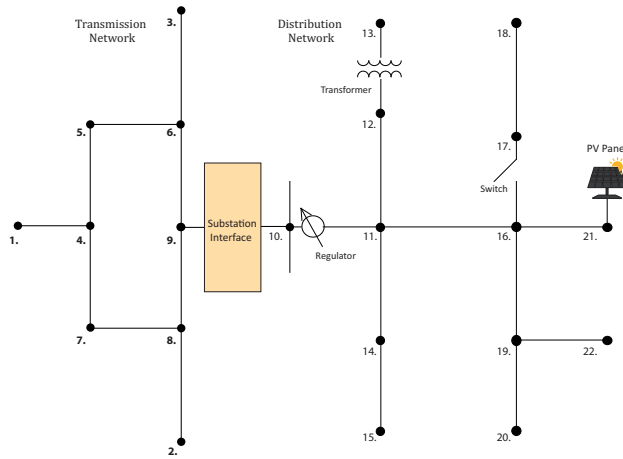
Figure 7.2: The T9-D13 test case visualised. The left part is the 9-bus meshed transmission network. It is connected at bus 9 via a substation interface to bus 10, which is the original slack bus of the distribution network. The special elements are visualised. The residential rooftop PV panel is located at bus 21 of the integrated network.

7.3.2. Amount of imbalance on transmission and distribution networks

The amount of PV penetration can lead to an increased imbalance in both distribution and transmission networks. Distribution networks are already unbalanced network and PV power penetration can increase the amount of imbalance. The National Electrical Manufacturers Association (NEMA) uses the following definition for the amount of imbalance:

$$V_{unb} = \frac{MaxDevfromV_{average}}{V_{average}} \cdot 100\% \tag{7.2}$$

Voltage unbalance of distribution systems should not exceed 5% according to the recommended standard under normal steady-state conditions [7], while the amount of imbalance on transmission systems should be as minimal as possible. Table 7.3 shows the amount of imbalance on distribution networks for the defined scenarios in three test cases.

7.3.3. Comparison to Homogeneous networks

We show the amount of imbalance in transmission networks by modelling the system in a homogeneous format. We only show this amount for:

1. The base case,

2. Scenario III: 50% PV penetration,

3. The extreme scenario (scenario IV), 200% PV penetration.

This is shown in table 7.3.

Table 7.3: The amount of imbalance on transmission and distribution systems using varying levels of PV penetration of a homogeneous network representation of the integrated system. The imbalance that exceeds operating limits are in bold.

	Network							
	Distribution					Transmission		
	Penetration Scenarios					Penetration Scenarios		
	0.	I.	II.	III.	IV.	0.	III.	IV.
Test case	V_{unb} %	V_{unb} %	V_{unb} %	V_{unb} %	V_{unb} %	V_{unb} %	V_{unb} %	V_{unb} %
T9-D13	2.33	2.40	2.47	2.69	**11.29**	0.04	0.04	0.36
T118-D123	2.15	2.19	2.19	2.27	**10.99**	0.03	0.04	0.27
T118-10D123	2.17	2.21	2.21	2.27	**11.14**	0.10	0.11	0.67

Table 7.3 shows that the amount of imbalance on distribution networks stays within a limit of 5% when penetrating the networks with a standard amount of PV penetration. Also, the amount of imbalance in transmission networks is limited. Only when penetrating the networks with an extreme amount of PV, one see that the imbalance increases beyond its limits. Even then, the amount of imbalance in transmission networks is limited. This means that as long the amount of PV penetration stays within its operating limits, hybrid network formulation is sufficient for doing integrated power flow computations. As soon as the amount of PV penetration reaches the critical limit for the amount of imbalance or voltage deviation, measures need to be taken at the distribution level as the imbalance increases already beyond its limits and will probably not influence transmission networks.

The authors of the MonoTri formulation [10] also assess the amount of unbalance on transmission networks. Their results confirm that the amount of unbalance is limited under certain levels of PV penetration [48].

7.4. Overview and Conclusion

The increasing amount of residential photovoltaic (PV) panels connected near the loads at the distribution network can lead to several effects which can be harmful to both the distribution and transmission networks. Residential rooftop panels are in general not capable of supplying reactive power. The lack of reactive power can lead to a voltage drop in the steady-state voltages and exceed the limits that are designed for safe operating conditions. Next to that, increased PV penetration can increase the amount of imbalance due to the design of the distribution network. The amount of imbalance can also have harmful consequences for electrical power systems and should therefore not exceed a certain limit.

Therefore it is important to analyse electrical power systems as integrated systems. Integrated systems are necessary to study the steady-state voltage levels of transmission and distribution networks simultaneously including the interaction that these

networks have on each other. Hybrid networks are numerically the most efficient representations of integrated networks, but not capable of showing possibly induced imbalance on transmission networks. As power flow studies become more complex and time-consuming, we need an efficient tool to analyse integrated systems while making sure any imbalance does not remain unnoticed due to the choice of a single-phase transmission network representation. Therefore, we simulated the effects of increased residential PV power generation and analysed whether hybrid networks are sufficiently capable of studying these networks or whether we should use a homogeneous network representation.

We ran several steady-state power flow simulations on integrated transmission-distribution networks to investigate whether the voltages exceed their safe operating limits and induce imbalance in distribution and transmission networks. We used these simulations to analyse the effects of increasing the amount of PV penetration by comparing various levels of PV penetration with a base case of zero PV power. We used standard penetration levels of 10, 20, and 50 %, and an extreme case of 200 %. In the extreme case, PV power is only injected through phase a. This is done, to intensify the effects that PV penetration can have on transmission networks.

The simulations show that under normal levels of PV penetration, the steady-state voltages of distribution networks slightly drop but never exceed the safe operating limits. The amount of imbalance increases slightly, but not to an extent that would be harmful to distribution networks. Only in the extreme scenario, do we see the effects on the transmission network. We see a slight drop in voltage magnitude in some buses and a tiny amount of extra imbalance compared to the base case. Yet, this extreme scenario is already so harmful for distribution networks, that measures should be taken at the distribution level to prevent harmful amounts of imbalance or voltage drop. We expect that these preventive measures will also decrease the effects on the transmission network. This means that the hybrid network representation of the integrated system is sufficient to analyse the steady-state behaviour of electrical power systems.

To summarise, we conclude that a hybrid network model is a sufficient tool to analyse the effects of increased PV penetration of integrated electrical power systems. The amount of induced imbalance and the increased voltage drop are still within safety margins according to distribution operating standards and transmission networks are not affected during these normal scenarios. The extreme case shows a slight increase in imbalance, but as the effects on distribution networks are much worse, we expect that preventive measures will be taken at the distribution level such that this will not influence transmission networks.

As a result of this study, our large system analysis (present in part III of this thesis) proceeds exclusively with simulations on hybrid network configurations.

7

III

Large Integrated Systems

8

Linear System Solvers

8.1. Introduction

We solve the non-linear power flow equations as described in equations 2.8, 3.3 and 3.4 with the Newton-Raphson (NR) method, using either power or current mismatches. As can be seen in equation 4.1, during every NR iteration ν, the following linear system is solved:

$$-J(\mathbf{x}^{\nu})\Delta\mathbf{x}^{\nu} = \mathbf{F}(\mathbf{x}^{\nu}) \tag{8.1}$$

where J is the Jacobian matrix and F is the power or current mismatch vector. To make this chapter better readable, we rewrite this linear system into the following standard form:

$$-J(\mathbf{x}^{\nu})\Delta\mathbf{x}^{\nu} = \mathbf{F}(\mathbf{x}^{\nu})$$
$$\Leftrightarrow$$
$$A\mathbf{x} = \mathbf{b}$$

We call A the coefficient matrix. When this system is solved using the Matpower library —which is done in the simulations in the previous chapters—, a direct method is used: the LU-factorisation. Direct methods are known to scale badly when linear systems get very large, which is the case for load flow studies on (integrated) transmission and distribution networks. Iterative methods are known to perform better on very large and sparse linear systems and are therefore considered to be better applicable when solving load flow problems [49]. Newton methods which use an iterative method to solve the linear system, are called inexact Newton methods because equation (8.1) is not solved with full accuracy, but until a certain stopping criterion η holds:

$$\frac{||\mathbf{r}||}{||\mathbf{b}||} \leqslant \eta,$$

The sections 8.1 until 8.5 of this chapter are based on the book of Y. Saad [49]

where $r = b - Ax$ is the residual. This chapter describes the theory of some direct and iterative methods —among which Krylov subspace and stationary methods— that work well in combination with Newton methods. As the performance of iterative methods often depends on preconditioners, we also explain how preconditioning works and which methods can be used as preconditioners. As the performance of preconditioners depends on the structure of linear systems, we also explain briefly how matrix columns and vectors can be reordered. Finally, we explain three of the most common preconditioned iterative methods that are used to solve Newton-Raphson-based power flow calculations on both transmission and distribution networks, from which we expect to work on integrated systems as well.

8.2. Direct methods

A direct method solves a linear system in a finite and predetermined number of steps. If we consider the general linear system $Ax = b$, it can be solved directly by using the inverse of the coefficient matrix (A^{-1}) as follows:

$$x = A^{-1}b$$

It is not very efficient to calculate the inverse of a matrix and therefore most direct methods perform a factorisation of the coefficient matrix and then solve this system. The best-known factorisation technique is LU-factorisation.

Solving a linear system with a sparse, positive-definite coefficient matrix using factorisation, works in four steps: a re-ordering step, a factorisation step, a forward sweep, and a backward sweep.

Re-ordering of matrix A is necessary to improve the quality of the factorisation.

The factorisation step is the factorisation of A into a lower and upper triangular matrix, L and U respectively, such that:

$$LUx = b, \quad \text{where}$$
$$A = LU$$

The forward and backward sweeps are applied to the following systems respectively:

$$Ly = b$$
$$Ux = y$$

Direct methods lead —in exact arithmetic— to an exact solution of the linear system, while iterative methods lead to an approximate solution. Nevertheless, the arithmetic of a computer is never exact, so round-off errors will always depend on the finite precision of the computer.

8.3. Iterative methods

To introduce iterative methods, we regard the following linear system:

$$A\mathbf{x} = \mathbf{b}.$$

We start with an initial iterate $\mathbf{x}_0$ and at each iteration k we keep updating the solution $\mathbf{x}_k$ until we consider $\mathbf{x}_k$ to be close enough to the exact solution $\mathbf{x}^*$. As we do not know the solution $\mathbf{x}^*$, we evaluate the residual of the linear system instead. The residual of this linear system is defined as:

$$\mathbf{r}_k = \mathbf{b} - A\mathbf{x}_k, \tag{8.2}$$

where $\mathbf{r}_k$ is the residual of the system at iteration k.

Using the residual as stopping criterion   To show how the residual is used to define a good stopping criterion for the iterative method, an estimate of the exact solution $\mathbf{x}^*$ is necessary. If we substitute $A\mathbf{x}^*$ into the residual relation for $\mathbf{b}$, we get the following:

$$\mathbf{r}_k = A\mathbf{x}^* - A\mathbf{x}_k = A(\mathbf{x}^* - \mathbf{x}_k)$$
$$\Leftrightarrow A^{-1}\mathbf{r}_k = \mathbf{x}^* - \mathbf{x}_k = \mathbf{e}_k,$$

where $\mathbf{e}_k$ is the error of the solution at iteration k. We can find an upper bound on the magnitude of the error by the following relation: By the multiplicative property of the norm $|| \cdot ||$, we know that

$$||\mathbf{e}_k|| = ||\mathbf{x}^* - \mathbf{x}_k|| = ||A^{-1}\mathbf{r}_k|| \leqslant ||A^{-1}||||\mathbf{r}_k||.$$

The relative error can be obtained by dividing this equation by $||\mathbf{x}^*||$:

$$\frac{||\mathbf{e}_k||}{||\mathbf{x}^*||} = \frac{||\mathbf{x}^* - \mathbf{x}_k||}{||\mathbf{x}^*||} \leqslant ||A^{-1}||\frac{||\mathbf{r}_k||}{||\mathbf{x}^*||}. \tag{8.3}$$

As we do not know the exact solution to the linear system, we need to get rid of $||\mathbf{x}^*||$ at the right-hand side of the equation. We use the following relationship:

$$||\mathbf{b}|| = ||A\mathbf{x}^*|| \leqslant ||A||||\mathbf{x}^*|| \tag{8.4}$$

$$\Leftrightarrow$$

$$\frac{1}{||\mathbf{x}^*||} \leqslant \frac{||A||}{||\mathbf{b}||}. \tag{8.5}$$

If we substitute (8.5) into (8.3) and use the condition number $\kappa(A) = ||A||||A^{-1}||$, we obtain:

$$\frac{||\mathbf{e}_k||}{||\mathbf{x}^*||} = \frac{||\mathbf{x}^* - \mathbf{x}_k||}{||\mathbf{x}^*||} \leqslant ||A^{-1}||||A||\frac{||\mathbf{r}_k||}{||\mathbf{b}||} = \kappa(A)\frac{||\mathbf{r}_k||}{||\mathbf{b}||} \tag{8.6}$$

If the condition number is not too large, we can use $\frac{||\mathbf{r}_k||}{||\mathbf{b}||}$ as a good approximate of the relative error such that it can be used as a stopping criterion for iterative methods: If it is lower than a certain tolerance value ε, we say that the linear system has converged.

The condition number and the machine precision, determine the loss in precision due to round-off errors. A general rule of thumb to make sure the condition number, $\kappa(A)$, is not too large for the machine precision that you are using, is to check whether the following relationship holds:

$$\kappa(A) \cdot \text{machine precision} < 10^{-3}$$

In the following subsections, we treat well-known basic iterative methods such as Jacobi and Gauss-Seidel, more advanced stationary methods, namely Algebraic Multigrid and Domain Decomposition methods, and, lastly, well-known Krylov subspace methods (non-stationary methods) such as GMRES and Conjugate Gradients.

8.3.1. Basic Iterative methods

Basic iterative methods to solve $A\mathbf{x} = \mathbf{b}$ are of the form:

$$\mathbf{x}_{k+1} = G\mathbf{x}_k + \mathbf{c}, \tag{8.7}$$

where G and $\mathbf{c}$ are to be defined. Most classical basis methods define a splitting of matrix A of the form:

$$A = M - N \tag{8.8}$$

G is therefore given by $G = I - M^{-1}A$, or by: $G = M^{-1}N$, while $\mathbf{c}$ by: $\mathbf{c} = M^{-1}\mathbf{b}$. We solve the system as follows:

$$\mathbf{x}_{k+1} = G\mathbf{x}_k + \mathbf{c}$$
$$\Leftrightarrow$$
$$\mathbf{x}_{k+1} = M^{-1}N\mathbf{x}_k + M^{-1}\mathbf{b} \tag{8.9}$$

The most simple version of this basic iterative method is Richardson iteration, where M is chosen as $M = I$ and N as $N = I - A$. The system is then solved as follows::

$$\mathbf{x}_{k+1} = (I - A)\mathbf{x}_k + \mathbf{b} \tag{8.10}$$
$$\Leftrightarrow \mathbf{x}_{k+1} = \mathbf{x}_k + \mathbf{r}_k.$$

Jacobi, Gauss-Seidel, and Successive Over Relaxation (SOR) methods are all based on this classical technique but use different splittings. They can also be seen as preconditioned versions of Richardson iterations [12].

Jacobi

The Jacobi method splits matrix A into $A = L + D + U$. If we use the standard notation of the splitting, equation (8.8), then $M = D$ and $N = -(L + U)$. Using (8.9), the iterative solution step of the system looks as follows:

$$\mathbf{x}_{k+1} = D^{-1}[\mathbf{b} - (L + U)\mathbf{x}_k] \tag{8.11}$$

The Jacobi method is guaranteed to converge when A is strictly row diagonally dominant.

Gauss-Seidel

Gauss-Seidel (GS) can be regarded as an improved version of Jacobi, where we again split A into $A = L + D + U$. For forward Gauss-Seidel, we put $M = D + L$ and $N = -U$, and for backward Gauss-Seidel, we put $M = D + U$ and $N = -L$. The solution step changes then respectively for forward and backward GS into:

$$x_{k+1} = (D + L)^{-1}[b - Ux_k] \tag{8.12}$$

$$(D + U)x_{k+1} = b - Lx_k \tag{8.13}$$

GS is guaranteed to converge when A is strictly diagonally dominant or when A is SPD. GS is in general faster than Jacobi.

Successive Over Relaxation

The Successive Over Relaxation method (SOR) is the accelerated version of GS by using a weight factor ω, also called the relaxation parameter. It is based on the splitting:

$$\omega A = (D + \omega L) - ((1 - \omega)D - \omega U) = \omega M - \omega N \tag{8.14}$$

The matrices M and N become as follows:

$$M = \frac{1}{\omega}D + L \tag{8.15}$$

$$N = (\frac{1}{\omega} - 1)D - U \tag{8.16}$$

Note that for $\omega = 1$, SOR is equal to Gauss-Seidel. If $\omega > 1$ we have over-relaxation and if $0 < \omega < 1$ we have under-relaxation.

8.3.2. Advanced stationary iterative methods

Two more advanced stationary methods that can be used to solve large, sparse linear systems are the Algebraic Multigrid (AMG) method and the Additive Schwarz Method (ASM). The AMG method is an extension of multigrid methods to general matrices. ASM is a domain-decomposition method.

Algebraic Multigrid (AMG)

In the AMG method, we solve the linear system $Ax = b$ by defining a coarse problem using the Galerkin approach:

$$A_H = I_h^H A_h I_H^h, \quad f^H = I_h^H f^h, \tag{8.17}$$

where I_h^H is the restriction operator and I_H^h, the prolongation operator. A_h is the original matrix A, it is derived from the underlying graph induced by the power network. As an example, a fine grid could contain details at household level, whereas nodes in a coarse grid could represent a neighbourhood or even a city. We will not go into further details of this method as it will not be used in our analyses.

Domain Decomposition: Additive Schwarz Method (ASM)

ASM is a domain-decomposition approach, where we solve the linear system $Ax = b$ using the partitioning of a graph into subsets. Consider a graph $G = \{W, E\}$, where

W is the set of vertices representing n unknowns and E is the set of edges, for which it holds that:

$$E = \{(i,j)|a_{ij} \neq 0\}.$$

We partition the set of vertices W into non-overlapping subsets W_i. We define W as the union of subsets as follows:

$$W = \bigcup_{i=1}^{N} W_i.$$

At each subset W_i, we define a restriction operator R_i, for which holds that:

$$R_i = \{r_{ii}|r_{ii} = 1 \text{ if } i \in W_i\}$$

We can define the coefficient matrix A_i belonging to each subset:

$$A_i = R_i A R_i^T$$

Our iterative process then becomes:

$$x_{k+1} = x_k + \sum_{i=1}^{n} R_i^T A_i^{-1} R_i (\mathbf{b} - A\mathbf{x}) \tag{8.18}$$

The overlapping ASM method divides the coefficient matrix A into blocks that overlap through a small number of elements. An obvious choice for the overlapping buses could be for example the connecting buses of the transmission and distribution networks. Each block is then related to a zone in the network where a zone can represent (a part of a) separate transmission or distribution system.

8.3.3. Non-stationary Iterative methods

Other important iterative methods available for large linear systems are the Krylov methods, which are non-stationary methods. Krylov subspace methods are more complex than basic iterative methods but do have better convergence properties. These methods are based on projection processes onto Krylov subspaces. A general Krylov subspace is a subspace spanned by vectors of the form $p(A)v$, where p is a polynomial. These techniques approximate $x = A^{-1}\mathbf{b}$ by using the polynomial $p(A)$:

$$x \approx p(A)\mathbf{b}.$$

A Krylov subspace of dimension m is the following set of vectors:

$$\mathcal{K}_m(A, v) = \text{span}\{v, Av, A^2v, \ldots, A^{m-1}v\} \tag{8.19}$$

A property of Krylov subspace methods is that $\mathcal{K}_m$ is the subspace of all vectors in $\mathbb{C}^n$ which can be written as $x = p(A)v$, p is a polynomial of degree uttermost $m-1$.

Computing Orthogonal bases

The Arnoldi method is a technique to compute an orthogonal basis of the Krylov subspace $\mathcal{K}_m$ for general non-Hermitian matrices. A Hermitian matrix is a matrix where

the conjugate transpose of A is equal to itself ($A = \overline{A^T}$). Arnoldi methods are mainly used to efficiently approximate eigenvalues of large sparse matrices and were later introduced to solve linear systems.

The idea is to start with a vector v_1 such that $||v_1||_2 = 1$. Then, at every iteration, Arnoldi's method multiplies the Arnoldi vector v_j by A and then normalizes the resulting vector w_j against all previous v_i's by, for example, a Gram-Schmidt procedure.

When we denote V_m as the matrix with column vectors $v_1, ...v_m$ (the Arnoldi vectors), $\overline{H}_m$ as the Hessenberg matrix whose nonzero entries h_{ij} are defined by the vectors that are the result of inner product between Av_j and v_i for $i = 1, 2, .., j$, and H_m which is obtained from $\overline{H}_m$ by deleting its last row. Then we can derive the following relations:

$$AV_m = V_m H_m + w_m e_m^T$$
$$= V_{m+1} \overline{H}_m$$
$$V_m^T A V_m = H_m$$

Lanczos iteration is equal to Arnoldi iteration but then applied to symmetric A. The Hessenberg matrix H_m then simplifies to a tridiagonal matrix.

The different Krylov subspace methods depend on the choice for subspace $\mathcal{L}_m$ and on the way the system is preconditioned. Common choices for $\mathcal{L}_m$ are simply $\mathcal{K}_m$ or the minimum residual version: $A\mathcal{K}_m$. In the following paragraphs, we treat some of the best-known Krylov subspace methods —amongst which are the Full Orthogonalisation Method, Conjugate Gradient Method, and GMRES— and describe how they depend on the different subspaces.

The Full Orthogonalisation Method

Arnoldi method used as a method to solve linear systems is called FOM: Full Orthogonalisation Method. The subspace $\mathcal{L}_m$ that is chosen is the subspace related to the coefficient matrix A and the residual $\mathbf{r}_0$: $\mathcal{L}_m = \mathcal{K}_m(A, \mathbf{r}_0)$, where $\mathbf{r}_0 = \mathbf{b} - A\mathbf{x}_0$. $\mathcal{K}_m(A, \mathbf{r}_0)$ is expressed as follows:

$$\mathcal{K}_m(A, \mathbf{r}_0) = \text{span}\{\mathbf{r}_0, A\mathbf{r}_0, A^2\mathbf{r}_0, \ldots, A^{m-1}\mathbf{r}_0\}.$$

The approximate solution $\mathbf{x}_m$ from the affine subspace $\mathbf{x}_0 + \mathcal{K}_m(A, \mathbf{r}_0)$ is extracted such that the Petrov-Galerkin condition holds, which is:

$$\mathbf{b} - A\mathbf{x}_m \perp \mathcal{L}_m.$$

Arnoldi is used to compute the orthogonal basis of this subspace, where we choose the Arnoldi vectors in relation to the residual where $v_1 = \frac{\mathbf{r}_0}{||\mathbf{r}_0||_2}$. We can rewrite $\mathbf{x}_m$ as $\mathbf{x}_m = \mathbf{x}_0 + V_m \mathbf{y}_m$ equivalently by using the relations to the Arnoldi method:

$$V_m^T A V_m = H_m,$$
$$V_m^T \mathbf{r}_0 = V_m^T(\beta v_1) = \beta \mathbf{e}_1,$$

where $\beta = ||\mathbf{r}_0||_2$. H_m is the upper Hessenberg matrix and V_m is the n by m matrix formed by the first m Arnoldi vectors v_m. We then compute $\mathbf{x}_m$, by solving the

following two equations subsequently:

$$y_m = H_m^{-1}(\beta e_1) \tag{8.20}$$

$$x_m = x_0 + V_m y_m \tag{8.21}$$

Conjugate Gradient

The Conjugate Gradient (CG) method is the best-known iterative technique to solve sparse symmetric positive definite (SPD) linear systems. It minimises the energy

$$E(x) = \frac{1}{2} x^T A x - x^T b \tag{8.22}$$

recursively. The conjugate gradient method is Lanczos iteration used to solve linear systems [50]. It is equivalent to FOM but it uses short recurrences. As CG is applied to SPD systems, the approximate solution is obtained as:

$$x_m = x_0 + V_m y_m,$$

where $y_m = T_m^{-1}(\beta e_1)$, with T_m is a tridiagonal matrix.

Bi-CG

Bi-CG is a Conjugate Gradient method that uses a dual system $\mathcal{L}_m = \overline{\mathcal{K}}_m = \mathcal{K}_m(A^T, r_0)$, where

$$\mathcal{K}_m = \text{span}\{v_1, A v_1, A^2 v_1, \ldots, A^{m-1} v_1\}$$

and

$$\mathcal{L}_m = \text{span}\{w_1, A^T w_1, (A^T)^2 w_1, \ldots, (A^T)^{m-1} w_1\}$$

are orthogonal. The solution is approximated from the to process onto $\mathcal{K}_m$. We select $v_1 = \frac{r_0}{||r_0||_2}$ and w_1 such that $(v_1, w_1) \neq 0$, but often w_1 is selected such that $v_1 = w_1$. This residual is orthogonal to $\mathcal{K}_j(A^T)$. The Bi-CG method is a natural extension of CG to unsymmetric A (using two Krylov subspaces).

Bi-CGSTAB   Bi-CGSTAB is also a Conjugate Gradient type of method. In Bi-CG, the subspace $\mathcal{L}_m$ is not used to improve the solution, while in Bi-CGSTAB also the computations to construct $\mathcal{L}_m$ are exploited to obtain a better approximation. For many problems, this makes Bi-CGSTAB converge faster than Bi-CG.

GMRES

GMRES is a Krylov subspace method that uses the following subspace $\mathcal{L}_m = A\mathcal{K}_m$. This technique minimizes the residual norm over all vectors in $x_0 + \mathcal{K}_m$. The method is similar to Arnoldi, so x_m is obtained by solving

$$x_m = x_0 + V_m y_m,$$

but y_m is now the value that minimizes the following function:

$$J(y) = ||b - A x_m||_2 = ||\beta e_1 - \overline{H}_m y||_2, \tag{8.23}$$

such that y_m can be written as:

$$y_m = \text{argmin}_y ||\beta e_1 - \overline{H}_m y||_2. \tag{8.24}$$

GMRES is a general-purpose method and can be applied to non-symmetric linear systems. Convergence is ensured for any non-singular matrix.

8.4. Preconditioners

Krylov subspace methods are likely to suffer from slow convergence. Therefore, preconditioning is necessary to obtain good convergence results for Krylov subspace methods. Preconditioning is the technique to transform the linear system in such a way that the solution does not change, but is likely to be obtained easier. Mathematically put, preconditioning means finding a matrix M such that the linear system $Mx = b$ can be inexpensively solved, where M should be close to A, and M must be non-singular. Three known ways of applying the preconditioner M to the linear system $Ax = b$, is by left or right multiplication or by using a factorisation of M and a simultaneous right and left multiplication, which is called split preconditioning:

- Left preconditioning:

$$M^{-1}Ax = M^{-1}b \tag{8.25}$$

- Right preconditioning:

$$AM^{-1}u = b, \quad x = M^{-1}u \tag{8.26}$$

- Split preconditioning:

$$M = M_L M_R$$
$$M_L^{-1}AM_R^{-1}u = M_L^{-1}b, \quad x = M_R^{-1}u \tag{8.27}$$

All stationary iterative methods can be used as preconditioners for Krylov subspace methods. In the following paragraphs, we explain some of these methods when used as preconditioners.

8.4.1. Incomplete factorisation as preconditioner

Direct methods are used to solve general linear systems. The LU-factorisation for example, decomposes the matrix A into a lower and upper triangular matrix, such that the system can be solved efficiently. A downside of this factorisation is that the original sparsity pattern of matrix A is not preserved, increasing the memory requirements of the system. Therefore, one can use an incomplete factorisation of matrix A, but you will lose accuracy in the solution to this system. For this reason, incomplete factorisation is often used as a preconditioner to the Krylov subspace method.

(Incomplete) LU

The first general technique we consider is an incomplete LU-factorisation (ILU) of A that has the form $A = LU - R$, where R is the residual of the factorisation. In this incomplete factorisation, the non-zero structure of L and U remain in the same order as matrix A such that the memory requirements do not increase. Generally, a larger R means that it is less expensive to compute the factorisation, but at the cost of accuracy. Therefore, several possibilities of ILU exist which are a trade-off between memory needed and the number of iterations, where LU is the complete LU-factorisation, without residuals. We express $ILU(p)$ as incomplete factorisation allowing a degree p of fill-in. Fill-in is a term that relates the amount of allowing additional non-zero entries in the factors L and U compared to A. The most simple

form, $ILU(0)$, has the same non-zero structure as A, so 0 additional fill-in. Allowing more fill-in will lead to a more accurate approximation but at the cost of efficiency. $ILU(1)$ allows first-order fill-ins such that the system has the same sparsity pattern as A^2. In general, $ILU(p)$ has the same sparsity pattern as A^{p+1}.

Another property for making an incomplete factorisation is to use a drop tolerance. This is a set of rules to replace elements with zero if it satisfies a certain set of criteria. For example for $ILU(0.1)$, a dropping rule could be to discard all elements in the factorisation that are smaller in absolute value than 0.1.

(Incomplete) Cholesky
The incomplete Cholesky (IC) factorisation of an SPD matrix is often used as a pre-conditioner for CG methods. The complete Cholesky factorisation is determined as $A = LL^T$. The incomplete factorisation can be based on the sparsity pattern of the original coefficient matrix A.

8.4.2. Iterative methods as preconditioners: Jacobi, GS, SOR, and SSOR
The iterative methods Jacobi, GS, SOR, and SSOR, can also be used as preconditioners. They split the coefficient matrix A into $A = M - N$, as described in the section on basic iterative methods. These preconditioned matrices are used in the Krylov subspace methods. We get the following preconditioned system:

$$M^{-1}Ax = M^{-1}b,$$

where M depends on the choice of preconditioning method: Jacobi, SOR, or SSOR. If we recall that we split our system as $A = M - N = D + L + U$, then we can define the following preconditioning matrices from the direct methods:

- Jacobi:

$$M = D \tag{8.28}$$

- GS:

$$M = D + L \tag{8.29}$$

- SOR:

$$M = \frac{1}{\omega}(D + \omega L) \tag{8.30}$$

- SSOR:

$$M = \frac{1}{\omega(2 - \omega)}(D + \omega L)D^{-1}(D + \omega U) \tag{8.31}$$

8.4.3. Stationary methods: Domain Decomposition as preconditioner

We can use the ideas of the additive Schwarz method to form a preconditioner. Recall that the iterative process of the ASM method is the following:

$$x_{k+1} = x_k + \sum_{i=1}^{n} R_i^{\mathsf{T}} A_i^{-1} R_i (b - Ax_k) \tag{8.32}$$

Note that $\sum_{i=1}^{n} R_i^{\mathsf{T}} A_i^{-1} R_i$ can also be used as explicit inverse of the preconditioner M and be applied to precondition any Krylov method, where $M^{-1} = \sum_{i=1}^{n} R_i^{\mathsf{T}} A_i^{-1} R_i$.

8.5. Re-ordering

Re-ordering is a necessary step that must be taken before a factorisation is constructed. Both when the factorisation is used as a direct method to solve the linear system or when it is used as a preconditioner to a non-stationary iterative method. Re-ordering improves the quality of incomplete factorisations [12]. Minimum Degree ordering methods work well on network types of problems [51]. These methods are used for re-ordering of structurally symmetric, sparse matrices before numerical factorisations. Both the Approximate Minimum Degree (AMD) and Quotient Minimum Degree (QMD) have been tested to solve power flow computations [12] [52]. As the performance of these methods is similar but as QMD is natively available in the library PETSc in which we work, we have decided to use QMD as the reordering method of use in our power flow simulations.

8.6. Newton-Krylov methods

A Newton-Krylov method is a combination of a Newton-Raphson method for the non-linear solve of the power flow equations and a Krylov method to update the linear step of the Newton-Raphson method. Remember that during every NR iteration (both in NR-power and NR-TCIM), we need to solve the following linear system:

$$-J(x^\nu)\Delta x^\nu = F(x^\nu),$$
$$\Leftrightarrow$$
$$Ax = b,$$

where J is the Jacobian matrix.

Preconditioned GMRES and preconditioned Bi-CGSTAB, with an (incomplete) LU factorisation as a preconditioner, are best-known methods to solve power flow systems for transmission networks [12], and have been proven to work for distribution networks as well [53]. As reordering improves the quality of (in)complete LU factorisations, this is a necessary step before the factorisation. Minimum Degree type of methods had the best performance. To work with protected data input —specifically for integrated system analysis— the Overlapping Additive Schwarz could be used as a preconditioner, where privacy of the separate network is obtained [9]. The separate networks are assigned to a different processor and solved as a separate linear system using a direct LU-solver. This method is visualised in figure 8.1. Instead of a direct method, one could also use another iterative method per electricity network or zone in this network.

> **Newton**: until non-linear residual is small. **Do:**
> $\nu \to \nu + 1$
>
> 1. Solve equation (8.1) using Krylov-Schwarz
>   **Krylov**: until linear residual is small **Do:**
> $k \to k + 1$
> 2. Solve equation (8.24)
> 3. Compute linear residual
> 4. Preconditioning using Schwarz
>   **Schwarz**:
>   5. Perform each block using $M^{-1}_{Schwarz} = R_i^T A_i^{-1} R_i$, where i represents a subset of the network

Figure 8.1: Algorithm of the Newton Krylov Schwarz method, taken from [9]

As seen in the first paragraph of section 8.4, preconditioners can be applied to matrix systems as a left, right, or split preconditioner. We illustrate how preconditioners can be used in combination with Krylov subspace methods by the example of a left preconditioner applied to a linear system:

$$M^{-1}A\mathbf{x} = M^{-1}\mathbf{b}$$

Both GMRES and Bi-CGSTAB are Krylov subspace methods. When left-preconditioning is used, they take their iterates from the left-preconditioned subspace $\mathcal{K}_m^L$:

$$\mathcal{K}_m^L = \text{span}\{z_0, M^{-1}Az_0, \dots, (M^{-1}A)^{m-1}z_0\},$$

where z_0 is the preconditioned residual: $z_0 = M^{-1}(\mathbf{b} - A\mathbf{x}_0)$. and the solution $\mathbf{x}_m$ is taken from

$$\mathbf{x}_m \in \mathbf{x}_0 + \mathcal{K}_m^L$$

The right and split preconditioners work similarly.

8

8.6.1. Numerical Experiments to test the performance of inexact Newton Methods on separate networks

It is difficult to judge upfront why certain preconditioned Krylov subspace combinations work best for specific problems. It is common practice to make a decision based on a comparison of the results of power flow simulations with different properties. Therefore, we first analyse the Newton-Krylov methods on separate electricity networks before we continue our analysis on integrated networks. The simulations on integrated networks are the topic of the next chapter (chapter 9).

In the remainder of this chapter, we run simulations on separate transmission and distribution networks. From these simulations, we conclude with which combinations we will continue integrated analyses.

To run the forthcoming simulations, we have used the PETSc library [54]. PETSc is an open-source library where the Newton-Raphson power mismatch to solve single-phase transmission power flow problems is already implemented. The details of this library are found in chapter 9. We have implemented the three-phase distribution power flow solver by continuing the work of [53].

The test cases used are taken from the Matpower library (Transmission networks) [38] and IEEE P&ES Library (Distribution networks) [39]. Details of these test cases are described in Appendix C. To test the performance of the inexact Newton methods, we run simulations on separate transmission networks and separate distribution networks. We used four standard transmission networks from Matpower and we have created nine larger transmission networks by connecting respectively 1, 2, 4, 8, 16, 32, 64, 128, and 264 copies of the T3120 test case to each other. The connections are made by connecting the original reference bus to the rest of the network. We have created these larger test cases to see how the performance of these inexact Newton methods would scale when the size of the test cases increases. We have done similarly for the distribution networks. We have worked with four standard distribution networks from the IEEE P&ES Library and created eight larger distribution test cases by connecting almost the same amount of copies (minus the 264) of the D8500 test case.

The results of the transmission network are presented in table 8.1 and figure 8.2 and these of the distribution network in table 8.2 and figure 8.3.

8

Table 8.1: Several transmission test cases of which the linear step is solved using different Krylov subspace-preconditioning combinations. The Iteration number of Newton-Raphson (NR) and the Krylov method (K) are presented, together with the CPU time to solve the system.

		Testcase											
		T9			T118			T2383			T3120		
		NR	K	Time	NR	K	Time	NR	K	Time	NR	K	sec
Method	**Prec**	$\mathcal{I}_{NR}$	$\mathcal{I}_{K}$	sec	$\mathcal{I}_{NR}$	$\mathcal{I}_{K}$	sec	$\mathcal{I}_{NR}$	$\mathcal{I}_{K}$	sec	$\mathcal{I}_{NR}$	$\mathcal{I}_{K}$	sec
Direct (LU)	-	5	1	3.71e-03	3	1	5.29e-03	6	1	4.13e-02	6	1	5.53e-02
GMRES	LU	5	1	4.05e-03	3	1	5.40e-03	6	1	4.24e-02	6	1	5.78e-02
	ILU(12)	5	1	4.21e-03	3	3	6.05e-03	6	7	5.04e-02	6	10	6.99e-02
	ILU(8)	5	1	4.15e-03	3	4	5.81e-03	6	11	5.37e-02	6	17	7.70e-02
	ILU(4)	5	1	3.83e-03	3	8	6.02e-03	6	27	6.85e-02	6	47	1.18e-01
	ILU(0)	5	5	3.89e-03	3	24	6.29e-03	6	193	1.95e-01	6	270	3.05e-01
BCGS	LU	5	1	3.96e-03	3	1	5.79e-03	6	1	4.29e-02	6	1	5.79e-02
	ILU(12)	5	1	4.05e-03	3	2	6.06e-03	6	4	5.25e-02	6	6	7.17e-02
	ILU(8)	5	1	4.09e-03	3	3	5.72e-03	6	7	5.60e-02	6	11	7.97e-02
	ILU(4)	5	1	3.82e-03	3	5	5.70e-03	6	17	7.04e-02	6	24	1.11e-01
	ILU(0)	5	5	4.05e-03	3	17	5.89e-03	6	77	1.42e-01	6	105	2.16e-01

Table 8.1 shows that all linear methods applied to the smaller transmission test cases have similar performance behaviour in terms of CPU time. The time to solve a network lies in the same order of magnitude per test case. The number of iterations differs per linear system solver. For the ILU(0) preconditioner combined with GMRES, we see that the high number of iterations leads to a higher CPU time.

Figure 8.2 shows the CPU time to solve larger test cases. We have decided to only show the time that it takes the method to solve the test case as the number of iterations stays on average the same as the T3120 network without additional connecting copies. As the different preconditioners performed similarly, except for the ILU(0) method, we decided to only show the LU and the ILU(0) preconditioners. This figure shows that initially, the ILU(0) preconditioned versions of GMRES and Bi-CGSTAB perform worse than the other methods, but when size increases they tend to take the same amount of time. Furthermore, the black dotted line shows how the methods would perform when they would scale one-to-one linearly.

8

Table 8.2: Several distribution test cases of which the linear step is solved using different Krylov subspace - preconditioning combinations. The Iteration number of Newton-Raphson (NR) and the Krylov method (K) are presented, together with the CPU time to solve the system.

		Testcase											
		D13			D37			D906			D2500		
		NR	K	Time	NR	K	Time	NR	K	Time	NR	K	sec
Method	Prec	$\mathfrak{I}_{\mathcal{NR}}$	$\mathfrak{I}_{\mathcal{K}}$	sec	$\mathfrak{I}_{\mathcal{NR}}$	$\mathfrak{I}_{\mathcal{K}}$	sec	$\mathfrak{I}_{\mathcal{NR}}$	$\mathfrak{I}_{\mathcal{K}}$	sec	$\mathfrak{I}_{\mathcal{NR}}$	$\mathfrak{I}_{\mathcal{K}}$	sec
Direct (LU)	-	3	1	6.21e-03	5	1	8.29e-03	2	1	3.33e-02	8	1	2.27e-01
GMRES	LU	3	1	5.94e-03	5	1	7.72e-03	2	1	3.67e-02	8	1	2.18e-01
	ILU(12)	3	1	5.99e-03	5	1	7.55e-03	2	1	3.50e-02	8	1	2.17e-01
	ILU(8)	3	1	6.13e-03	5	1	7.15e-03	2	1	3.54e-02	8	1	2.20e-01
	ILU(4)	3	1	5.75e-03	5	1	7.90e-03	2	1	3.57e-02	8	1	2.18e-01
	ILU(0)	3	1	5.67e-03	5	1	7.32e-03	2	1	3.38e-02	8	1	2.17e-01
BCGS	LU	3	1	5.91e-03	5	1	7.71e-03	2	1	3.51e-02	8	1	2.22e-01
	ILU(12)	3	1	5.70e-03	5	1	7.39e-03	2	1	3.53e-02	8	1	2.25e-01
	ILU(8)	3	1	5.83e-03	5	1	6.93e-03	2	1	3.53e-02	8	1	2.24e-01
	ILU(4)	3	1	5.65e-03	5	1	7.30e-03	2	1	3.52e-02	8	1	2.29e-01
	ILU(0)	3	1	6.37e-03	5	1	7.25e-03	2	1	3.58e-02	8	1	2.09e-01

Table 8.2 show similar results as the transmission networks. But as every preconditioned method only takes one Krylov iteration, all the methods perform similarly. The reason that distribution networks take only one inner iteration is that these networks are diagonal dominant and radial, and every bus in the network is only connected to uttermost one previous and one (sometimes two) subsequent buses. Appendix C shows the sparsity pattern of the admittance matrix of the test cases used. Applying the right reordering technique results in an almost diagonal sparsity structure, making direct methods preferable for these test cases. We have redone the simulations in Matpower which resulted in the same results.

Following the same reasoning as transmission networks, we only run simulations with the LU and ILU(0) preconditioners for the larger distribution test cases. Figure 8.3 shows that all these methods perform similarly when the size of the distribution test cases increases.
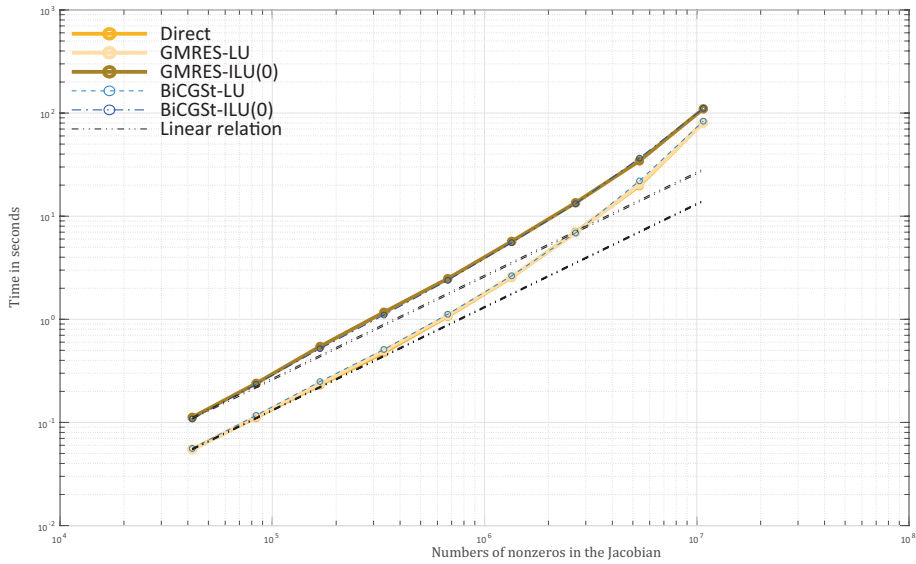
8

Figure 8.2: The CPU time in seconds to solve large transmission systems. The time is plotted against the number of nonzeros in the Jacobian to see how the efficiency of the methods scales when size increases. The black dotted line shows a linear relationship between the method and size.
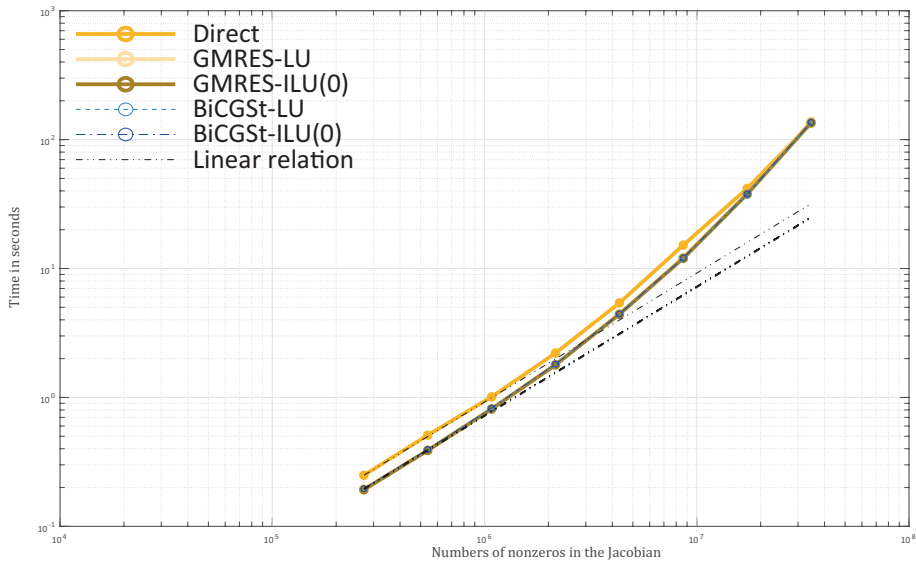
8

Figure 8.3: The CPU time in seconds to solve large distribution systems. The time is plotted against the number of nonzeros in the Jacobian to see how the efficiency of the methods scales when size increases. The black dotted line shows a linear relationship between the method and size.

8.7. Overview

Linear systems are of the form

$$Ax = b.$$

They are solved using direct or iterative methods. Iterative methods are often preferred for large systems. Therefore, we would like to apply them to large electricity networks.

The most straightforward direct method is taking the inverse multiplication of the system. In practice, this is often impossible such that factorisation methods, such as LU or Cholesky factorisation are preferred.

A basic iterative method is of the form:

$$x_{k+1} = Gx_k + c,$$

where G and c are to be defined and A is splitted as $A = M - N$, such that the system can be expressed as:

$$x_{k+1} = M^{-1}Nx_k + M^{-1}b.$$

Table 8.3 gives an overview of the specifications of G, M, N, and c to solve the linear system.

A Krylov subspace method approximates the solution x_m to the linear system $A^{-1}b$ by taking a solution x_m from $x_0 + \mathcal{K}_m(A, r_0)$ such that $b - Ax_m$ is orthogonal to the subspace $\mathcal{L}_m$ (known as the Petrov-Galerkin condition). The choice of the subspace $\mathcal{L}_m$ defines the subspace method. An overview of the explained subspace methods is shown in Tab. 8.4. The Additive Schwarz Method partitions the linear system into subsets W_i where the restriction operator R_i belongs to this subset. Then we can solve the linear system iteratively using:

$$x_{k+1} = x_k + \sum_{i=1}^{n} R_i^T A_i^{-1} R_i (b - Ax_k)$$

Table 8.3: Overview of the matrices in basic iterative methods

Method	Matrix			
	M	N	G	c
Richardson	I	$I - A$	$I - A$	b
Jacobi	D	$-(L + U)$	$-D^{-1}(L + U)$	$D^{-1}b$
forward GS	$D + L$	$-U$	$-(D + L)^{-1}U$	$(D + L)^{-1}b$
backward GS	$D + U$	$-L$	$-(D + U)^{-1}L$	$(D + U)^{-1}b$
SOR	$\frac{1}{\omega}D + L$	$(\frac{1}{\omega} - 1)D - U$	$-(\frac{1}{\omega}D + L)^{-1}U$	$(\frac{1}{\omega}D + L)^{-1}b$

Table 8.4: Summary of the properties of Krylov subspace methods

	Properties		
Method	$\mathcal{L}_m$	Applications	Extra
GMRES	$A\mathcal{K}_m(A, \mathbf{r}_0)$	A not symmetric	Optimality
CG	$\mathcal{K}_m(A, \mathbf{r}_0)$	A is SPD	Optimality
Bi-CG	$\mathcal{K}_m(A^\mathsf{T}, \mathbf{r}_0) = \overline{\mathcal{K}}_m$	-	Short recurrences
Bi-CGSTAB	$\mathcal{K}_m(A^\mathsf{T}, \mathbf{r}_0) = \overline{\mathcal{K}}_m$	-	Short recurrences

Preconditioners are used to obtain better convergence for Krylov subspace methods. It means finding a matrix M such that the linear system does not change, but a solution is obtained more efficiently. It is essentially a matrix (or a factorisation of this matrix) multiplication of a linear system, which is then solved. The preconditioner choice can be an (incomplete) LU-factorisation, an incomplete Cholesky factorisation, any basic iterative method, or a stationary iterative method such as the ASM.

For power flow systems, either GMRES or Bi-CGSTAB is used together with a preconditioner and reordering using QMD. As our separate analyses showed, GMRES combined with an $(I)LU$ factorisation worked best for transmission and distribution systems, which is similar to the work of [12] [53] and [52]. As the inexact Newton methods did not show any unexpected behaviour, we will continue the analysis of integrated power flow simulations in a similar way. These results are shown in the next chapter.

8

9

Results of Large Integrated Power Flow Simulations

9.1. Introduction

We have built a framework to conduct power flow analyses on integrated transmission-distribution systems. We have considered two network representations to conduct these analyses on integrated systems: hybrid and homogeneous networks and two solution methods for the integrated network: unified and splitting methods. The goal of this thesis is to execute these analyses efficiently by using numerical analysis (NA) techniques to make the underlying computations faster. In this chapter, we focus on the efficiency of these methods by analysing the methods on large test cases.

We have shown in chapter 7 and chapter 6 that hybrid network representations are sufficient to analyse integrated power systems and, respectively, that they are also more efficient. Therefore, we restrict ourselves in the remainder of this chapter to analyses of hybrid network representations. In chapter 6, we have tested besides numerical performances the accuracy and realistic conditions of the methods to prove the concept of the framework. In this section, we solely focus on the numerical performance to find the most efficient combination of preconditioned Newton-Krylov solvers for large electrical power grids. For this, we run simulations of up to 1 million unknown variables. The test cases that we use are simplified versions of the ones used in chapters 6 and 7.

We perform our simulations in The Portable, Extensible Toolkit for Scientific Computation (PETSc). PETSc is "an open-source library of advanced data structures and methods for solving linear and nonlinear equations and for managing discretisations" [54]. It contains numerical libraries and an implementation of the transmission power system and the Newton-Raphson Power mismatch solver, from which we will implement the distribution system, the current mismatch solver and the integration frameworks. It contains a wide variety of Krylov methods and preconditioners which we can use to solve our systems.

To summarise, this chapter contains the following content:

1. Recap of the methods that are the object of study: Hybrid network representation and Unified and Manager-Fellow Splitting methods

2. Explanation of the PETSc library and its possibilities to apply Krylov subspace methods and preconditioners to non-linear systems

3. Description of the test cases used

4. Results of the simulations

5. Conclusion and overview

9.2. Methods

In chapter 5, we have described four methods to model and solve integrated power systems that are the objects of review. In chapter 6, we saw that all methods can solve integrated systems —even when they are applied to different conditions— but we concluded that hybrid networks and unified methods were most efficient. As we have illustrated in chapter 7, we could conclude that hybrid networks are sufficient to analyse integrated power systems —and as they are faster than homogeneous network representations— we have decided to proceed exclusively with hybrid networks in this part of the research. Therefore, we only review the Unified and Manager-Fellow Splitting (MFS) methods applied to hybrid networks: The interconnected method and the MFS-hybrid method, respectively. We provide a brief recap of the details of these methods. Also, we repeat the visualisations of these methods in chapter 5 through figures 9.1 and 9.4 (at the end of this chapter).

9.2.1. The interconnected method: Unified method applied to hybrid networks

Hybrid networks contain a single-phase representation of the transmission network while leaving the distribution network in three-phase. Unified methods solve the integrated system as a whole. A substation, which is placed in between the two networks, takes care of the dimension mismatch. It connects a load bus on the transmission side to the original reference bus — which changes therefore in a load bus — at the distribution side. It then solves the new system as a whole.

9.2.2. The MFS-hybrid method: Splitting method applied to hybrid networks

The Manager-Fellow Splitting method keeps two separate systems. It starts by solving the distribution network (the Fellow) and injects the solution obtained at the coupling (also known as the boundary) bus into the Manager. It then solves the transmission network (the Manager) and obtains the updated solution at the boundary bus. This process continues until the voltage of the boundary bus between two subsequent iterations is lower than a certain tolerance value.
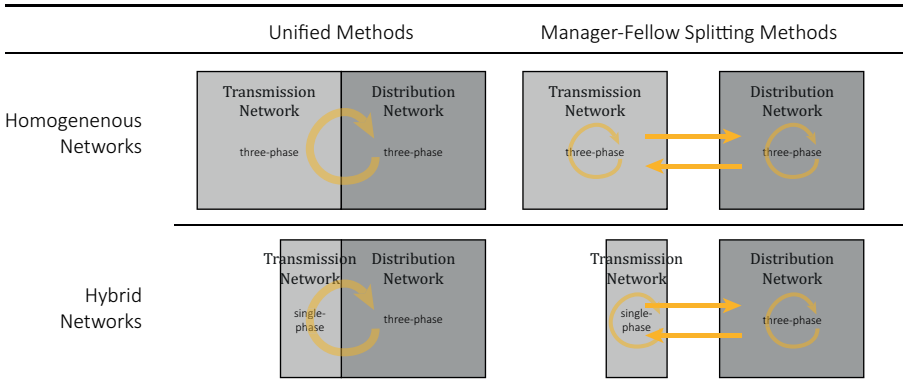
Figure 9.1: Overview of the Modelling (Hybrid and Homogeneous) and Solution (Unified and Splitting) Methods

The boundary bus is the original reference bus of the distribution network and a load bus of the transmission network. As this is a reference bus of the Fellow, the voltage should be initialised before running the Fellow. As a result, we get the power output at this bus that is specified for the Manager. As the boundary bus at the manager side is a load bus, power should be known (see table 2.1). After every MFS run, we get the voltage output of the boundary bus of the Manager which we compare to its output of the previous MFS run. Before voltage and power are injected into their respective network, the quantities have to be scaled to either single-phase or three-phase equivalent. This is explained in section 5.4.2.

9.3. PETSc

PETSc is an open-source library that can handle sequential and parallel computations (supported by the Message Processing Interface (MPI)) to solve large-scale problems. It contains several routines and packages that are built on top of each other to support different types of equations and to allow for flexibility at the level of the non-linear solve, linear solve, and preconditioner [54].

The KSP and PC packages manage the choice for the iterative method and preconditioner to solve linear equations. The SNES package is built on top of the linear solvers and provides numerical routines for solving large-scale nonlinear problems [53]. The power flow problem is part of the DMNetwork structure. DMNetwork is a library that manages the mapping of the network data structure and its physical components to the available PETSc solvers. It provides the underlying infrastructure for managing the network topology and the physics components. Figure 9.2 contains an overview of the build-in routines, packages, and libraries in PETSc. We use DM, SNES, KSP, and PC packages within PETSc that are built in this hierarchical order.

9

9.3.1. DMNetwork

One can view DMNetwork as the library that models the concept of electricity networks by taking care of the network topology (buses, edges) and matching it with the physical components (loads, generators, etc.) in an efficient and scalable framework. It was originally designed for single-network applications but was developed to handle multiple networks such that the interaction between networks can be studied.

The way that DMNetwork is designed allows for solving the subnetwork in a unified or splitting manner by respecting its underlying individual physics. A model for the transmission power flow network was already present in this library, as well as a framework to solve a coupled power-water network. We have added the distribution network to PETSc, based on [53], and the physical coupling framework as described in chapter 5, that manages the correct physical interaction of subnetworks (which was not yet present in PETSc). It uses the concept of shared vertices of DMNetwork. A shared vertex is a vertex that is shared by all processors, in case of parallel computations, which is then the only information that needs to be read by both system operators. PETSc is built in such a way that the rest of the network can remain in the ownership of the respective operator. The shared vertex is the coupling bus of both networks. The information on this bus is thus shared by both operators. The structure of DMNetwork also allows for specifically tailored power or current mismatch functions that correspond to individual networks. This means that as well in the unified methods as in the splitting methods, distribution networks can be solved using NR-TCIM and transmission networks using NR-Power.

9.3.2. SNES

The Scalable Nonlinear Equations Solvers (SNES) library handles the solve of the nonlinear equations and it employs linear solvers from the KSP and PC libraries. The library is based on Newton methods, amongst which Newton line search, to which the user should provide its mismatch function [53]. For both the transmission and distribution network, we have implemented the power and current mismatch formulation. As our designed coupling framework can only handle power mismatch equations, we restrict our simulations to power mismatch.

The SNES module allows us to specify the nonlinear solve, see figure 9.2 for the options. The absolute and relative tolerance for the non-linear solve can be defined as well.

The user can specify the choice for the non-linear solve and of the mismatch function at run time. Although PETSc is designed to respect the different solvers for subnetworks for both unified and splitting methods, this flexibility is only available at runtime for splitting methods. For unified methods, one has to agree on the same non-linear solver and mismatch function at runtime. Nevertheless, the underlying models can be adapted and recompiled to allow for specific solvers for the unified methods as well.
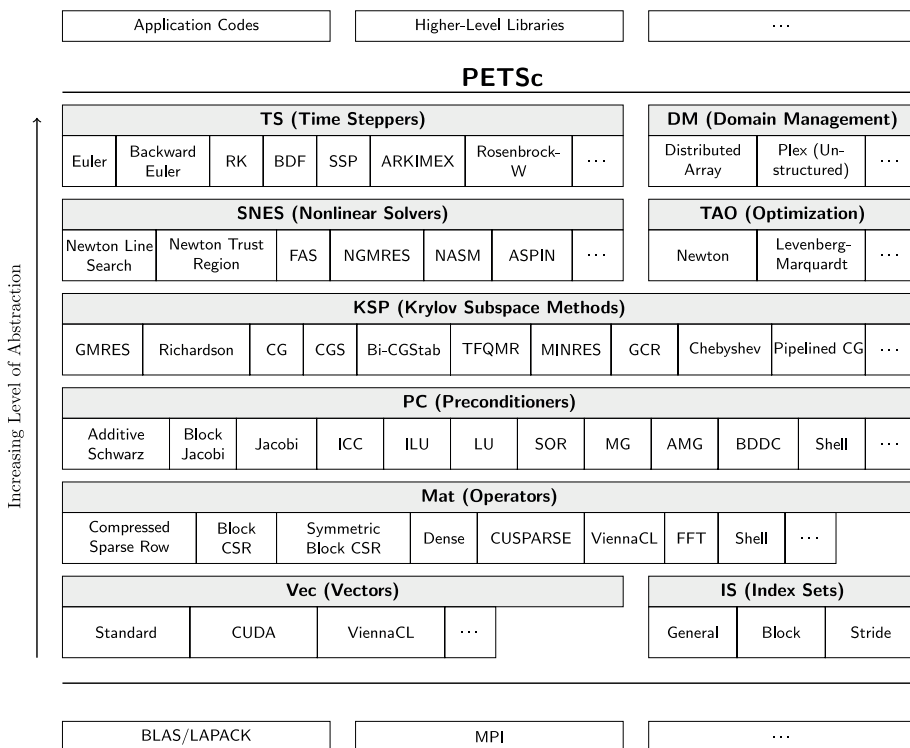
9

Figure 9.2: Petsc structure [54]

9.3.3. KSP and PC

The linear step within the non-linear Newton-Raphson is taken care of by the Krylov Subspace (KSP) and Preconditioners (PC) packages. It can solve systems of the form $Ax = b$ and contains a wide range of Krylov Subspace methods, as described in chapter 8, amongst which GMRES, CG, and Bi-CGSTAB, and preconditioners, such as LU, ILU and Jacobi.

The specific subspace methods are chosen at runtime. The same as for the SNES options, the user has to specify the same KSP and PC method for the unified methods, whereas, for splitting methods, they can differ. The selected runtime options are described in section 9.5.

9

9.4. Test cases

The test cases we use are combined Transmission and Distribution test cases of which the Transmission test cases are taken from the Matpower library [38] and the distribution test cases from the IEEE P&ES library [39]. We have created four cases to test that the framework works, and we have created one large test case to show its performance when running simulations up to roughly 1 million unknowns. Appendix C contains an overview of the separate transmission and distribution test cases including its details on the number of buses, branches, and non-zeros in the Jacobian.

9.4.1. Details

We have simplified the test cases to get the focus of our study on its numerical performance. We have made the following adjustments, the test cases contain:

1. Only constant power models (as described in section 3.5)

2. All loads in distribution networks are modelled as Wye load models (as described in section 3.5.1)

3. All transformers in distribution networks have a Wye-Wye configuration (as described in section 3.8.1)

4. Distribution networks do not contain any PV-bus

9.4.2. Substation

The test cases are connected via a substation to connect the single-phase network to the three-phase network and to match the base quantities. For simplicity reasons, we model every substation as a Wye-Wye transformer (See Table 3.2 for details of the matrix configuration).

9.4.3. Integrated test cases

We have created a total of 5 integrated test cases to perform our simulations. The first four are (relatively) small test cases to show the behaviour of unified and splitting models in general. The fifth test case is a range of large test cases. It is made of one large transmission network and one large distribution network, that differ in size such that we can investigate how these methods scale when the size gets larger.

The large test case is a combination of the 2T3120 transmission network and a range of large distribution networks. This 2T3120 transmission network is the original T3120 network coupled with itself. For the large distribution networks, we select a range of multiple copies of the D2500 network. The first network in the range is the 2T3120 network coupled to a single copy of D2500, the second network is the 2T3120 network coupled to a double copy of D2500 case, and the third is the 2T3120 network coupled to a quadruple copy of D2500 test case. We repeat this process until we have created 8 test cases in this way, which means that the largest test case is the 2T3120 network coupled to a 128 copy of the D2500 case. This last test case contains around 1 million unknown variables.

In total, we have the following four smaller test cases:

1. T9 - D13

2. T118 - D37

3. T2383 - D906

4. T3120 - D2500

and 8 large test cases consisting of copies, as explained in the previous paragraph.

9.5. Numerical Results

The goal is to find good combinations of preconditioners and Krylov methods to solve integrated test cases. We have selected two Krylov methods: GMRES and Bi-CGSTAB. We make use of LU and incomplete LU (ILU) factorisation applied as left preconditioners together with QMD as a reordering method. We compared all the results with a direct method: LU factorisation. We use an Intel(R) Core(TM) i5-6500 CPU @ 3.20GHz with 4 cores. 64 GB of memory is used.

In PETSc, you are allowed to specify certain options at runtime, such as the Newton-Raphson mismatch formulation. The runtime options for both the unified and splitting methods are specified in table 9.1. Although we have the availability to use the NR-TCIM method, we only run simulations for the NR-power mismatch formulation.

Table 9.1: Available options (a selection) that can be selected at runtime. There are more options available in PETSc, but these are the ones that we have incorporated into our analysis.

Runtime options				
Newton	Mismatch	Linear Solve	Preconditioner	Ordering
Line search	Power	Direct	LU	QMD
	Current	GMRES	$ILU(12)$	
⋮		Bi-CGSTAB	$ILU(8)$	⋮
			$ILU(4)$	
		⋮	$ILU(0)$	
			⋮	

Note that in the splitting methods, we can define different runtime options for each subnetwork. Nevertheless, we have chosen to select the same runtime options for each subnetwork.

9.5.1. General test cases

We first run simulations on the four small test cases to get insight into which Krylov subspace methods perform best so that we can select these combinations to solve the range of large integrated systems. We apply the interconnected and MFS-hybrid methods to these test cases and check their iteration number —both the NR method and the Krylov subspace method— and the CPU time. These results are presented in table 9.2.

The first thing that we notice is that both GMRES, Bi-CGSTAB and the direct method have a similar performance. The $ILU(4)$ and $ILU(0)$ preconditioner has a much higher Krylov iteration number which results in a higher CPU time, therefore these methods —both GMRES and Bi-CGSTAB— perform less combined with these preconditioners. Furthermore, the performance of GMRES and Bi-CGSTAB is similar. We, therefore, decide to continue the analysis of large test cases with GMRES together with an LU and $ILU(12)$ and $ILU(0)$ preconditioner.

9.5.2. Large test cases

For the large test cases, we only focus on the CPU performance as we saw that the Krylov and NR iterations stay roughly similar when size increases. We presented the times that it takes to run integrated power flow simulations in figure 9.3 where the time in seconds is plotted against the number of unknown variables. We have used a log-log plot to show the relationship.

The most interesting of these results is that in PETSc, the MFS method is in general faster than unified methods. Especially when size increases, the interconnected method scales worse with size. It is not straightforward to argue why this is the case as we do not know exactly how PETSc provides the solver to this system. One of the reasons could be that the methods in PETSc are optimised for multiple, smaller blocks to run parallel computations. As the unified method solves one large block and the MFS method keeps two separate smaller blocks, this could explain the difference in time.

Secondly, we see that direct methods are performing better than iterative methods. As we argued previously, it is difficult to deduce why this is the case. A reason for this is related to how the test cases are designed. The large separate networks are hardly interconnected which makes the direct methods more efficient. Furthermore, we see that when the size of the large test case increases, is that the methods tend to converge to the same CPU time. This is because the size of the large test cases only increases with extra distribution networks. As chapter 8 showed the distribution networks only require one inner Krylov iteration, and all preconditioner methods perform the same. The integrated test cases tend to perform similarly to the separate distribution test cases, so also all the inexact Newton methods on these test cases tend to perform similarly.

Table 9.2: The Interconnected and MFS-hybrid method applied to several transmission-distribution test cases of which the linear step is solved using different Krylov subspace-preconditioning combinations. The iteration number of the MFS method (MFS), the Newton-Raphson (NR) method, and the Krylov method (K) is presented, together with the CPU time to solve the system.

		The interconnected method													
	Test case	T9-D13			T118-D37			T2383-D906			T3120-D2500		
		NR	K	$Time$	NR	K	$Time$	NR	K	$Time$	NR	K	sec
Method	Prec	$\mathfrak{I}_{NR}$	$\mathfrak{I}_K$	sec	$\mathfrak{I}_{NR}$	$\mathfrak{I}_K$	sec	$\mathfrak{I}_{NR}$	$\mathfrak{I}_K$	sec	$\mathfrak{I}_{NR}$	$\mathfrak{I}_K$	sec
Direct (LU)	-	5	1	1.47e-02	12	1	5.00e-02	8	1	8.64e-01	6	1	1.70e+00
GMRES	LU	5	1	1.53e-02	12	1	4.54e-02	8	1	8.72e-01	6	1	1.68e+00
	ILU(12)	5	1	1.53e-02	12	3	4.57e-02	8	7	9.20e-01	6	10	1.91e+00
	ILU(8)	5	1	1.83e-02	12	1	4.82e-02	8	11	9.37e-01	6	17	2.08e+00
	ILU(4)	5	1	1.52e-02	12	5	4.94e-02	8	26	1.04e+00	7	47	2.48e+00
	ILU(0)	5	5	1.63e-02	12	21	5.49e-02	9	165	1.78e+00	6	240	4.52e+00
BCGS	LU	5	1	1.48e-02	12	1	4.58e-02	8	1	8.79e-01	6	1	1.70e+00
	ILU(12)	5	1	1.56e-02	12	1	4.70e-02	8	5	9.31e-01	6	6	1.83e+00
	ILU(8)	5	1	1.51e-02	12	1	4.71e-02	8	7	9.52e-01	6	11	2.12e+00
	ILU(4)	5	1	1.64e-02	12	4	4.90e-02	8	17	1.06e+00	7	24	2.39e+00
	ILU(0)	5	5	1.62e-02	12	16	5.57e-02	8	67	1.45e+00	6	103	3.74e+00

| | | The MFS-hybrid method | | | | | | | | | | | |
| --- | --- | --- | --- | --- | --- | --- | --- | --- | --- | --- | --- | --- |
| | Test case | T9-D13 | | | | | | T118-D37 | | | | | |
| | | MFS | NR_D | K_D | NR_T | K_T | $Time$ | MFS | NR_D | K_D | NR_T | K_T | $Time$ |
| Method | Prec | $\mathfrak{I}_{MFS}$ | $\mathfrak{I}_{NR_D}$ | $\mathfrak{I}_{K_D}$ | $\mathfrak{I}_{NR_T}$ | $\mathfrak{I}_{K_T}$ | sec | $\mathfrak{I}_{MFS}$ | $\mathfrak{I}_{NR_D}$ | $\mathfrak{I}_{K_D}$ | $\mathfrak{I}_{NR_T}$ | $\mathfrak{I}_{K_T}$ | sec |
| Direct (LU) | - | 2 | 3 | 1 | 4 | 1 | 2.03e-02 | 2 | 6 | 1 | 3 | 1 | 4.43e-02 |
| GMRES | LU | 2 | 3 | 1 | 4 | 1 | 2.03e-02 | 2 | 6 | 1 | 3 | 1 | 4.48e-02 |
| | ILU(12) | 2 | 3 | 1 | 4 | 1 | 2.11e-02 | 2 | 6 | 1 | 3 | 1 | 4.54e-02 |
| | ILU(8) | 2 | 3 | 1 | 4 | 1 | 2.05e-02 | 2 | 6 | 1 | 3 | 2 | 4.54e-02 |
| | ILU(4) | 2 | 3 | 1 | 4 | 1 | 2.04e-02 | 2 | 6 | 1 | 3 | 3 | 4.61e-02 |
| | ILU(0) | 2 | 3 | 1 | 4 | 5 | 2.09e-02 | 2 | 6 | 1 | 3 | 23 | 5.41e-02 |
| BCGS | LU | 2 | 3 | 1 | 4 | 1 | 2.30e-02 | 2 | 6 | 1 | 3 | 1 | 4.76e-02 |
| | ILU(12) | 2 | 3 | 1 | 4 | 1 | 2.28e-02 | 2 | 6 | 1 | 3 | 1 | 4.83e-02 |
| | ILU(8) | 2 | 3 | 15 | 4 | 1 | 2.22e-02 | 2 | 6 | 1 | 3 | 2 | 4.89e-02 |
| | ILU(4) | 2 | 3 | 20 | 4 | 1 | 2.39e-02 | 2 | 6 | 1 | 3 | 2 | 4.99e-02 |
| | ILU(0) | 2 | 3 | 75 | 4 | 5 | 2.39e-02 | 2 | 6 | 1 | 3 | 17 | 5.88e-02 |
| | Test case | T2383-D906 | | | | | | T3120-D2500 | | | | | |
| Direct | LU | 2 | 4 | 1 | 6 | 1 | 7.27e-01 | 2 | 5 | 1 | 6 | 1 | 1.57e+00 |
| GMRES | LU | 2 | 4 | 1 | 6 | 1 | 7.42e-01 | 2 | 5 | 1 | 6 | 1 | 1.59e+00 |
| | ILU(12) | 2 | 4 | 1 | 6 | 7 | 8.17e-01 | 2 | 5 | 1 | 6 | 10 | 1.81e+00 |
| | ILU(8) | 2 | 4 | 1 | 6 | 11 | 8.49e-01 | 2 | 5 | 1 | 6 | 18 | 1.99e+00 |
| | ILU(4) | 2 | 4 | 1 | 6 | 27 | 1.03e+00 | 2 | 5 | 1 | 6 | 47 | 2.69e+00 |
| | ILU(0) | 2 | 4 | 1 | 6 | 193 | 2.60e+00 | 2 | 5 | 1 | 6 | 270 | 7.13e+00 |
| BCGS | LU | 2 | 4 | 1 | 6 | 1 | 7.68e-01 | 2 | 5 | 1 | 6 | 1 | 1.68e+00 |
| | ILU(12) | 2 | 4 | 1 | 6 | 4 | 8.56e-01 | 2 | 5 | 1 | 6 | 6 | 1.94e+00 |
| | ILU(8) | 2 | 4 | 1 | 6 | 7 | 9.02e-01 | 2 | 5 | 1 | 6 | 11 | 2.11e+00 |
| | ILU(4) | 2 | 4 | 1 | 6 | 17 | 1.07e+00 | 2 | 5 | 1 | 6 | 26 | 2.63e+00 |
| | ILU(0) | 2 | 4 | 1 | 6 | 76 | 1.86e+00 | 2 | 5 | 1 | 6 | 105 | 5.08e+00 |

9
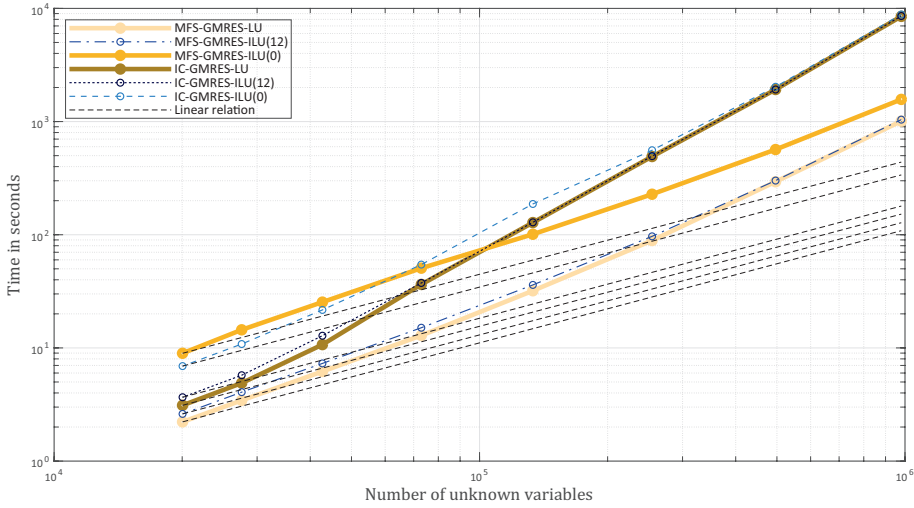
Figure 9.3: The CPU time in seconds to solve large transmission-distribution test cases. The time is plotted against the number of variables to solve, to see how the efficiency of the methods scales when the size of the test cases increases. The black dotted line shows how the time would scale with size in a one-to-one linear relationship.

9.6. Overview and conclusion

In this part of the thesis, we focus on the performance of large methods. We have run simulations in the library PETSc as we have several Krylov subspaces and preconditioning available that are necessary to solve large systems efficiently.

Currently, only the hybrid network configuration is still the object of study as its performance was better, more in line with how SOs are currently running power flow simulations, and sufficient to analyse the interaction between power systems. We have therefore two methods remaining that we will use to run integrated power flow simulations: The interconnected method and the MFS-hybrid method.

In chapter 6, we concluded that unified methods are faster than MFS methods which were as expected as they require less communication between the two networks and do not need an extra iterative scheme. In this chapter, we saw something different: the performance of the MFS methods is much better. We cannot argue why this is the case, but we expect that the solvers in PETSc are optimised for solving multiple smaller blocks in parallel. It can therefore more efficiently process a couple of smaller blocks than one large block.

Besides the comparison between the two methods, we are also interested in which Krylov subspace combination performs best. At this point, the GMRES method preconditioned with a LU factorisation performs the best. This could be related to how the test cases are designed as the range of test cases are connected with only a couple of intermediate branches.

In summary, we can conclude that for these types of test cases and available meth-
ods, the GMRES-LU method works best to solve large-scale power flow simulations
on integrated transmission and distribution networks and that the splitting methods
are more efficient for large test cases. We would recommend focusing future analysis
on the properties of the test cases and PETSc to get a better insight into the perfor-
mance of different test cases. Secondly, it would be interesting to adapt the methods
to be solved in parallel such that even larger integrated power flow simulations can
be done. More of the recommendations are part of the conclusions in chapter 11.
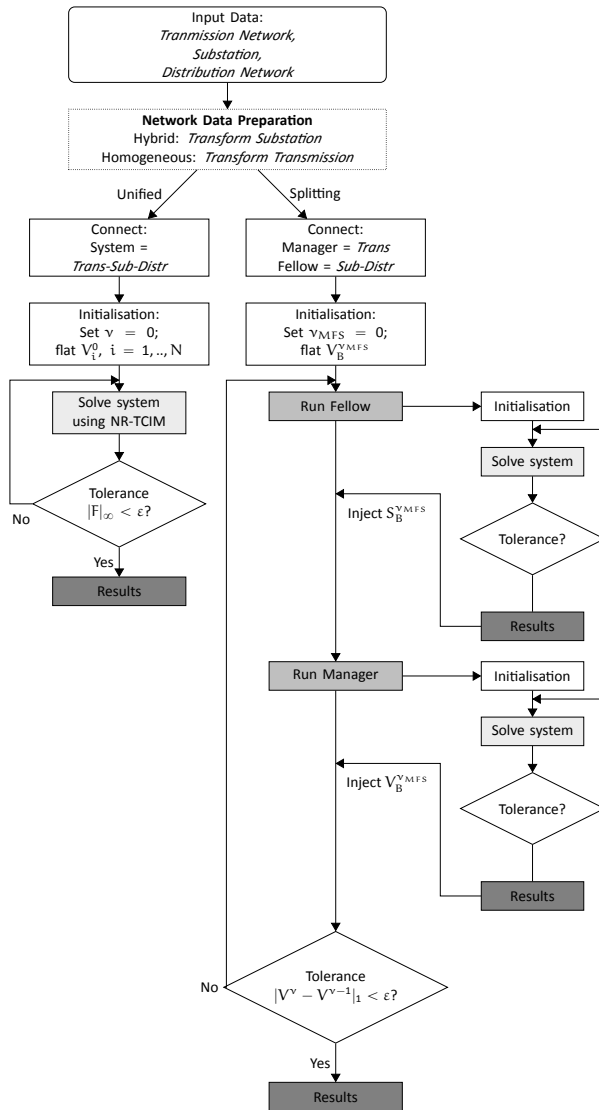
Figure 9.4: Repetition of the visualisation of the processes of the Unified and Splitting methods.

IV

Looking Ahead

10

Policy notes on TSO-DSO interaction

10.1. Introduction

The goal of this thesis is to develop a framework to run power flow simulations on integrated transmission-distribution power systems efficiently. The motivation to develop such a framework is to assist transmission and distribution system operators (TSOs and DSOs) in operating the electrical power system of the future safely and reliably. This power system of the future should be robust to changes related to the energy transition and at the same time take advantage of technical and digital innovations. These advances include both innovations related to the energy sector itself, such as the development of renewable energy resources (RES) and electrification of energy consumers, and innovations in digitisation, such as the Internet-of-Things; increased IT infrastructure; and availability of (real-time) data, changing the power system into a smart grid.

The amounts of reports written by European institutes ENTSO-E, ISGAN, and JRC show the need for increased TSO-DSO cooperation specifically when the power system is challenged due to the energy transition [55], [56], [57], [58], [59], [60]. The reports investigate the potential of increased SO cooperation through conducted pilot studies and stakeholder interviews, and collected best practices. We will point out the most important insights from these reports in this chapter. In the introduction, we have touched briefly upon the motivation to create an efficient integrated solution framework. The reports make the motivation more concrete which results in clear arguments to create a computationally efficient integrated power flow framework.

This chapter summarises the main findings of the reports we have consulted. It is divided as follows: First, we explain the original historic state of our power system including current developments that drive the need for intensive TSO-DSO cooperation. The energy and digitisation transition creates not only challenges but also opportunities for TSOs and DSOs which increased cooperation can benefit from. These opportunities are explained in the similarly named chapter. Thirdly, we summarise three of
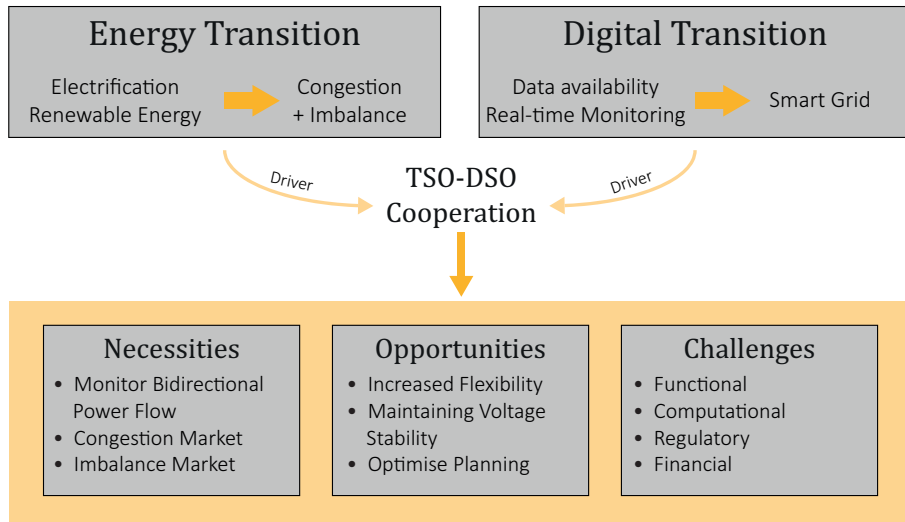
Figure 10.1: Overview of chapter

the pilot projects that were conducted by the initiative of the European Commission and the International Smart Grid Action Network (ISGAN) [57] where different case studies for SO cooperation were investigated. Increased cooperation leads to challenges on an economic, operational, functional, and digital level. We explain these challenges and show how our developed framework can overcome some of these challenges.

The European grid and operations and management of that grid differ from that of other continents. Not only in size, topology, and voltage levels but also in the way energy systems are operated. The focus here is on applications in the European region, and for that reason, we have consulted European reports. Note that our framework itself is not restricted to European grids, but can be used for any single-phase / three-phase electrical power system in the world.

10.2. Current state

The original design of the electrical power system is that of an active, leading transmission network and several passive distribution networks. The transmission network is responsible for the supply of power and transport over large distances to substations. The distribution networks bring power from the substations to end-consumers. Transmission System Operators (TSOs) are responsible for daily operation and long-term planning. Planning includes making grid expansion plans to facilitate the generation and consumption of electrical energy and investigating whether the grid is still safe under changing future conditions. TSOs need to run intensive year-round power flow and contingency analysis calculations to investigate this.

The other responsibility of TSOs is daily operation, which includes maintaining a constant balance[1] between instantaneous supply and demand of electrical energy and preventing any form of congestion [55]. Congestion is the overloading of transmission cables or transformers such that the transport of energy gets obstructed. TSOs have a complex market structure in place, where trading of electricity is done on different time intervals (weekly, daily, hourly) to make sure an all-time balance is maintained. TSOs run computationally intensive optimal dispatch problems to maintain this balance which are also based on power flow calculations.

The design of the passive distribution network is according to a 'fit-and-forget' approach, where the transmission system leads the allocation of energy. The original distribution system is overdesigned, which means that distribution cables and transformers are designed with sufficient capacity to always supply energy [56] [61]. TSOs can therefore leave out the detailed topology of distribution systems when doing their analyses.

SOs do separate system analyses and supply each other with data on a pro-rata basis [56]. This data is aggregated and supplied at different moments in time [60]. Furthermore, distributed loads and generation cannot participate in the trading markets of TSOs, and DSOs do not have their own wholesale or trading markets.

10.2.1. Changing Environment

We are currently in an era of transitioning from polluting and exhausting energy resources towards renewable energy resources (RES) to supply electricity in a clean, inexpensive, but of course still reliable manner [57]. The increase in RES comes with challenges that affect the operations of SOs. Energy resources such as Photo-Voltaic (PV) power and wind are highly volatile and intermittent, their connections are spread over large areas, and encountered in smaller volumes at distribution levels [56] [58] [59]. Their volatile, decentralised character makes it difficult to forecast and control their production [56] [59]. Furthermore, their connection at the distribution level can cause the voltage to flow upstream, which leads to a bidirectional power flow system [57] [59]. As the PV output depends on weather conditions, it is difficult to rely on this type of generation. All these factors add complexity to keep the supply and demand in balance.

Another factor of the energy transition is the electrification of different sectors, such as the transport sector (electric cars, electric buses) and the cooling and heating industry (ventilators, refrigerators, heat pumps), and the rise of data centres [58]. This leads to an increase in electrical loads. The increase in electrical loads and distributed generation can lead to congestion. Transformer and distribution cables can become critically loaded and prevent a decent supply of electrical power [55].

On the other hand, the digitisation transition leads to a growth in IT infrastructure, advanced data management systems, and better operational material making our electricity grid a smart grid. This is a necessary development that allows for better management of the grid as forecasts can be optimised due to the availability of data resources and computational power. On top of that, we get a better insight into real-

10

---

[1]The term balance might lead to confusion. It is different from the (im)balance we encounter at the distribution level. Balance means that supply and demand are equal to each other, which keeps the frequency constant.

time operation as we can monitor and measure our appliances and obtain information from suppliers, grid operators, and consumers continuously [56] [57].

10.3. Opportunities

To monitor and resolve 1) bidirectional power flow issues, 2) congestion, and 3) imbalance, TSOs and DSOs should work more intensively together. To simulate bidirectional power flow, TSOs should incorporate the generation and power flow at the distribution level in their models. Furthermore, as transformers and distribution cables are expected to get more often critically loaded, TSOs cannot assume to take the capacity of the distribution grid for granted and should incorporate the topology and capacity of distribution grids in their power flow simulations. Furthermore, the exchange of information between SOs is necessary to operate wholesale and trading markets.

The changing electrical environment leads besides these necessities to opportunities. Distributed Energy Resources (DERs) lead to increased system flexibility[2] that can be harvested by TSOs to reduce imbalance [58] by allowing DSOs to sell into wholesale and trading markets [55] [57]. Several use cases in Europe have demonstrated this potential and several balancing service providers exist that are aggregating distributed generation and loads to participate in TSO markets.

SOs can support each other in maintaining voltage stability [55]. The distribution voltage level can be controlled by changing the tap settings of the substation transformer, which is in some countries in control of the TSO [56]. The transmission voltage level can be supported by the DSO by activating flexibility at the distribution grid [55]. Also, investments in grid infrastructure can be optimised by making integrated simulations to identify areas that need extra capacity [58].

The smart grid allows SOs to activate resources from a distance and to operate in real-time such that production and consumption can be spread to off-peak moments to avoid congestion and network reinforcement duties of DSOs [57]. For example, a pilot study with electric vehicles (EVs) [62] has shown that aggregating loads of a decently sized pool of EVs and charging them during the night instead of during peak hours between 5:00 and 9:00 AM can reduce the effect on the grid significantly. For customers, this is also attractive as electricity prices will be cheaper during these hours.

To manage power systems in this changing environment, the role of distribution systems is transforming into a more active role; potentially taking on the same role as transmission system operators, where DSOs will become market facilitators and congestion managers [56] [61]. DSOs can benefit from the acquired knowledge of TSOs on energy system management.

10

---

[2]Flexibility is a term that incorporates both loads and generation that are flexible. Meaning that they can be switched on or turned down when necessary. An example of load flexibility is a refrigerator. Over a certain time interval, the temperature of a refrigerator should stay constant, but certain fluctuations are allowed. With this information, one can allow the temperature to rise by switching off the refrigerator when the electricity demand is high, as long as it is restarted quickly after.

10.4. Current Developments

The European Union has facilitated six pilot projects throughout Europe to investigate the potential of TSO-DSO cooperation. Three of these projects (SmartNet, CoordiNet and Interplan) were specifically designed to investigate TSO-DSO interaction for imbalance and congestion management and planning purposes. We summarise the goals and key outcomes of these projects [57].

SmartNet

SmartNet was the first out of the six pilot projects which lasted from 2016 to 2019 throughout Italy, Spain, and Denmark. The goal was to build a coordination scheme that allows flexibility at the distribution level to participate in TSO markets, such that the potential of ancillary services provided by distribution networks can be investigated. Ancillary service is an umbrella term for services beyond the generation and transport of electricity to maintain a safe grid. Balancing, congestion management, and voltage stability services provided by DSOs were part of the ancillary services in this pilot.

The focus of this pilot project was to create an operable simulation framework which was challenging considering the complexity of representing both transmission and distribution networks simultaneously, all the flexibility providers, the several scenarios, and the amount of equations and constraints that incorporate the objectives and interaction of and between stakeholders. As the participating DSOs were currently not doing any power flow computations, these needed to be modelled. Eventually, the project resulted in some regulatory guidelines that can form a starting point for integrating and coordinating different networks.

Coordinet

Coordinet — executed between 2019 and 2022 — was a pilot study to develop a universal framework for a new market structure to manage congestion and load settlement by improved TSO-DSO interaction. The hope was that this would lead to a more environmentally friendly grid and a cheaper supply of electricity to consumers. The main goal was to demonstrate which regulation is necessary to make a basic framework applicable to individual needs and which key objectives should be defined to enable the participation of different stakeholders.

A cooperation platform has been developed for TSOs, DSOs, and consumers to participate in. The platform has demonstrated that better coordination between these parties can help alleviate network congestion as the number of violations decreased when the flexibility market was available and operating. This has led to reaching the original goal: to supply cheaper energy in a clean way.

10

A challenge was that many potential flexibility owners were not aware of the services they could provide to stabilise the grid, so their potential could not be harnessed yet. Awareness amongst these stakeholders should be created. Furthermore, it is necessary that grid data and grid models are available and shared to make the platform interoperable.

Interplan

Interplan — conducted between 2017 and 2021 — was not a pilot study but comprised the theoretical development of a tool. This tool should enable TSOs and DSOs to simultaneously plan and operate the Pan-European Network. It had to be so extensive and multi-purpose to include both long-term planning and short-term operational issues by implementing sufficient control functions for both applications. The tool should focus on the interaction between TSOs and DSOs and incorporate the efficient use of emerging products such as RES, storage, demand response and EVs to support the European Union in maintaining sustainability goals while maintaining a safe and reliable grid.

One of the experienced challenges was to scale up the platform from the country level to the European level as countries have their individually specified products and local constraints. It was also difficult to make the platform compatible with existing platforms.

Summary

The three projects have shown the potential for increased TSO-DSO interaction. The developed tools helped in reducing congestion and provided better balancing techniques. Furthermore, improved communication has led to better coordination of unplanned events. Also, the long-term planning for a robust, efficient, and sustainable network considering harnessed distributed flexibility was successfully shown by adequate TSO-DSO interaction.

10.5. Challenges

Besides the successes and recommendations gained from the demonstration pilot projects, some challenges for TSO-DSO interaction were identified. These challenges arise when TSO-DSO cooperation is intensified and are considered from the perspectives of all the stakeholders within the power system [57]. The main outcome of the pilot projects was that a TSO-DSO coordination platform was required to optimise flexible resources at the distribution level. Such a platform has to be built, which comes with challenges which can be categorised into four categories:

1. Operational: Related to stakeholder management and coordination of the framework

2. Computational: Related to data, ICT, and computational power

3. Regulatory: Related to legal concerns, cyber security, and other regulatory aspects

4. Economic: Related to financial aspects, and return on investments

10

Operational

One of the biggest operational challenges is to align all stakeholders that are part of an integrated power system and identify their concerns. Some might have a reserved attitude, which would hinder functional TSO-DSO cooperation. The pilot projects have shown the potential benefit for all stakeholders which might convince them to participate [55]. Furthermore, awareness amongst potential partakers should be created to increase the participation of distributed flexibility in TSO markets.

Next to that, new roles should be clearly defined. Increased TSO-DSO cooperation might require a new independent system operator, a market platform coordinator, and a responsible substation coordinator. These concerns were currently not sufficiently handled in the pilot projects [56].

Lastly, there is a current lack of operational procedures concerned with the implementation of TSO-DSO interaction. Furthermore, the implementation of an integrated coordination framework itself is challenging as it should contain so many different possibilities, scenarios, and requests [55] [57].

Computational
To create a coordination platform, the current ICT infrastructure should be extended and data should be exchanged. Data exchange is required on network conditions, real-time measurements, generation and demand forecasts and is preferably supplied at varying frequencies. Currently, SOs are not always willing to provide data due to economic, security, and privacy issues [55] [57].

Furthermore, the increased level of detail in grid simulation models results in very large grid models [58]. On top of that, the additional constraints arising from the distribution capacity limit add to the complexity of this model [57]. This level of detail and these additional constraints are necessary to get an accurate representation of the grid, but this is currently limited due to computational burdens [57].

Legal and regulatory
An interconnected grid and increased data sharing create extra cyber-security risks. Furthermore, the level of detail which allows distributed resources to participate in flexibility markets or to create simultaneously planning simulations is currently legally not allowed as this data contains private, personal data which is protected for privacy reasons. One can think of EV or residential solar panel owners, who would like to participate in markets. A workaround could be to aggregate these participants in an aggregation platform, such that personal data is only shared with the responsible balancing party and not with the entire market structure. Currently, better TSO-DSO interaction requires an update in current regulations [55] [57].

Economical
An important financial consideration for DSOs is whether they should invest in grid capacity — by reinforcing distribution cables— or in intelligence —monitoring devices to participate with resources in flexibility markets— [57]. The current capacity of distribution cables is not sufficient to provide the transport of electrical power during peak hours. These cables should be replaced by bigger ones to increase their capacity. Another option would be to shift loads and generation from peak hours to quiet hours by allowing flexibility at the distribution level to participate in markets. To enable this, one should invest in the intelligence of the grid and the participating devices. DSOs do not have the financial capability to invest in both.

10

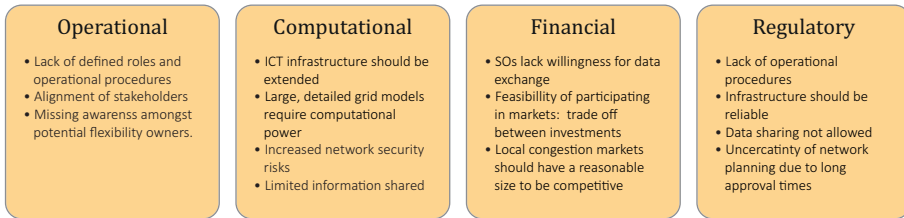# Challenges

Operational	Computational	Financial	Regulatory
• Lack of defined roles and operational procedures • Alignment of stakeholders • Missing awarenss amongst potential flexibility owners.	• ICT infrastructure should be extended • Large, detailed grid models require computational power • Increased network security risks • Limited information shared	• SOs lack willingness for data exchange • Feasibillity of participating in markets: trade off between investments • Local congestion markets should have a reasonable size to be competitive	• Lack of operational procedures • Infrastructure should be reliable • Data sharing not allowed • Uncercatinty of network planning due to long approval times

Figure 10.2: Challenges on different levels/categories for TSOs and DSOs

Furthermore, DSOs should switch their core task from being passive operators to being active, intelligent operators. They need incentives to create this mindset switch. Therefore, they would like to know whether investments in ICT infrastructure and market participation are economically feasible [57]. Pilot projects help in showing this potential.

Finally, participating in flexibility markets is only competitive when loads are aggregated and a large pool of distributed flexibility owners are participating [55] [58]. Likewise, awareness should be created amongst potential flexibility owners.

Figure 10.2 contains an overview of the identified challenges that arise when cooperation between TSOs and DSOs is identified.

10.5.1. Our work

The platform that we have created as part of this thesis overcomes some of the challenges identified. First of all, the computational burden of the size and level of detail of integrated simulations is reduced when using a unified framework and applying specific numerical analysis tools to solve large systems. Research on this topic is ongoing and SOs are not always aware of numerical techniques that reduce computational power [63]. We would therefore recommend SOs to not be held back by computational burden.

Another concern of SOs was that network data sharing is currently not allowed. PETSc has the option to keep the private data of individual networks separate and only allow sharing of a small amount of information of the connecting substations [9]. The only requirement is that an independent system operator would be in charge of coordinating this.

Another aspect that was identified is that different SOs have their models in place and it is difficult to align these models or to create a new platform. Co-simulation seems to be a better resolution to coordinate TSO-DSO cooperation as it can respect individual needs. However, even as this would be preferred, there is still a need for a demonstration platform to show the potential benefits of TSO-DSO cooperation to get more flexibility owners on board. Our framework could also play a role in this demonstration platform.

10.6. Overview

The energy and digitisation transition are driving the need and possibilities for TSO-DSO cooperation. The energy transition will increase the chance of bidirectional power flow, congestion, and imbalance in transmission systems. TSO-DSO cooperation is necessary to overcome bidirectional power flow issues, alleviate congestion, and reduce imbalance. On the other hand, the digitisation transition makes TSO-DSO cooperation easier as it allows distributed flexibility to participate in balancing and trading markets, planning to be optimised, and ancillary services to be better integrated to maintain a stable grid.

Challenges arise when TSO-DSO cooperation is intensified. System operators have legal concerns about sharing data. Furthermore, the scale of the combined models increases the computational burden of the simulations. During the development of this integrated power flow simulation framework, we have considered these challenges and paid attention to numerical analysis and efficient modelling techniques to decrease the computational burden of integrated power flow simulations. Furthermore, other researchers working in PETSc have been involved with the legal concerns that SOs have by creating a platform in which full data sharing between SOs is not necessary.

Another challenge that was mentioned in the EU reports is that DSO participation in flexibility markets is only beneficial when multiple flexibility owners start offering their electrical loads to these markets. Many of these potential owners are currently not aware of the possibilities of TSO market participation and they can be somewhat reluctant as they do not know the benefits for them. This platform can serve as a basis for a TSO-DSO market structure demonstration project in which the potential for stakeholders of intensified cooperation is shown.

10

11

Conclusion

We have developed an open-source framework to run power flow simulations on integrated transmission-distribution electricity networks. Such a framework is necessary to simulate how transmission and distribution networks interact. Until recently, system operators (SOs) that run these power flow simulations were able to operate their power systems by running separate power flow simulations only. The energy transition drives the need for doing integrated power flow simulations. SOs have a reserved attitude towards more intensive cooperation, amongst others due to the computational burden of integrated power flow simulations. Therefore, we have created a platform and used numerical analysis to make sure SOs can run these simulations efficiently. In this chapter, we share the most important insights of what we have created, review the obtained results and give recommendations for future improvements.

11.1. Conclusion

Transmission and distribution electricity networks are currently separately analysed by their respective system operator. Due to the difference in design, topology, and elements, these systems are modelled and solved differently. The main difference is that the balanced transmission system is modelled in single-phase and preferably solved using the power mismatch formulation of the Newton-Raphson (NR) method, while the unbalanced distribution system is modelled in three-phase and preferably solved using the NR current mismatch formulation. When running integrated simulations, we must be cautious in determining the system's modelling approach while having a phase dimension mismatch and in determining its solution approach while having different preferred solution methods.

We have conducted a review study and found two ways of modelling the integrated network. The first is as a homogeneous network: The transmission network is modelled in three phases such that it can be connected directly to the distribution network. The second method is a hybrid network: The transmission network remains in single-phase, but the substation placed in between the two networks takes care of the dimension mismatch.

From the same literature study, we found two ways of solving the integrated network: Unified and Manager-Fellow Splitting (MFS) methods. The unified methods solve the system as one new system, while the MFS method keeps two separate systems and iterates between the two systems until convergence on the coupling bus has been reached. An advantage of the MFS methods is that the separate systems can be solved using their preferred NR method, while the unified system should select either the power or current mismatch formulation for the new, integrated system. On the other hand, we expect that the MFS methods are slower than unified methods as they require more communication between the two systems. In total, we obtained four methods: Unified methods applied to hybrid networks (the interconnected method) and to homogeneous networks (the full three-phase method) versus MFS methods applied to hybrid networks (MFS-hybrid) and homogeneous networks (MFS-homo).

We have conducted a numerical assessment study to compare these methods on their numerical performance. We have done this in two stages. The first stage was to test the performance of these methods on small test networks. Therefore, we have implemented these —in total four— methods in Matpower. Matpower is easy to work with and gives us the flexibility to test the methods under different conditions. A downside of Matlab is that it is not optimised for speed. Nevertheless, it was a comprehensive software to prove the concept of the methods and to subject them to several physical conditions, such as increased distributed generation and multiple distribution networks.

From this performance study, we concluded that the methods behaved as we expected: The unified methods were in general faster than the MFS methods and it was more convenient to model integrated networks as a hybrid network compared to homogeneous networks. The interconnected method was therefore showing the best performance. Furthermore, we showed that hybrid networks are sufficient to analyse integrated systems when the amount of distributed generation is rising due to the increased photo-voltaic (PV) penetration of residential rooftop solar panels. The increased PV penetration could lead to an induced imbalance in transmission networks, which is very much unwanted. We showed that normal PV penetration levels would not lead to extra imbalance in transmission systems. Therefore — and because hybrid networks are more sufficient — we have decided to continue the second part of our analysis exclusively with hybrid network configurations.

The second stage of this research was to apply numerical techniques, such as Krylov subspace methods, preconditioners, and reordering, to efficiently solve power systems. Therefore, we switched from Matpower to PETSc, an open-source library where many of these numerical techniques are available to us. We have implemented a hybrid version of the integrated transmission and distribution network and compared the unified and MFS methods. The objective was to find the right combination of the Krylov method and preconditioner to solve integrated systems. As general power flow systems contain millions of buses, we have scaled our test networks to similar sizes.

Some interesting conclusions came out of this second-stage analysis. First of all, the performance of direct methods and preconditioned iterative methods behave similarly when the size of the integrated power system grows. This could be the result of the way the large test cases are formed with few interconnections and as the distribution network is radial so with few interconnections as well. Furthermore, during

11

this analysis, the MFS methods were faster than the unified methods. This could be caused by the fact that the unified methods require a much larger block to solve every iteration and PETSc may be optimised for handling smaller blocks.

It is therefore important to continue the analysis of integrated systems to see the performance on differently designed test cases. Also, the integrated analysis could benefit from High-Performance Computing advances which could lead to additional speed-up of the methods. SOs can be hesitant to more intensive transmission-distribution cooperation because of the expected computational burden, as concluded in chapter 10, but we have high expectations to run integrated power systems efficiently when all these techniques are combined and would recommend system operators not to be held back towards more intensive cooperation.

11.2. Discussion

As stated previously, we have identified opportunities to advance the analysis of integrated power flow simulations on certain topics. We have made several recommendations for future research, that we categorised into two categories: electrical engineering-related and numerical analysis-related.

Electrical engineering

The test cases that we used to run power flow simulations were taken from existing libraries that provide test cases based on real networks. These test cases should reflect real power system conditions. Nevertheless, some simplifications were made in the PETSc model of the distribution network. One of these simplifications made in the distribution network of PETSc was to only include constant power Wye load models and Wye-Wye transformer configurations in the network compared to the original design (summarised in appendix C). The distribution network did not contain any step-voltage regulator or generator buses. These simplifications could have affected the behaviour of the methods.

The integration framework also contained some simplifications, both in Matlab and in PETSc. It was based on the fact that the bus connecting the two networks was balanced and that any imbalance could not flow from one network to the other. A way to improve the substation is by connecting the two networks by incorporating the zero and negative sequences of the transmission network into the substation model [10]. Furthermore, the type of transformer connecting the two networks can also influence the performance of the simulations. It is therefore important to investigate if a specific transformer configuration is required to connect the two networks.

The large test cases created for the analyses in chapter 9 were created by connecting multiples of the same network by placing one extra branch between them. The fact that these networks were loosely connected might have caused the obtained results.

Lastly, we would recommend doing a more extensive analysis of the influence of PV penetration on integrated systems. This study was quite preliminary.

Numerical Analysis

First of all, we think it is important to do a solid convergence analysis. It is difficult to state why certain test cases require more iterations than others and why some are slower than others. It would be valuable if we could relate certain power system

11

elements — such as capacitors, loads, and transformers — and the topology of the network directly to the performance of the electrical power system and decide on a smart choice of the method to solve this system.

Improvements in the performance of the methods can be obtained by solving the integrated systems in parallel. This can be easily implemented when one continues the analysis in PETSc, as it is built using MPI. An interesting topic could be to investigate the potential of the splitting methods versus the unified methods. We expect that their performance should be more equal. Moreover, the construction of the Jacobian can be made cheaper as the configuration of the Jacobian consists of elements in the power or current mismatch vector which can be directly used to build the Jacobian.

General
Besides these recommendations, we have two more general ones. First of all, we were not able to do a comparison on the accuracy of the methods as we do not have access to real data. Next, it is not possible to compare the outcome of the integrated simulations with separate simulations as they differ from each other, shown in the work of [37]. It is always a burden to validate numerical results with real-life data, but with improvements in software and the rise of digital twins — such as the digital twin of the Dutch electricity network created by the group of P. Palensky in Delft — it will be easier in the future.

Lastly, we would recommend combining this framework with the grid partitioning framework [59] also constructed in PETSc. This grid partitioning framework takes care of the privacy concerns of SOs by only allowing a small number of buses that need to be shared with the other SOs. In this way, distribution and transmission system operators should have fewer concerns about data ownership.

11.2.1. Applications
The last point we would like to highlight is that this framework can be utilised in other ways than being used for transmission distribution network analysis only. First of all, the concept of the framework works for any form of energy carrier network integration or any system operator interaction.

Next to that, it could also be used by distribution or transmission system operators for separate system analysis. TSOs could face induced imbalance soon on their electricity grid, but probably only on a part of the grid. It is not efficient to start modelling the entire system in three-phase. Connections between single-phase and three-phase lines could be made using the idea of the hybrid network configuration such that only a couple of lines have to be modelled in three-phase, keeping an efficient power system [10]. The same could work for distribution systems where large parts of the system are balanced. These lines then only have to be modelled in single-phase.

11

To summarise, we have created an open-source framework to run efficient steady-state power flow simulations on integrated transmission and distribution networks. This framework is tested on simplified test cases but shows potential for large system simulations. Moreover, it takes into account the considerations of system operators and can be utilised in other applications besides integrated analysis.

Bibliography

[1] Industrial power distribution: Introduction. industrial electronics, 2018.

[2] P. Schavemaker and L. van der Sluis. Introduction to Power System Analysis. In *Electrical Power System Essentials*, chapter 1. John Wiley & Sons, Inc., Sussex, United Kingdom, 2008.

[3] B. Palmintier, E. Hale, T.M. Hansen, W. Jones, D. Biagioni, K. Baker, H. Wu, J. Giraldez, H. Sorensen, M. Lunacek, N. Merket, J. Jorgenson, and B.M. Hodge, National Renewable Energy Laboratory. Final Technical Report: Integrated DistributionTransmission Analysis for Very High Penetration Solar PV, 2016.

[4] K. Balasubramaniam and S. Abhyankar. A combined transmission and distribution system co-simulation framework for assessing the impact of volt/var control on transmission system. *2017 IEEE Power & Energy Society General Meeting*, pages 1–5, 2017.

[5] H. Jain, B.A. Bhatti, T. Wu, B. Mather, and R. Broadwater. Integrated transmission-and-distribution system modeling of power systems: State-of-the-art and future research directions. *Energies*, 14(1), 2021.

[6] G. Krishnamoorthy and A. Dubey. A Framework to Analyze Interactions between Transmission and Distribution Systems. In *2018 IEEE Power Energy Society General Meeting (PESGM)*, pages 1–5, 2018.

[7] William H. Kersting. The whys of distribution system analysis. Requirements for a power-flow study. *IEEE Industry Applications Magazine*, 17(5):59–65, 2011.

[8] M. Bollen and F. Hassan. *Integration of Distributed Generation in the Power System*. Wiley, 2011.

[9] S.G. Rinaldo, A. Ceresoli, D.J.P. Lahaye, M. Merlo, M. Cvetković, S. Vitiello, and G. Fulli. Distributing Load Flow Computations Across System Operators Boundaries Using the Newton − Krylov − Schwarz Algorithm Implemented in PETSc. *Energies*, 11(2910), 2018.

[10] G.N. Taranto and J.M. Marinho. A Hybrid Three-Phase Single-Phase Power Flow Formulation. *IEEE Transactions on Power Systems*, 23(3):1063–1070, 2008.

[11] H. Sun, Q. Guo, B. Zhang, and Y. Guo. Master − Slave-Splitting Based Distributed Global Power Flow Method for Integrated Transmission and Distribution Analysis. *IEEE Transactions on Smart Grid*, 6(3):1484–1492, 2015.

[12] R. Idema and D.J.P. Lahaye. *Computational Methods in Power System Analysis*. Atlantis Press, Paris, 2014.

[13] C.A. Gross. *Power System Analysis*. John Wiley & Sons, Inc., New York, second edition, 1986.

[14] P. Schavemaker and L. van der Sluis. Energy Management Systems. In *Electrical Power System Essentials*, chapter 6. John Wiley & Sons, Inc., Sussex, United Kingdom, 2008.

[15] Entso-e transmission system map, 2019.

[16] Tennet grid maps | grid map de onshore corporate, 2023.

[17] S.M. Alizadeh, C. Ozansoy, and T. Alpcan. The impact of x/r ratio on voltage stability in a distribution network penetrated by wind farms. In *2016 Australasian Universities Power Engineering Conference (AUPEC)*, pages 1–6, 2016.

[18] B. Sereeter, C. Vuik, and C. Witteveen. Newton power flow methods for unbalanced three-phase distribution networks. *Energies*, 10(10):1658, 2017.

[19] S. Eftekharnejad, V. Vittal, G.T. Heydt, B. Keel, and J. Loehr. Impact of increased penetration of photovoltaic generation on power systems. *IEEE Transactions on Power Systems*, 28(2):893–901, 2013.

[20] J. Liu, M.M.A. Salama, and R.R. Mansour. An efficient power flow algorithm for Distribution Systems with Polynomial Load. *International Journal of Electrical Engineering Education*, 39(4):371–386, 2002.

[21] J.B.V. Subrahmanyam and C. Radhakrishna. A simple approach of three phase distribution system modeling for power flow calculations. *International Journal of Electrical and Computer Engineering*, 4:571–576, 2010.

[22] W.H. Kersting. *Distribution System Modeling and Analysis, Third edition*. CRC Press Taylor & Francis Group LLC, Las Cruces, New Mexico, 3 edition, 2012.

[23] M. Bazrafshan and N. Gatsis. Comprehensive modeling of three-phase distribution systems via the bus admittance matrix. *IEEE Transactions on Power Systems*, 33(2):2015–2029, 2018.

[24] P.A.N. Garcia, J.L.R. Pereira, S. Carneiro, and M. Da Costa. Three-phase power flow calculations using the current injection method. *IEEE Transactions on Power Systems*, 15(2):508–514, 2000.

[25] J.H. Teng. A modified Gauss–Seidel algorithm of three-phase power flow analysis in distribution networks. *International Journal of Electrical Power & Energy Systems*, 24(2):97–102, 2002.

[26] J.A. Martinez and J. Mahseredjian. Load Flow Calculations in Distribution Systems with Distributed Resources. A Review. In *2011 IEEE Power and Energy Society General Meeting*, pages 1–8, San Diego, CA, USA, 2011. IEEE.

[27] P. Rousseaux and T. Van Cutsem. Quasi steady-state simulation diagnosis using newton method with optimal multiplier. In *2006 IEEE Power Engineering Society General Meeting*, pages 7 pp.–, 2006.

[28] G. Andersson. Modelling and Analysis of Electric Power Systems, Lecture 227-0526-00, 3 2004.

[29] U. Eminoglu and M.H. Hocaoglu. Distribution Systems Forward/Backward Sweep based Power Flow Algorithms: A Review and Comparison Study. *Electric Power Components and Systems*, dec 2008.

[30] B. Sereeter, C. Vuik, and C. Witteveen. Newton Power Flow Methods for Unbalanced Three-Phase Distribution Networks. *Energies*, 10(10):1658, 10 2017.

[31] M.E. Kootte and C. Vuik. Steady-state stand-alone power flow solvers for integrated transmission-distribution networks: A comparison study and numerical assessment. *Energies*, 14(18), 2021.

[32] G. Huang and V. Vittal. Integrated Transmission and Distribution System Power Flow and Dynamic Simulation Using Mixed Three-Sequence Three-phase modeling. *IEEE Transactions on Power Systems*, 32(5):3704–3714, 2017.

[33] H. Sun and B. Zhang. Distributed Power Flow Calculation for Whole Networks Including Transmission and Distribution. In *IEEE/PES Transmission and Distribution Conference and Exposition*, pages 1–6, 2008.

[34] M.E. Kootte and C. Vuik. The Master-Slave Splitting Extended to Power Flow Problems on Integrated Networks with an Unbalanced Distribution Network. *Lecture Notes in Computational Science and Engineering*, 139(Numerical Mathematics and Advanced Applications, ENUMATH 2019 - European Conference):625– 632, 2021.

[35] H.B. Sun and B.M. Zhang. Global state estimation for whole transmission and distribution networks. *Electric Power Systems Research*, 74(2):187–195, 2005.

[36] H. Sun, D. Nikovski, T. Ohno, T. Takano, and Y. Kojima. A fast and robust load flow method for distribution systems with distributed generations. *Energy Procedia*, 12:236–244, 2011.

[37] B. Sereeter, W. van Westering, C. Vuik, and C. Witteveen. Linear power flow method improved with numerical analysis techniques applied to a very large network. *Energies*, 12(21), 2019.

[38] R.D. Zimmerman, C.E. Murillo-Sánchez, and R.J. Thomas. MATPOWER: Steady-state operations, planning, and analysis tools for power systems research and education. *IEEE Transactions on Power Systems*, 26(1):12–19, 2011.

[39] K. P. Schneider, B. A. Mather, B. C. Pal, C. W. Ten, G. J. Shirek, H. Zhu, J. C. Fuller, J. L.R. Pereira, L. F. Ochoa, L. R. De Araujo, R. C. Dugan, S. Matthias, S. Paudyal, T. E. McDermott, and W. Kersting. Analytic Considerations and Design Basis for the IEEE Distribution Test Feeders. *IEEE Transactions on Power Systems*, 33(3):3181–3188, 2018.

[40] M.E. Kootte and C. Vuik. The influence of the increasing penetration of photovoltaic generation on integrated transmission-distribution power systems. In *Control of Smart Buildings - An Integration to Grid and Local Energy Communities*. Springer Nature, to appear.

[41] Bilal Ahmad Bhatti, Robert Broadwater, and Murat Dilek. Analyzing Impact of Distributed PV Generation on Integrated Transmission & Distribution System - A Graph Trace Based Approach. *Energies*, 13(4526):6–9, 2020.

[42] V. Ramachandran, S.K. Solanki, and J. Solanki. Steady State Analysis of Three Phase Unbalanced Distribution Systems with Interconnection of. In *2011 IEEE/PES Power Systems Conference and Exposition*, pages 1–7. IEEE, 2011.

[43] R. Yan and T.K. Saha. Voltage Variation Sensitivity Analysis for Unbalanced Distribution Networks Due to Photovoltaic Power Fluctuations. *IEEE Transactions on Power Systems*, 27(2):1078–1089, 2012.

[44] K. Balamurugan and D. Srinivasan. Review of Power Flow Studies on Distribution Network with Distributed Generation. *IEEE PEDS*, pages 411–417, 12 2011.

[45] R.C. Dugan. *Electrical power system quality*. The McGraw Hill Companies, 2000.

[46] B.A. Bhatti, R. Broadwater, and M. Dilek. Analyzing Impact of Distributed PV Generation on Integrated Transmission & Distribution System - A Graph Trace Based Approach. *Energies*, 13(4526):6–9, 2020.

[47] Sandia National Laboratories. Pv performance modeling collaborative, 2020.

[48] G.N. Taranto. Simulation of Integrated Transmission and Distribution Networks with a Hybrid Three- Phase / Single-Phase Formulation. *Conference Proceedings, IREP*, 101(July), 2017.

[49] Y. Saad. *Iterative Methods for Sparse Linear Systems*. Society for Industrial and Applied Mathematics, second edition, 2003.

[50] L.N. Trefethen and D. Bau. *Numerical Linear Algebra*. Other Titles in Applied Mathematics. Society for Industrial and Applied Mathematics, 1997.

[51] P. Heggernes, S.C. Eisenstat, G. Kumfert, and A. Pothen. The computational complexity of the minimum degree algorithm. 5 2002.

[52] S. Abhyankar. Development of an implicitly coupled electromechanical and electromagnetic transients simulator for power systems. 2011.

[53] J.A. Cedeno. A three-phase unbalanced load flow solver for large-scale distribution power systems. Technical report, Delft University of Technology, 2017.

[54] S. Balay, S. Abhyankar, M.F. Adams, S. Benson, J. Brown, P. Brune, K. Buschelman, E. Constantinescu, L. Dalcin, A. Dener, V. Eijkhout, J. Faibussowitsch, W.D. Gropp, V. Hapla, T. Isaac, P. Jolivet, D. Karpeev, D. Kaushik, M.G. Knepley, F. Kong, S. Kruger, D.A. May, L. Curfman McInnes, R. Tran Mills, L. Mitchell, T. Munson, J.E. Roman, K. Rupp, P. Sanan, J. Sarich, B.F. Smith, S. Zampini, H. Zhang, H. Zhang, and J. Zhang. PETSc/TAO users manual. Technical Report ANL-21/39 - Revision 3.19, Argonne National Laboratory, 2023.

[55] A. Zegers and H. Brunner. Tso-dso interaction: An overview of current interaction between transmission and distribution system operators and an assessment of their cooperation in smart grids. Technical report, Annex 6 Power T&D Systems, Task 5, ISGAN Discussion Papers, September 2014.

[56] S. Rinaldo, A. Ceresoli, and G. Prettico. A distributed approach to solve power flow problems in new emerging scenarios, eur 29998 en. *Joint Research Centre Europe*, 2019.

[57] B. Herndler (Austrian Institute of Technology). Lessons learned from international projects on tsodso interaction. Technical report, ISGAN Annex 6 Power Transmission and Distribution Systems, ISGAN Discussion Papers, 12 2020.

[58] B. Herndler, C.Y. Evrenosoglu, G. Migliavacca, H. Gerard, I. Vilgan, J.P. Chaves Ávila, K. Kessels, M. Rossi, P. Lo, and S. Wong. Flexibility harvesting and its impact on stakeholder interaction. Technical report, ISGAN Discussion Papers, 12 2022.

[59] S.G. Rinaldo, A. Ceresoli, and G. Prettico. A distributed load flow application for multipartite grid operators'coordination. In *2019 16th International Conference on the European Energy Market (EEM)*, pages 1–5, 2019.

[60] G. Prettico, A. Marinopoulos, and S. Vitiello. Distribution system operator observatory 2020: An in-depth look on distribution grids in europe, eur 30561 en. *Joint Research Centre Europe*, 2021.

[61] S.Y. Hadush and L. Meeus. Dso-tso cooperation issues and solutions for distribution grid congestion management. *Energy Policy*, 120:610–621, 2018.

[62] L.R. Visser, M.E. Kootte, A.C. Ferreira, O. Sicurani, E.J. Pauwels, C. Vuik, W.G.J.H.M. Van Sark, and T.A. AlSkaif. An operational bidding framework for aggregated electric vehicles on the electricity spot market. *Applied Energy*, 308:118280, 2022.

[63] S. Chipli. Automating ac power flow simulations. Technical report, Delft University of Technology, 2021.

Appendices

A

Derivation of the MonoTri formulation in polar coordinates

This appendix derives the MonoTri formulation for power and current injections in polar coordinates. The first section shows the derivation for power injections and the second section for current injections.

A.1. Derivation of power injections in polar coordinates

The MonoTri formulation describes the concept of connecting single-phase quantities to three-phase quantities by transforming the nodal admittance matrix. This transformation is shown by expressing the complex power of the single-phase transmission connection bus (S_k^a) and of three-phase distribution connection bus (S_m^{abc}) in terms of the voltage, admittance, and transformer matrices. These expressions were derived in chapter 5 and shown in equations (5.13) and (5.14), which we will repeat here:

$$S_k^a = \mathrm{diag}(V_k^a)\overline{(\mathbf{T_5}Y_{kk}^{abc}\mathbf{T_1}V_k^a)} + \mathrm{diag}(V_k^a)\overline{(\mathbf{T_5}Y_{km}^{abc}\mathbf{V}_m^{abc})},$$

$$\mathbf{S}_m^{abc} = \mathrm{diag}(\mathbf{V}_m^{abc})\overline{(Y_{mk}^{abc}\mathbf{T_1}V_k^a)} + \mathrm{diag}(\mathbf{V}_m^{abc})\overline{(Y_{mm}^{abc}\mathbf{V}_m^{abc})}.$$

If we use polar coordinates, we have to rewrite these equations. We will do so in several steps, for which we have to split the equation into four parts as follows:

$$S_k^a = \underbrace{\mathrm{diag}(V_k^a)\overline{(\mathbf{T_5}Y_{kk}^{abc}\mathbf{T_1}V_k^a)}}_{S_{k,\mathrm{I}}^a} + \underbrace{\mathrm{diag}(V_k^a)\overline{(\mathbf{T_5}Y_{km}^{abc}\mathbf{V}_m^{abc})}}_{S_{k,\mathrm{II}}^a},$$

$$\mathbf{S}_m^{abc} = \underbrace{\mathrm{diag}(\mathbf{V}_m^{abc})\overline{(Y_{mk}^{abc}\mathbf{T_1}V_k^a)}}_{\mathbf{S}_{m,\mathrm{I}}^{abc}} + \underbrace{\mathrm{diag}(\mathbf{V}_m^{abc})\overline{(Y_{mm}^{abc}\mathbf{V}_m^{abc})}}_{\mathbf{S}_{m,\mathrm{II}}^{abc}}.$$

We will derive the polar description of the four parts separately in the following paragraphs. We start with $\mathbf{S}_{m,\mathrm{I}}^{abc}$.

A

Derivation of polar coordinates for $S_{m,I}^{abc}$ We start by rewriting the matrix vector product $Y_{mk}^{abc}T_1$. This matrix-vector product looks as follows:

$$
Y_{mk}^{abc}T_1 = \begin{bmatrix} y^{aa} & y^{ab} & y^{ac} \\ y^{ba} & y^{bb} & y^{bc} \\ y^{ca} & y^{cb} & y^{cc} \end{bmatrix}_{mk} \begin{bmatrix} 1 \\ \mathbf{a}^2 \\ \mathbf{a} \end{bmatrix},
$$

where the parameters within the product are the following:

$$
\mathbf{a} = \quad e^{\frac{2}{3}\pi\iota} = \cos\frac{2}{3}\pi + \iota\sin\frac{2}{3}\pi
$$

$$
y^{pq} = \quad g^{pq} + \iota b^{pq}, \quad p,q \in \alpha_p
$$

The outcome of the product is a 3 by 1 vector which contains the following row entries of which every row corresponds to its respective phase a, b, and c.

$$
Y_{mk}^{abc}T_1[1] = y^{aa} + y^{ab}\cdot\mathbf{a}^2 + y^{ac}\cdot\mathbf{a}
$$
$$
= (g^{aa} + \iota b^{aa}) + (g^{ab} + \iota b^{ab})\cdot(\cos\frac{2}{3}\pi - \iota\sin\frac{2}{3}\pi)
$$
$$
+ (g^{ac} + \iota b^{ac})\cdot(\cos\frac{2}{3}\pi + \iota\sin\frac{2}{3}\pi)
$$

$$
Y_{mk}^{abc}T_1[2] = y^{ba} + y^{bb}\cdot\mathbf{a}^2 + y^{bc}\cdot\mathbf{a}
$$
$$
= (g^{ba} + \iota b^{ba}) + (g^{bb} + \iota b^{bb})\cdot(\cos\frac{2}{3}\pi - \iota\sin\frac{2}{3}\pi)
$$
$$
+ (g^{bc} + \iota b^{bc})\cdot(\cos\frac{2}{3}\pi + \iota\sin\frac{2}{3}\pi)
$$

$$
Y_{mk}^{abc}T_1[3] = y^{ca} + y^{cb}\cdot\mathbf{a}^2 + y^{cc}\cdot\mathbf{a}
$$
$$
= (g^{ca} + \iota b^{ca}) + (g^{cb} + \iota b^{cb})\cdot(\cos\frac{2}{3}\pi - \iota\sin\frac{2}{3}\pi)
$$
$$
+ (g^{cc} + \iota b^{cc})\cdot(\cos\frac{2}{3}\pi + \iota\sin\frac{2}{3}\pi)
$$

We factorize and reassemble the entries, to obtain following expressions at each row which we name according its respective phase and split simultaneously into a real and imaginary part:

$$
Y_{mk}^{abc}T_1[1] = \underbrace{g^{aa} + (g^{ab} + g^{ac})\cdot\cos\frac{2}{3}\pi + (b^{ab} - b^{ac})\cdot\sin\frac{2}{3}\pi}_{Re_{YT1}^a}
$$
$$
+ \iota\underbrace{\left(b^{aa} + (b^{ab} + b^{ac})\cdot\cos\frac{2}{3}\pi + (g^{ac} - g^{ab})\cdot\sin\frac{2}{3}\pi\right)}_{Im_{YT1}^a}
$$

$$Y_{mk}^{abc}T_1[2] = \underbrace{g^{ba} + (g^{bb} + g^{bc}) \cdot \cos \frac{2}{3}\pi + (b^{bb} - b^{bc}) \cdot \sin \frac{2}{3}\pi}_{Re_{YT1}^b}$$

$$+ \iota \underbrace{\left(b^{ba} + (b^{bb} + b^{bc}) \cdot \cos \frac{2}{3}\pi + (g^{bc} - g^{bb}) \cdot \sin \frac{2}{3}\pi \right)}_{Im_{YT1}^b}$$

$$Y_{mk}^{abc}T_1[3] = \underbrace{g^{ca} + (g^{cb} + g^{cc}) \cdot \cos \frac{2}{3}\pi + (b^{cb} - b^{cc}) \cdot \sin \frac{2}{3}\pi}_{Re_{YT1}^c}$$

$$+ \iota \underbrace{\left(b^{ca} + (b^{cb} + b^{cc}) \cdot \cos \frac{2}{3}\pi + (g^{cc} - g^{cb}) \cdot \sin \frac{2}{3}\pi \right)}_{Im_{YT1}^c}$$

Summarised, the per-phase expression of the polar multiplication is :

$$Y_{mk}^{abc}T_1{}^p = Re_{YT1}^p + \iota Im_{YT1}^p, \quad p \in \alpha_p. \tag{A.1}$$

In order to find the expressions for complex power per phase, we need to fill-in the newly obtained matrix into the first part of equation (5.14), which is:

$$S_{m,I}^{abc} = \text{diag}(V_m^{abc})\overline{(Y_{mk}^{abc}T_1 V_k^a)}.$$

We rewrite this as follows:

$$\begin{aligned} S_{m,I}^{abc} &= \text{diag}(V_m^{abc})\overline{(Y_{mk}^{abc}T_1 V_k^a)} \\ &= \overline{(V_k^a)}\text{diag}(V_m^{abc})\overline{(Y_{mk}^{abc}T_1)} \\ &= \overline{(V_k^a)}\text{diag}(V_m^{abc})\overline{(Re_{YT1} + \iota Im_{YT1p})} \end{aligned}$$

The polar expression for a part of the per-phase complex power ($S_{m,I}^p$) is:

$$S_{m,I}^p = |V_m^p||V_k^a|(\cos \delta_m^p - \delta_k^a + \iota \sin \delta_m^a - \delta_k^a) \cdot (Re_{YT1}^p - \iota Im_{YT1}^p) \tag{A.2}$$

If you write this all out, then you get the following expressions for active and reactive power parts per-phase:

$$P_{m,I}^a = |V_m^a||V_k^a| \cdot (Re_{YT1}^a \cos(\delta_m^a - \delta_k^a) + Im_{YT1}^a \sin(\delta_m^a - \delta_k^a))$$
$$Q_{m,I}^a = |V_m^a||V_k^a| \cdot (Re_{YT1}^a \sin(\delta_m^a - \delta_k^a) - Im_{YT1}^a \cos(\delta_m^a - \delta_k^a))$$
$$P_{m,I}^b = |V_m^b||V_k^a| \cdot (Re_{YT1}^b \cos(\delta_m^b - \delta_k^a) + Im_{YT1}^b \sin(\delta_m^b - \delta_k^a))$$
$$Q_{m,I}^b = |V_m^b||V_k^a| \cdot (Re_{YT1}^b \sin(\delta_m^b - \delta_k^a) - Im_{YT1}^b \cos(\delta_m^b - \delta_k^a))$$
$$P_{m,I}^c = |V_m^c||V_k^a| \cdot (Re_{YT1}^c \cos(\delta_m^c - \delta_k^a) + Im_{YT1}^c \sin(\delta_m^c - \delta_k^a))$$
$$Q_{m,I}^c = |V_m^c||V_k^a| \cdot (Re_{YT1}^c \sin(\delta_m^c - \delta_k^a) - Im_{YT1}^c \cos(\delta_m^c - \delta_k^a))$$

Derivation of polar coordinates for $S_{k,II}^a$ We continue by rewriting the second part of equation (5.13), which is:

$$S_{k,II}^a = (V_k^a)\overline{(T_5 Y_{km}^{abc} V_m^{abc})}.$$

We proceed in the same manner as previous paragraph: We start by rewriting the following matrix-vector product:

$$T_5 Y_{km}^{abc} = \frac{1}{3} \begin{bmatrix} 1 \\ a^2 \\ a \end{bmatrix}^T \begin{bmatrix} y^{aa} & y^{ab} & y^{ac} \\ y^{ba} & y^{bb} & y^{bc} \\ y^{ca} & y^{cb} & y^{cc} \end{bmatrix}_{km} \quad ,$$

where the parameters within the product are the following:

$$a = e^{\frac{2}{3}\pi\iota} = \cos\frac{2}{3}\pi + \iota\sin\frac{2}{3}\pi$$
$$y^{pq} = g^{pq} + \iota b^{pq}, \quad p, q \in \alpha_p$$

The obtained vector contains the following entries on its rows, respectively:

$$T_5 Y_{mk}^{abc}[1] = \frac{1}{3}\left(y^{aa} + y^{ba} \cdot a^2 + y^{ca} \cdot a\right)$$
$$= \frac{1}{3}((g^{aa} + \iota b^{aa}) + (g^{ba} + \iota b^{ba}) \cdot (\cos\frac{2}{3}\pi - \iota\sin\frac{2}{3}\pi)$$
$$+ (g^{ca} + \iota b^{ca}) \cdot (\cos\frac{2}{3}\pi + \iota\sin\frac{2}{3}\pi))$$

$$T_5 Y_{mk}^{abc}[2] = \frac{1}{3}\left(y^{ab} + y^{bb} \cdot a^2 + y^{cb} \cdot a\right)$$
$$= \frac{1}{3}((g^{ab} + \iota b^{ab}) + (g^{bb} + \iota b^{bb}) \cdot (\cos\frac{2}{3}\pi - \iota\sin\frac{2}{3}\pi)$$
$$+ (g^{cb} + \iota b^{cb}) \cdot (\cos\frac{2}{3}\pi + \iota\sin\frac{2}{3}\pi))$$

$$T_5 Y_{mk}^{abc}[3] = \frac{1}{3}\left(y^{ac} + y^{bc} \cdot a^2 + y^{cc} \cdot a\right)$$
$$= \frac{1}{3}((g^{ac} + \iota b^{ac}) + (g^{bc} + \iota b^{bc}) \cdot (\cos\frac{2}{3}\pi - \iota\sin\frac{2}{3}\pi)$$
$$+ (g^{cc} + \iota b^{cc}) \cdot (\cos\frac{2}{3}\pi + \iota\sin\frac{2}{3}\pi))$$

We factorise, reassemble, rename, and split these equations to obtain the following:

$$T_5 Y_{mk}^{abc}[1] = \frac{1}{3}\underbrace{\left(g^{aa} + (g^{ba} + g^{ca}) \cdot \cos\frac{2}{3}\pi + (b^{ba} - b^{ca}) \cdot \sin\frac{2}{3}\pi\right)}_{\mathrm{Re}_{T5Y}^a}$$
$$+ \iota\frac{1}{3}\underbrace{\left(b^{aa} + (b^{ba} + b^{ca}) \cdot \cos\frac{2}{3}\pi + (g^{ca} - g^{ba}) \cdot \sin\frac{2}{3}\pi\right)}_{\mathrm{Im}_{T5Y}^a}$$

$$T_5 Y_{mk}^{abc}[2] = \frac{1}{3}\underbrace{\left(g^{ab} + (g^{bb} + g^{cb}) \cdot \cos\frac{2}{3}\pi + (b^{bb} - b^{cb}) \cdot \sin\frac{2}{3}\pi\right)}_{Re_{T5Y}^{b}}$$

$$+ \iota\frac{1}{3}\underbrace{\left(b^{ab} + (b^{bb} + b^{cb}) \cdot \cos\frac{2}{3}\pi + (g^{cb} - g^{bb}) \cdot \sin\frac{2}{3}\pi\right)}_{Im_{T5Y}^{b}}$$

$$T_5 Y_{mk}^{abc}[3] = \frac{1}{3}\underbrace{\left(g^{ac} + (g^{bc} + g^{cc}) \cdot \cos\frac{2}{3}\pi + (b^{bc} - b^{cc}) \cdot \sin\frac{2}{3}\pi\right)}_{Re_{T5Y}^{c}}$$

$$+ \iota\frac{1}{3}\underbrace{\left(b^{ac} + (b^{bc} + b^{cc}) \cdot \cos\frac{2}{3}\pi + (g^{cc} - g^{bc}) \cdot \sin\frac{2}{3}\pi\right)}_{Im_{T5Y}^{c}}$$

Summarised, the per-phase expression of the polar multiplication is :

$$(T_5 Y_{km}^{abc})^p = \frac{1}{3}(Re_{T5Y}^p + \iota Im_{T5Y}^p), \quad p \in \alpha_p. \tag{A.3}$$

In order to find the expressions for complex power per phase, we need to fill-in the newly obtained matrix into the second part of equation (5.13), which is:

$$\begin{aligned} S_{k,II}^a &= (V_k^a)\overline{(T_5 Y_{km}^{abc} V_m^{abc})} \\ &= \overline{(T_5 Y_{km}^{abc})}(V_k^a)\overline{(V_m^{abc})} \\ &= \frac{1}{3}\overline{(Re_{T5Y} + \iota Im_{T5Y})}(V_k^a)\overline{(V_m^{abc})} \end{aligned}$$

The polar expression for a part of the complex power ($S_{k,II}^a$) is:

$$S_{k,II}^a = \frac{1}{3}\sum_{p\in\alpha_q} |V_k^a||V_m^p|(\cos(\delta_k^a - \delta_m^p) + \iota\sin(\delta_k^a - \delta_m^p)) \cdot (Re_{T5Y}^p - \iota Im_{T5Y}^p)$$

$$\tag{A.4}$$

If we express this in a real and active part, we obtain:

$$P_{k,II}^a = \frac{1}{3}\sum_{p\in\alpha_q} |V_k^a||V_m^p|\left(Re_{T5Y}^p \cos(\delta_k^a - \delta_m^p) + Im_{T5Y}^p \sin(\delta_k^a - \delta_m^p)\right)$$

$$Q_{k,II}^a = \frac{1}{3}\sum_{p\in\alpha_q} |V_k^a||V_m^p|\left(Re_{T5Y}^p \sin(\delta_k^a - \delta_m^p) - Im_{T5Y}^p \cos(\delta_k^a - \delta_m^p)\right)$$

Derivation of polar coordinates for $S_{k,I}^a$ Lastly, we have to rewrite the first part of equation (5.13), which is:

$$S_{k,I}^a = (V_k^a)\overline{(T_5 Y_{kk}^{abc} T_1 V_k^a)}.$$

We start by rewriting the matrix-vector product:

$$T_5 Y_{kk}^{abc} T_1 = \frac{1}{3} \begin{bmatrix} 1 \\ a^2 \\ a \end{bmatrix}^T \begin{bmatrix} y^{aa} & y^{ab} & y^{ac} \\ y^{ba} & y^{bb} & y^{bc} \\ y^{ca} & y^{cb} & y^{cc} \end{bmatrix}_{kk} \begin{bmatrix} 1 \\ a^2 \\ a \end{bmatrix},$$

with the following parameters:

$$a = e^{\frac{2}{3}\pi\iota} = \cos\frac{2}{3}\pi + \iota\sin\frac{2}{3}\pi$$

$$y^{pq} = g^{pq} + \iota b^{pq}, \quad p, q \in \alpha_p$$

We do matrix multiplications from left till right, so we first regard the matrix-vector product of $T_5 Y_{km}^{abc}$, this expression results in the same row vector as described in paragraph A.1.

This row vector is then multiplied to T_1, which results in the following scalar as result:

$$T_5 Y T_1 = \frac{1}{3}((\mathrm{Re}_{T5Y}^a + \iota\mathrm{Im}_{T5Y}^a) + (\mathrm{Re}_{T5Y}^b + \iota\mathrm{Im}_{T5Y}^b)(\cos\frac{2}{3}\pi - \iota\sin\frac{2}{3}\pi)$$

$$+ (\mathrm{Re}_{T5Y}^c + \iota\mathrm{Im}_{T5Y}^c)(\cos\frac{2}{3}\pi + \iota\sin\frac{2}{3}\pi)) \tag{A.5}$$

If we split this in a real and imaginary part, then we get the following expressions:

$$\mathrm{Re}_{T5YT1} = \mathrm{Re}_{T5Y}^a + (\mathrm{Re}_{T5Y}^b + \mathrm{Re}_{T5Y}^c) \cdot \cos\left(\frac{2}{3}\pi\right) + (\mathrm{Im}_{T5Y}^b - \mathrm{Im}_{T5Y}^c) \cdot \sin\left(\frac{2}{3}\pi\right)$$

$$\mathrm{Im}_{T5YT1} = \mathrm{Im}_{T5Y}^a + (\mathrm{Im}_{T5Y}^b + \mathrm{Im}_{T5Y}^c) \cdot \cos\left(\frac{2}{3}\pi\right) + (\mathrm{Re}_{T5Y}^c - \mathrm{Re}_{T5Y}^b) \cdot \sin\left(\frac{2}{3}\pi\right)$$

In order to find the expressions for complex power per phase, we need to fill-in the newly obtained matrix into the first part of equation (5.13), which is:

$$S_{k,I}^a = (V_k^a)\overline{(T_5 Y_{kk}^{abc} T_1 V_k^a)}$$

$$= (V_k^a)\overline{(V_k^a)}\overline{(T_5 Y_{kk}^{abc} T_1)}$$

$$= \frac{1}{3}|V_k^a|^2 (\mathrm{Re}_{T5YT1} - \iota\mathrm{Im}_{T5YT1}) \tag{A.6}$$

The active and reactive expressions for complex power part are then:

$$P_{k,I}^a = \frac{1}{3}|V_k^a|^2 \mathrm{Re}_{T5YT1}$$

$$Q_{k,I}^a = -\frac{1}{3}|V_k^a|^2 \mathrm{Im}_{T5YT1}$$

A

A.2. Derivation of current injections in polar coordinates

The derivation of current injections in polar coordinates works in a similar manner as power injections, but instead we express the complex current of both connection buses (I_k^a and I_m^{abc}). These expressions were shown in equations (5.18) and (5.19), which we will repeat here:

$$I_k^a = T_3 I_k^{abc} = T_3 Y_{kk}^{abc} T_1 V_k^a + T_3 Y_{km}^{abc} V_m^{abc},$$
$$I_m^{abc} = Y_{mk}^{abc} T_1 V_k^a + Y_{mm}^{abc} V_m^{abc}.$$

We will rewrite these equations, for which split the equation into four parts as follows:

$$I_k^a = \underbrace{T_3 Y_{11}^{abc} T_1 V_k^a}_{I_{k,I}^a} + \underbrace{T_3 Y_{12}^{abc} V_m^{abc}}_{I_{k,II}^a},$$
$$I_m^{abc} = \underbrace{Y_{21}^{abc} T_1 V_k^a}_{I_{m,I}^{abc}} + \underbrace{Y_{22}^{abc} V_m^{abc}}_{I_{m,II}^{abc}}.$$

We start with $I_{m,I}^{abc}$

Derivation of polar coordinates for $I_{m,I}^{abc}$ The expression for $I_{m,I}^{abc}$ contains the same matrix-vector product as in the power polar description, see paragraph A.1. The per-phase expression of the polar multiplication of this matrix-vector product is (see eq. (A.1)):

$$Y_{mk}^{abc} T_1{}^p = Re_{YT1}^p + \iota Im_{YT1}^p, \quad p \in \alpha_p.$$

We plug this expression into the first part of eq. (5.19) and rewrite as follows:

$$I_{m,I}^{abc} = Y_{mk}^{abc} T_1 V_k^a$$
$$= V_k^a \cdot (Re_{YT1} + \iota Im_{YT1p})$$

The polar expression for a part of the per-phase complex power ($I_{m,I}^p$) is:

$$I_{m,I}^p = |V_k^a|(\cos \delta_k^a + \iota \sin \delta_k^a) \cdot (Re_{YT1}^p + \iota Im_{YT1}^p), \quad p \in \alpha_p. \qquad (A.7)$$

If you write this out, then you get the following expressions for active and reactive power parts per-phase:

$$Re(I_{m,I}^a) = |V_k^a| \cdot (Re_{YT1}^a \cos(\delta_k^a) - Im_{YT1}^a \sin(\delta_k^a))$$
$$Im(I_{m,I}^a) = |V_k^a| \cdot (Re_{YT1}^a \sin(\delta_k^a) + Im_{YT1}^a \cos(\delta_k^a))$$
$$Re(I_{m,I}^b) = |V_k^a| \cdot (Re_{YT1}^b \cos(\delta_k^a) - Im_{YT1}^b \sin(\delta_k^a))$$
$$Im(I_{m,I}^b) = |V_k^a| \cdot (Re_{YT1}^b \sin(\delta_k^a) + Im_{YT1}^b \cos(\delta_k^a))$$
$$Re(I_{m,I}^c) = |V_k^a| \cdot (Re_{YT1}^c \cos(\delta_k^a) - Im_{YT1}^c \sin(\delta_k^a))$$
$$Im(I_{m,I}^c) = |V_k^a| \cdot (Re_{YT1}^c \sin(\delta_k^a) + Im_{YT1}^c \cos(\delta_k^a))$$

Derivation of polar coordinates for $I_{k,II}^a$ We continue by rewriting the second part of equation (5.18), which is:

$$I_{k,II}^a = T_3 Y_{12}^{abc} V_m^{abc}.$$

143

A

We rewrite the following matrix-vector product:

$$
\mathbf{T}_3 Y_{km}^{abc} = \frac{1}{3}
\begin{bmatrix} 1 \\ \mathbf{a} \\ \mathbf{a}^2 \end{bmatrix}^{\mathsf{T}}
\begin{bmatrix}
y^{aa} & y^{ab} & y^{ac} \\
y^{ba} & y^{bb} & y^{bc} \\
y^{ca} & y^{cb} & y^{cc}
\end{bmatrix}_{km} ,
$$

which has the following parameters:

$$
\begin{aligned}
\mathbf{a} &= e^{\frac{2}{3}\pi\iota} = \cos\frac{2}{3}\pi + \iota\sin\frac{2}{3}\pi \\
y^{pq} &= g^{pq} + \iota b^{pq}, \quad p,q \in \alpha_p.
\end{aligned}
$$

The obtained vector contains the following entries on its rows, respectively:

$$
\begin{aligned}
I_{k,II}^{a}[1] &= \frac{1}{3}\left(y^{aa} + y^{ba}\cdot\mathbf{a}^2 + y^{ca}\cdot\mathbf{a}\right) \\
&= \frac{1}{3}((g^{aa} + \iota b^{aa}) + (g^{ba} + \iota b^{ba})\cdot(\cos\frac{2}{3}\pi + \iota\sin\frac{2}{3}\pi) \\
&+ (g^{ca} + \iota b^{ca})\cdot(\cos\frac{2}{3}\pi - \iota\sin\frac{2}{3}\pi))
\end{aligned}
$$

$$
\begin{aligned}
I_{k,II}^{a}[2] &= \frac{1}{3}\left(y^{ab} + y^{bb}\cdot\mathbf{a}^2 + y^{bc}\cdot\mathbf{a}\right) \\
&= \frac{1}{3}((g^{ab} + \iota b^{ab}) + (g^{bb} + \iota b^{bb})\cdot(\cos\frac{2}{3}\pi + \iota\sin\frac{2}{3}\pi) \\
&+ (g^{cb} + \iota b^{cb})\cdot(\cos\frac{2}{3}\pi - \iota\sin\frac{2}{3}\pi))
\end{aligned}
$$

$$
\begin{aligned}
I_{k,II}^{a}[3] &= \frac{1}{3}\left(y^{ac} + y^{bc}\cdot\mathbf{a}^2 + y^{cc}\cdot\mathbf{a}\right) \\
&= \frac{1}{3}((g^{ac} + \iota b^{ac}) + (g^{bc} + \iota b^{bc})\cdot(\cos\frac{2}{3}\pi + \iota\sin\frac{2}{3}\pi) \\
&+ (g^{cc} + \iota b^{cc})\cdot(\cos\frac{2}{3}\pi - \iota\sin\frac{2}{3}\pi))
\end{aligned}
$$

We factorise, reassemble, rename, and split these equations to obtain the following:

$$
\begin{aligned}
I_{k,II}^{a}[1] &= \frac{1}{3}\underbrace{\left(g^{aa} + (g^{ba} + g^{ca})\cdot\cos\frac{2}{3}\pi + (b^{ca} - b^{ba})\cdot\sin\frac{2}{3}\pi\right)}_{\mathrm{Re}_{T3Y}^{a}} \\
&+ \iota\frac{1}{3}\underbrace{\left(b^{aa} + (b^{ba} + b^{ca})\cdot\cos\frac{2}{3}\pi + (g^{ba} - g^{ca})\cdot\sin\frac{2}{3}\pi\right)}_{\mathrm{Im}_{T3Y}^{a}}
\end{aligned}
$$

$$I^a_{k,II}[2] = \frac{1}{3}\underbrace{\left(g^{ab} + (g^{bb} + g^{cb}) \cdot \cos\frac{2}{3}\pi + (b^{cb} - b^{bb}) \cdot \sin\frac{2}{3}\pi\right)}_{Re^b_{T3Y}}$$

$$+ \iota\frac{1}{3}\underbrace{\left(b^{ab} + (b^{bb} + b^{cb}) \cdot \cos\frac{2}{3}\pi + (g^{bb} - g^{cb}) \cdot \sin\frac{2}{3}\pi\right)}_{Im^b_{T3Y}}$$

$$I^a_{k,II}[3] = \frac{1}{3}\underbrace{\left(g^{ac} + (g^{bc} + g^{cc}) \cdot \cos\frac{2}{3}\pi + (b^{cc} - b^{bc}) \cdot \sin\frac{2}{3}\pi\right)}_{Re^c_{T3Y}}$$

$$+ \iota\frac{1}{3}\underbrace{\left(b^{ac} + (b^{bc} + b^{cc}) \cdot \cos\frac{2}{3}\pi + (g^{bc} - g^{cc}) \cdot \sin\frac{2}{3}\pi\right)}_{Im^c_{T3Y}}$$

Summarised, the per-phase expression of the polar multiplication is :

$$(T_3 Y^{abc}_{km})^p = \frac{1}{3}(Re^p_{T3Y} + \iota Im^p_{T3Y}) \tag{A.8}$$

In order to find the expressions for complex power per phase, we need to fill-in the newly obtained matrix into the right-side of equation (5.13), which is:

$$I^a_{k,II} = T_3 Y^{abc}_{km} V^{abc}_m$$
$$= \frac{1}{3}(Re_{T3Y} + \iota Im_{T3Y}) \cdot V^{abc}_m$$

The polar expression of $(I^a_{k,II})$ is:

$$I^a_{k,II} = \frac{1}{3}\sum_{p \in \alpha_q}(|V^p_m|(\cos(\delta^p_m) + \iota\sin(\delta^p_m))(Re^p_{T5Y} + \iota Im^p_{T5Y})) \tag{A.9}$$

If we express this in a real and complex part, we obtain:

$$Re(I^a_{k,II}) = \frac{1}{3}\sum_{p \in \alpha_q}|V^p_m|\left(Re^p_{T5Y}\cos(\delta^p_m) - Im^p_{T5Y}\sin(\delta^p_m)\right)$$

$$Im(I^a_{k,II}) = \frac{1}{3}\sum_{p \in \alpha_q}|V^p_m|\left(Re^p_{T5Y}\sin(\delta^p_m) + Im^p_{T5Y}\cos(\delta^p_m)\right)$$

Derivation of polar coordinates for $I^a_{k,I}$ Lastly, we rewrite the first part of equation (5.18), which is:

$$I^a_{k,I} = T_3 I^{abc}_k = T_3 Y^{abc}_{kk} T_1 V^a_k$$

We start by rewriting matrix-vector product

$$T_3 Y^{abc}_{kk} T_1 = \frac{1}{3}\begin{bmatrix} 1 \\ a \\ a^2 \end{bmatrix}^T \begin{bmatrix} y^{aa} & y^{ab} & y^{ac} \\ y^{ba} & y^{bb} & y^{bc} \\ y^{ca} & y^{cb} & y^{cc} \end{bmatrix}_{kk} \begin{bmatrix} 1 \\ a^2 \\ a \end{bmatrix}$$

A

with the following parameters:

$$\mathbf{a} = e^{\frac{2}{3}\pi\iota} = \cos\frac{2}{3}\pi + \iota\sin\frac{2}{3}\pi$$

$$y^{pq} = g^{pq} + \iota b^{pq}, \quad p, q \in \alpha_p.$$

We do matrix multiplications from left till right, so we first regard the matrix-vector product $T_3 Y^{abc}_{km}$, this expression results in the same row vector as described in paragraph (A.2).

This row vector is then multiplied to T1, which results in the following scalar as result:

$$\mathbf{T_3 Y T_1} = \frac{1}{3}((Re^a_{T3Y} + \iota Im^a_{T3Y}) + (Re^b_{T3Y} + \iota Im^b_{T3Y})(\cos\frac{2}{3}\pi + \iota\sin\frac{2}{3}\pi)$$
$$+ (Re^c_{T3Y} + \iota Im^c_{T3Y})(\cos\frac{2}{3}\pi - \iota\sin\frac{2}{3}\pi)) \qquad (A.10)$$

If we split this in a real and imaginary part, then we get the following expressions:

$$Re_{T3YT1} = Re^a_{T3Y} + (Re^b_{T3Y} + Re^c_{T3Y}) \cdot \cos\left(\frac{2}{3}\pi\right) + (Im^c_{T3Y} - Im^b_{T3Y}) \cdot \sin\left(\frac{2}{3}\pi\right)$$

$$Im_{T3YT1} = Im^a_{T3Y} + (Im^b_{T3Y} + Im^c_{T3Y}) \cdot \cos\left(\frac{2}{3}\pi\right) + (Re^b_{T3Y} - Re^c_{T3Y}) \cdot \sin\left(\frac{2}{3}\pi\right)$$

In order to find the expressions for complex power per phase, we need to fill-in the newly obtained matrix into the left side of equation (5.18), which is:

$$I^a_{k,I} = \mathbf{T_3 Y^{abc}_{kk} T_1} V^a_k$$
$$= \frac{1}{3}|V^a_k|(\cos(\delta^a_k) + \iota\sin(\delta^a_k))(Re_{T3YT1} + \iota Im_{T3YT1}) \qquad (A.11)$$

The real and imaginary expressions for single-phase current become then:

$$Re(I^a_{k,I}) = \frac{1}{3}|V^a_k|Re_{T3YT1}\cos(\delta^a_k) - Im_{T3YT1}\sin(\delta^a_k)$$

$$Im(I^a_{k,I}) = \frac{1}{3}|V^a_k|Im_{T3YT1}\cos(\delta^a_k) + Re_{T3YT1}\sin(\delta^a_k)$$

B

The Jacobian for the MonoTri Formulation

This appendix contains the entries of the Jacobian matrix for the power and current power flow equations after transformation according the MonoTri Formulation.

Table B.1: Overview of the derivatives in the Jacobian in polar coordinates. It shows the derivatives of active power (real part of complex power) with respect to voltage of the current injections in the MonoTri formulation

Real part		
System	**Derivative system**	**Derivative**
Transmission	Trans	$\frac{\partial P_T^+}{\partial \delta_T^+} = \|V_T^+\| \sum_{r \in \alpha_p} \|V_D^r\| \left(-Re_{T5}^r \sin(\delta_T^+ - \delta_D^r) + Im_{T5}^r \cos(\delta_T^+ - \delta_D^r) \right)$
		$\frac{\partial P_T^+}{\partial \|V_T^+\|} = 2\|V_T^+\| Re_{T5YT1} + \sum_{r \in \alpha_p} \|V_D^r\| \left(Re_{T5}^r \cos(\delta_T^+ - \delta_D^r) + Im_{T5}^r \sin(\delta_T^+ - \delta_D^r) \right)$
	Distr	$\frac{\partial P_T^+}{\partial \delta_D^+} = \|V_T^+\|\|V_D^p\| \left(Re_{T5}^p \sin(\delta_T^+ - \delta_D^p) - Im_{T5}^p \cos(\delta_T^+ - \delta_D^p) \right) \quad \{p \in \alpha_p\}$
		$\frac{\partial P_T^+}{\partial \|V_D^p\|} = \|V_T^+\| \left(Re_{T5}^p \cos(\delta_T^+ - \delta_D^p) + Im_{T5i}^p \sin(\delta_T^+ - \delta_D^p) \right) \quad \{p \in \alpha_p\}$
Distribution	Distr $p = q$	$\frac{\partial P_D^p}{\partial \delta_D^p} = \|V_D^p\| \sum_{\substack{r \in \alpha_p \\ p \neq r}} \|V_i^r\| \left(-G_{DD}^{pr} \sin(\delta_D^p - \delta_D^r) + B_{DD}^{pr} \cos(\delta_D^p - \delta_D^r) \right)$
		$\qquad + \|V_D^p\|\|V_T^+\| \left(-Re_{T1}^p \sin(\delta_D^p - \delta_T^+) + Im_{T1}^p \cos(\delta_D^p - \delta_T^+) \right)$
		$\frac{\partial P_D^p}{\partial \|V_D^p\|} = 2\|V_D^p\| G_{DD}^{pp} + \sum_{\substack{r \in \alpha_p \\ p \neq r}} \|V_D^r\| \left(G_{DD}^{pr} \cos(\delta_D^p - \delta_D^r) + B_{DD}^{pr} \sin(\delta_D^p - \delta_D^r) \right)$
		$\qquad + \|V_T^+\| \left(Re_{T1}^p \cos(\delta_D^p - \delta_T^+) + Im_{T1}^p \sin(\delta_D^p - \delta_T^+) \right)$
	Distr $p \neq q$	$\frac{\partial P_D^p}{\partial \delta_D^q} = \|V_D^p\|\|V_D^q\| \left(G_{DD}^{pq} \sin(\delta_D^p - \delta_D^q) - B_{DD}^{pq} \cos(\delta_D^p - \delta_D^q) \right)$
		$\frac{\partial P_D^p}{\partial \|V_D^q\|} = \|V_D^p\| \left(G_{DD}^{pq} \cos(\delta_D^p - \delta_D^q) + B_{DD}^{pq} \sin(\delta_D^p - \delta_D^q) \right)$
	Trans	$\frac{\partial P_D^p}{\partial \delta_T^+} = \|V_D^p\|\|V_T^+\| \left(Re_{T1}^p \sin(\delta_D^p - \delta_T^+) - Im_{T1}^p \cos(\delta_D^p - \delta_T^+) \right)$
		$\frac{\partial P_D^p}{\partial \|V_T^+\|} = \|V_D^p\| \left(Re_{T1}^p \cos(\delta_D^p - \delta_T^+) + Im_{T1}^p \sin(\delta_D^p - \delta_T^+) \right)$

Table B.2: Overview of the derivatives in the Jacobian in polar coordinates. It shows the derivatives of reactive power (imaginary part of complex power) with respect to voltage of the current injections in the MonoTri formulation

Imaginary part		
System	**Derivative system**	**Derivative**
Transmission	Trans	$\frac{\partial Q_T^+}{\partial \delta_T^+} = \|V_T^+\| \sum_{r\in\alpha_p} \|V_D^r\| \left(Re_{T5}^r \cos(\delta_T^+ - \delta_D^r) + Im_{T5}^r \sin(\delta_T^+ - \delta_D^r)\right)$ $\frac{\partial Q_T^+}{\partial \|V_T^+\|} = -2\|V_T^+\| Im_{T5YT1} + \sum_{r\in\alpha_p} \|V_D^r\| \left(Re_{T5}^r \sin(\delta_T^+ - \delta_D^r) - Im_{T5}^r \cos(\delta_T^+ - \delta_D^r)\right)$
	Distr	$\frac{\partial Q_T^+}{\partial \delta_D^p} = \|V_T^+\|\|V_D^p\| \left(-Re_{T5}^p \cos(\delta_T^+ - \delta_D^p) - Im_{T5}^p \sin(\delta_T^+ - \delta_D^p)\right) \quad \{p\in\alpha_p\}$ $\frac{\partial Q_T^+}{\partial \|V_D^p\|} = \|V_T^+\| \left(Re_{T5}^p \sin(\delta_T^+ - \delta_D^p) - Im_{T5i}^p \cos(\delta_T^+ - \delta_D^p)\right) \quad \{p\in\alpha_p\}$
Distribution	Distr $p = q$	$\frac{\partial Q_D^p}{\partial \delta_D^p} = \|V_D^p\| \sum_{\substack{r\in\alpha_p \\ p\neq r}} \|V_i^r\| \left(G_{DD}^{pr} \cos(\delta_D^p - \delta_D^r) + B_{DD}^{pr} \sin(\delta_D^p - \delta_D^r)\right)$ $\qquad + \|V_D^p\|\|V_T^+\| \left(Re_{T1}^p \cos(\delta_D^p - \delta_T^+) + Im_{T1}^p \sin(\delta_D^p - \delta_T^+)\right)$ $\frac{\partial Q_D^p}{\partial \|V_D^p\|} = -2\|V_D^p\| B_{DD}^{pp} + \sum_{\substack{r\in\alpha_p \\ p\neq r}} \|V_D^r\| \left(G_{DD}^{pp} \sin(\delta_D^p - \delta_D^r) - B_{DD}^{pr} \cos(\delta_D^p - \delta_D^r)\right)$ $\qquad + \|V_T^+\| \left(Re_{T1}^p \sin(\delta_D^p - \delta_T^+) - Im_{T1}^p \cos(\delta_D^p - \delta_T^+)\right)$
	Distr $p \neq q$	$\frac{\partial Q_D^p}{\partial \delta_D^q} \quad \{p\neq q\} = \|V_D^p\|\|V_D^q\| \left(-G_{DD}^{pq} \cos(\delta_D^p - \delta_D^q) - B_{DD}^{pq} \sin(\delta_D^p - \delta_D^q)\right)$ $\frac{\partial Q_D^p}{\partial \|V_D^q\|} = \|V_D^p\| \left(G_{DD}^{pq} \sin(\delta_D^p - \delta_D^q) - B_{DD}^{pq} \cos(\delta_D^p - \delta_D^q)\right)$
	Trans	$\frac{\partial Q_D^p}{\partial \delta_T^+} = \|V_D^p\|\|V_T^+\| \left(-Re_{T1}^p \cos(\delta_D^p - \delta_T^+) - Im_{T1}^p \sin(\delta_D^p - \delta_T^+)\right)$ $\frac{\partial Q_D^p}{\partial \|V_T^+\|} = \|V_D^p\| \left(Re_{T1}^p \sin(\delta_D^p - \delta_T^+) - Im_{T1}^p \cos(\delta_D^p - \delta_T^+)\right)$

Table B.3: Overview of the derivatives in the Jacobian in polar coordinates. It shows the derivatives of real part of current injections with respect to voltage in the MonoTri formulation

Real part		
System	**Derivative system**	**Derivative**
Transmission	Trans	$\frac{\partial I_T^+}{\partial \delta_T^+} = \|V_T^+\| \left(-Re_{T3YT1} \sin(\delta_T^+) - Im_{T3YT1} \cos(\delta_T^+)\right)$ $\frac{\partial I_T^+}{\partial \|V_T^+\|} = \left(Re_{T3YT1} \cos(\delta_T^+) - Im_{T3YT1} \sin(\delta_T^+)\right)$
	Distr	$\frac{\partial I_T^+}{\partial \delta_D^p} = \|V_D^p\| \left(-Re_{T3Y}^p \sin(\delta_D^p) - Im_{T3Y}^p \cos(\delta_D^p)\right) \quad \{p\in\alpha_q\}$ $\frac{\partial P_T^+}{\partial \|V_D^p\|} = \left(Re_{T3Y}^p \cos(\delta_D^p) - Im_{T3Y}^p \sin(\delta_D^p)\right) \quad \{p\in\alpha_q\}$
Distribution	Distr $p = q$	$\frac{\partial I_D^p}{\partial \delta_D^p} = \|V_D^p\| \left(-G_{DD}^{pp} \sin(\delta_D^p) - B_{DD}^{pp} \cos(\delta_D^p)\right)$ $\frac{\partial I_D^p}{\partial \|V_D^p\|} = \left(G_{DD}^{pp} \cos(\delta_D^p) - B_{DD}^{pp} \sin(\delta_D^p)\right)$
	Distr $p \neq q$	$\frac{\partial I_D^p}{\partial \delta_D^q} = \|V_D^q\| \left(-G_{DD}^{pq} \sin(\delta_D^q) - B_{DD}^{pq} \cos(\delta_D^q)\right)$ $\frac{\partial I_D^p}{\partial \|V_D^q\|} = \left(G_{DD}^{pq} \cos(\delta_D^q) - B_{DD}^{pq} \sin(\delta_D^q)\right)$
	Trans	$\frac{\partial I_D^p}{\partial \delta_T^+} = \|V_T^+\| \left(-Re_{T1}^p \sin(\delta_T^+) - Im_{T1}^p \cos(\delta_T^+)\right)$ $\frac{\partial I_D^p}{\partial \|V_T^+\|} = \left(Re_{T1}^p \cos(\delta_T^+) - Im_{T1}^p \sin(\delta_T^+)\right)$

Table B.4: Overview of the derivatives in the Jacobian in polar coordinates. It shows the derivatives of imaginary part of current injections with respect to voltage in the MonoTri formulation

	Imaginary part	
System	**Derivative system**	**Derivative**
Transmission	Trans	$\frac{\partial I_T^+}{\partial \delta_T^+} = \lvert V_T^+ \rvert \left(Re_{T3YT1} \cos(\delta_T^+) - Im_{T3YT1} \sin(\delta_T^+) \right)$ $\frac{\partial I_T^+}{\partial \lvert V_T^+ \rvert} = \left(Re_{T3YT1} \sin(\delta_T^+) + Im_{T3YT1} \cos(\delta_T^+) \right)$
	Distr	$\frac{\partial I_T^+}{\partial \delta_D^p} = \lvert V_D^p \rvert \left(Re_{T3Y}^p \cos(\delta_D^p) + Im_{T3Y}^p \sin(\delta_D^p) \right) \quad \{p \in \alpha_q\}$ $\frac{\partial P_T^+}{\partial \lvert V_D^p \rvert} = \left(Re_{T3Y}^p \sin(\delta_D^p) + Im_{T3Y}^p \cos(\delta_D^p) \right) \quad \{p \in \alpha_q\}$
Distribution	Distr $p = q$	$\frac{\partial I_D^p}{\partial \delta_D^p} = \lvert V_D^p \rvert \left(G_{DD}^{pp} \cos(\delta_D^p) - B_{DD}^{pp} \sin(\delta_D^p) \right)$ $\frac{\partial I_D^p}{\partial \lvert V_D^p \rvert} = \left(G_{DD}^{pp} \sin(\delta_D^p) + B_{DD}^{pp} \cos(\delta_D^p) \right)$
	Distr $p \neq q$	$\frac{\partial I_D^p}{\partial \delta_D^q} = \lvert V_D^q \rvert \left(G_{DD}^{pq} \cos(\delta_D^q) - B_{DD}^{pq} \sin(\delta_D^q) \right)$ $\frac{\partial I_D^p}{\partial \lvert V_D^q \rvert} = \left(G_{DD}^{pq} \sin(\delta_D^q) + B_{DD}^{pq} \cos(\delta_D^q) \right)$
	Trans	$\frac{\partial I_D^p}{\partial \delta_T^+} = \lvert V_T^+ \rvert \left(Re_{T1}^p \cos(\delta_T^+) - Im_{T1}^p \sin(\delta_T^+) \right)$ $\frac{\partial I_D^p}{\partial \lvert V_T^+ \rvert} = \left(Re_{T1}^p \sin(\delta_T^+) + Im_{T1}^p \cos(\delta_T^+) \right)$

C

Details of the used test cases

C.1. Transmission test cases

Table C.1: Elements of four transmission test cases.

Transmission test cases (Matpower [38])				
	Test case			
	T9	T118	T2383	T3120
Element	*Case 9*	*Case 118*	*Case 2383wp*	*Case 3120sp*
Buses	9	118	2383	3120
Generators	3	54	327	505
Branches	9	185	2895	3693
Loads	6	64	2056	2615

C
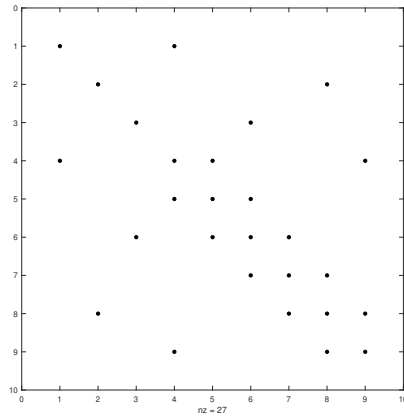
Figure C.1: Sparsity Pattern of Transmission test case T9
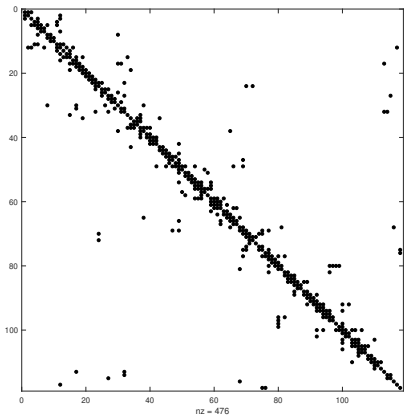
Figure C.2: Sparsity Pattern of Transmission test case T118
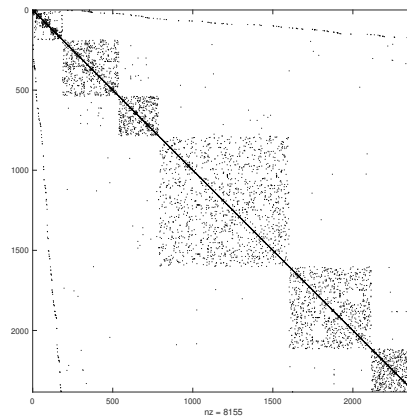
Figure C.3: Sparsity Pattern of Transmission test case T2383
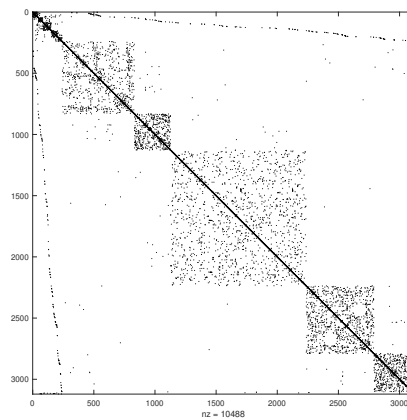
Figure C.4: Sparsity Pattern of Transmission test case T3120

C.2. Distribution test cases

Table C.2: Elements of five distribution test cases. The Dxx is the name I use in my chapters. The italic case name is the one used by Matpower. There are two types of loads (Wye and Delta) in distribution networks. The first two gives the number of Wye loads and the subsequent row the number of Delta loads. The first transformer-configuration row gives the configuration of the first transformer and the subsequent row the configuration of the second.

C

Distribution test cases taken from IEEE [39]

Element		Test case				
		D13	D37	D123	D906	D2500
		Case 13	*Case 37*	*Case 123*	*Case LV*	*Case 8500*
Buses		13	37	123	906	2500
Generators		1	1	1	1	1
Branches		12	36	122	905	2499
Loads	Wye	5	-	113	55	1138
	Delta	3	25	3	-	-
Transformers		2	2	2	1	1
Configuration		D-Yg	D-D	D-Yg	D-Y	D-Y
		Yg-Yg	D-D	D-Yg		
SVRs		1	1	3	-	4
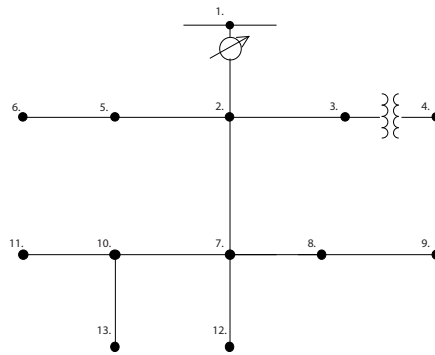
Figure C.5: Network outlook of Distribution test case D13 [39]
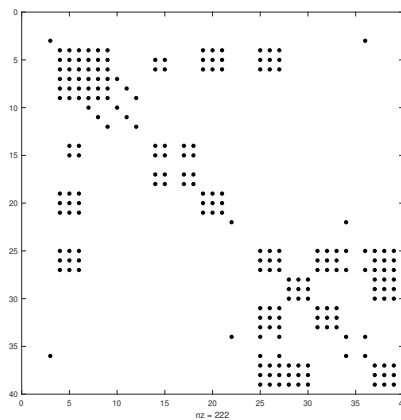
Figure C.6: Sparsity pattern of Distribution test case D13
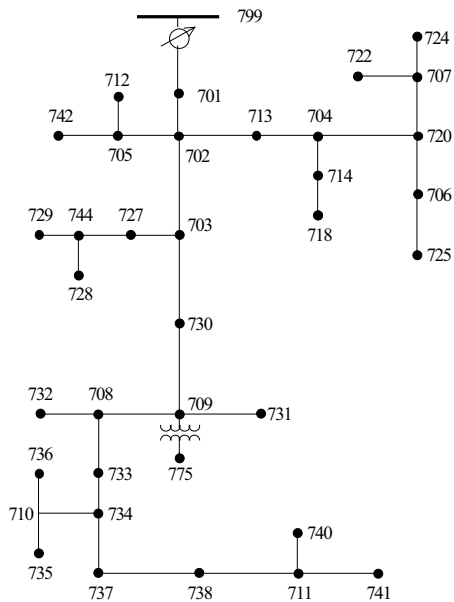
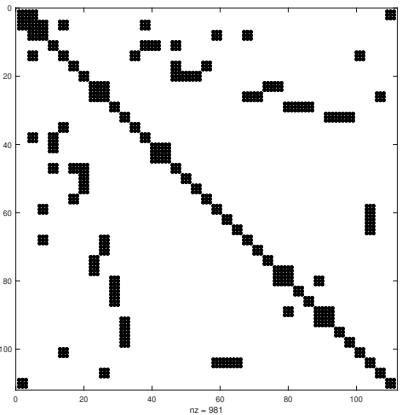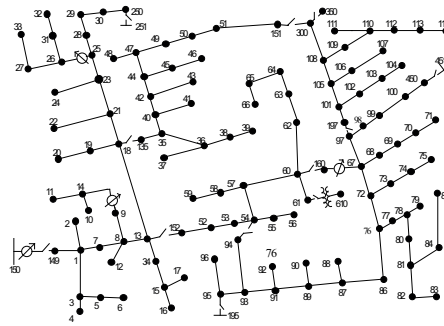Figure C.7: Network outlook of Distribution test case D37 [39]

Figure C.8: Sparsity pattern of Distribution test case D37

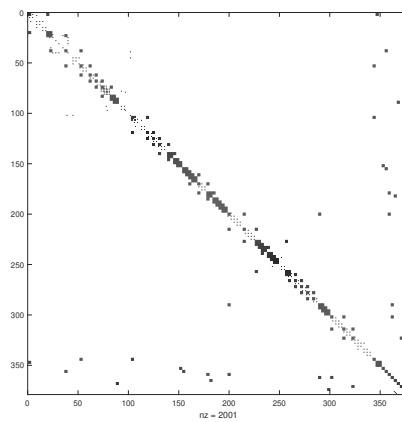Figure C.9: Network outlook of Distribution test case D123 [39]

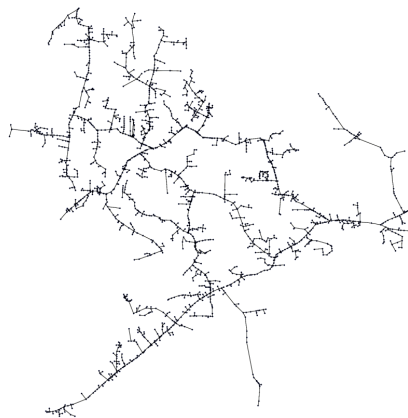Figure C.10: Sparsity pattern of Distribution test case D123

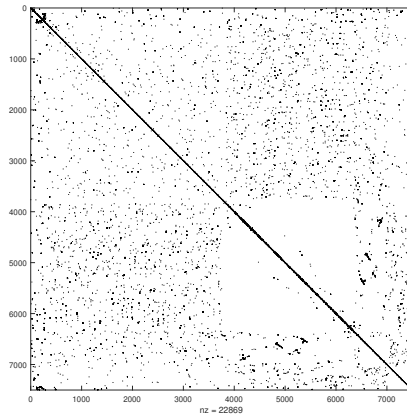Figure C.11: Network outlook of Distribution test case D8500 [39]

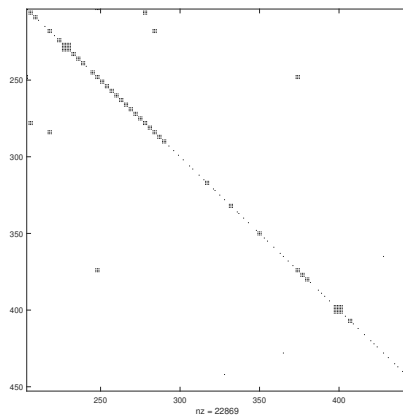Figure C.12: Sparsity pattern of Distribution test case D8500

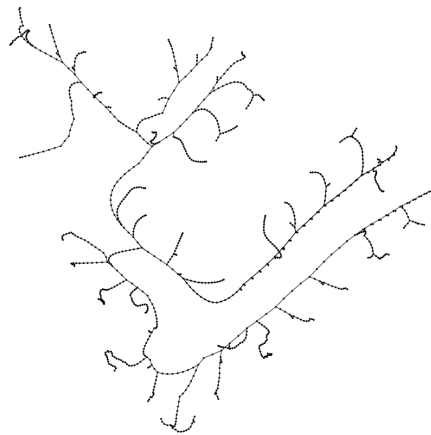Figure C.13: Close-up of the sparsity pattern of the diagonal of Distribution test case D8500

C

Figure C.14: Network outlook of Distribution test case D906 [39]